Extended Investigations into Recovery of Water and Salts from Multi-component Hypersaline Brines using Eutectic Freeze Crystallization

Report to the
Water Research Commission

by

Dyllon Randall, Alison Lewis, Marcos Rodriguez-Pascual, Jeeten Nathoo, Traci Reddy, Grant Apsey, Michael Kapembwa, Tim Egan, Jemitias Chivavava
Crystallization and Precipitation Research Unit
Department of Chemical Engineering, University of Cape Town

This project is a follow-on project from the one entitled
Novel Technology for Recovery of Water and Solid Salts from Hypersaline Brines: Eutectic Freeze Crystallization (WRC Project No. K5/1727)

WRC Report No. 2012/1/13
ISBN 978-1-4312-0495-5

September 2013

Obtainable from

Water Research Commission

Private Bag X03
Gezina, 0031

orders@wrc.org.za or download from www.wrc.org.za

DISCLAIMER

This report has been reviewed by the Water Research Commission (WRC) and approved for publication. Approval does not signify that the contents necessarily reflect the views and policies of the WRC, nor does mention of trade names or commercial products constitute endorsement or recommendation for use.

©Water Research Commission

EXECUTIVE SUMMARY

Hypersaline inorganic brines are generated by a number of industries, including mining operations, power generation and petrochemical refining. In addition, because of pressures on water resources, and thus further water recycling and reuse, these brines present an increasingly significant global problem. Brine management consists mainly of disposal to lined evaporation ponds, which is both a costly and unsustainable solution. Viable brine treatment solutions do not currently exist, thus there is an urgent need to both develop and implement such treatment options.

Eutectic Freeze Crystallization (EFC) has been identified as a possible novel brine treatment method, but to date it has not been applied to multi-component streams such as brines. Therefore, the overall aim of this project was to investigate the applicability of EFC to the multi-component hypersaline brines produced by major South African industries. The first objective was to establish the thermodynamic and kinetic factors governing the operation of a Sequential Eutectic Freeze Crystallization process. The second objective was to summarise the effect of real brines compared to synthetic brines on the operation and control of a Eutectic Freeze Crystallization process. For the third objective, the effect of impurities and contaminants on the ice product formed during a Eutectic Freeze Crystallization process was investigated. For the fourth objective, the effect of impurities and contaminants on the ice product produced in an EFC process was investigated. The fifth and last objective was to investigate how operating temperatures affect the yield and purity of the final products formed in an EFC process.

Four brines were studied overall: **two** from the coal mining industry (**Brine 1** and **Brine 2**), and **two** different brines from the platinum mining industry in South Africa. A comprehensive brine analysis had to be conducted before the thermodynamic modelling of the brine could proceed. A combination of standard water analysis techniques and wet chemistry were used to characterize the brine, while a commercial thermodynamic modelling package (OLI Stream Analyser) was used to perform the thermodynamic modelling of the brine. It was found that the difference between the total cations and total anions (ion imbalance) from the analysis of two brine samples, **Brine 1** and **Brine 2** (both brines were obtained from coal mining), were 5.8% and 6.3% respectively. The brines were also very dilute with a total dissolved solid content of 29.77 g/L for **Brine 1** and 31.26 g/L for **Brine 2**. The conclusion to this is that the ion imbalances were so small as to be considered negligible.

The thermodynamic modelling software was able to predict and simulate the phase equilibria of a multicomponent aqueous system over a wide temperature range by estimating the standard state terms and the excess terms with the use of various thermodynamic models. This was an important step because the identities of the potential salts, the temperatures at which they would crystallize and the potential yields of the various products could be predicted before any experiments were conducted. The thermodynamic modelling predicted that the brine samples were saturated with respect to $CaSO_4 \cdot 2H_2O$. The modelling also predicted that ice, $Na_2SO_4 \cdot 10H_2O$ as well as $K_2SO_4 \cdot CaSO_4 \cdot 1H_2O$ would crystallize in a narrow temperature range from -0.8°C to -2.2°C. The thermodynamic results also showed that a high overall ion recovery (85% for **Brine 1** and 71% for **Brine 2**) would be obtained at an operating temperature of -5°C.

However, the thermodynamics only offered an equilibrium prediction. It was only by investigating the kinetic aspects of the system that the identity, crystallization temperatures and yield of products under real operating conditions could be confirmed.

The experiments for the kinetic phase focused primarily on the sequential removal of pure salts from a single brine under EFC conditions. The experimental work showed that relatively pure calcium sulphate (98.0% purity), sodium sulphate (96.4% purity) and potable water (ice) could be formed with a brine mass reduction of ~97%. The problem with the brines initially being saturated with respect to calcium sulphate was also solved by successfully removing calcium sulphate and ice under EFC conditions. This meant that pure sodium sulphate and ice could be removed in the subsequent stage.

The validity of using synthetic versus real brines for experimental studies was established. The criterion for testing the validity was that the conductivity, pH, density measurements and ion imbalance were similar. The research showed that synthetic brine resulted in the same ice and salt nucleation temperatures as real brine and therefore could be substituted for real brine for the purposes of experimental work.

Impurity incorporation was investigated using the **third** brine: a platinum industry brine. It was found that the sodium sulphate crystals formed from the brine were relatively pure, but had a small quantity of selenium as an impurity incorporated in the crystal product due to isomorphic substitution. The form of the selenium was identified as selenate.

It was found that the purity of ice could be improved by adopting agitation in a vessel with a larger surface area together with washing of the final ice product. The agitation of the ice bulk resulted in the release of trapped salt and thus an improved ice purity while washing removed any entrained brine on the surface of the ice crystals.

From a fundamental point of view, the mechanisms that characterise ice crystal growth include heat and mass diffusion and, depending on how they interact with each other, they affect crystal growth, morphology and ultimately the purity of ice.

In terms of yield and purity in an EFC process, the system is dependent on temperature and must be analysed on a case-by-case basis. Thermodynamic modelling was used to identify prominent features of a brine system, in particular the eutectic temperature.

A **fourth** brine, an alkaline sodium carbonate brine, was used to study the effects of operating temperature on yield and purity of the salt formed in the Eutectic Freeze Crystallization process. In the sodium carbonate system, high yields of salt were observed above to its eutectic point. Ice yields increased substantially at sub-eutectic temperatures.

The concentration of impurities in the sodium carbonate decahydrate salt was found to be low, indicating a highly pure compound affected largely by entrained impurities, and not liquid inclusions or isomorphous incorporations.

ACKNOWLEDGEMENTS

The writers wish to express their gratitude:

- To the staff of the Crystallization and Precipitation Research Unit and the Mechanical Workshop, in the Chemical Engineering Department at the University of Cape Town for their contribution to the research reported here;
- To the Water Research Commission (WRC) for the funding support;
- To Coaltech, Mr Johan Beukes and Mr Dick Kruger for their support and input to the project;
- To the members of the Reference Group for their contributions to and guidance of the project, namely:

Dr JE Burgess – WRC (chairperson)
Prof LF Petrik – University of the Western Cape
Mr A Wurster – Golder Associates Africa (Pty) Limited
Dr NE Ristow – Phathamanzi Water Treatment (Pty) Limited
Mr IW van der Merwe – Proxa (Pty) Limited
Mr G van Dyk – AngloGold Ashanti
Mr P Günther – Anglo Coal
Mr JA Steenkamp – Eskom
Ms R Mühlbauer BHP Billiton Energy Coal South Africa Limited
Mr JS Beukes – Coaltech
Ms S Mudau – Chamber of Mines of South Africa
Mr HM du Plessis – Private Consultant
Mr TM Morokane – Department of Water Affairs
Dr LM Baratta – Sasol Technology Research and Development

TABLE OF CONTENTS

TABLE OF FIGURES

TABLE OF TABLES

Abbreviations

CMOS	Complementary Metal-Oxide Semiconductor
EFC	Eutectic Freeze Crystallization
ICP	Inductively Coupled Plasma
ICP-OES	Inductively Coupled Plasma Optical Emission Spectrometry
MSZ	Metastable Zone
MSZW	Metastable Zone Width
RO	Reverse Osmosis

1 INTRODUCTION

One of the most important environmental issues in many industries of South Africa is hypersaline brine production. Major methods aimed at reducing these brine volumes consist of either brine disposal in evaporation ponds, or brine treatment using evaporative crystallization. Brine disposal has a negative impact on the environment because of potential ground-water contamination, while evaporative crystallization is costly because of the high energy requirements. Both of these methods can reduce the volume of brine, but the final salt product is always contaminated with other salts. This makes separation of the salt waste to create a usable product extremely unlikely. In addition, these current methods of brine disposal and treatment only offer short-term solutions and have not been shown to be sustainable in the long-term.

A novel technology known as Eutectic Freeze Crystallization (EFC) has the potential to treat brines by operating near the eutectic temperature of a specific salt. Not only is water produced in the form of ice, but pure salts are also produced when EFC conditions are reached. Thus, the problem of salt contamination is avoided by the fact that each salt has its own unique eutectic temperature, therefore providing the possibility of crystallizing many pure salts from the brine individually. Eutectic Freeze Crystallization is an attractive water treatment technology, but to date it has not been utilized for complex systems such as brines. Therefore, a protocol for the treatment of hypersaline brines using EFC is necessary in order to test the feasibility of this technology.
This research is an extension of an earlier research project (Novel Technology for Recovery of Water and Solid Salts from Hypersaline Brines: Eutectic Freeze Crystallization (WRC Project No. K5/1727). The earlier project had three main aims: (1) Establish the eutectic freeze crystallization phase diagrams for the hypersaline brines and saline effluents under investigation; (2) Establish the effect of the complex aqueous chemistry and impurities on the applicability of eutectic freeze crystallization to these aqueous systems and (3) Establish the expected costs and economic benefits of applying eutectic freeze crystallization to these aqueous systems.

2 OBJECTIVES

The main aim of this research project was to further the understanding of the applicability of EFC to the multi-component hypersaline brines produced by major South African industries. The objectives to date for the study are (see Appendix for original project deliverables as well as revised project deliverables):

1. Establish the thermodynamic and kinetic factors governing the operation of a Sequential Eutectic Freeze Crystallization process;
2. Establish how the treatment of real brines differs from that of synthetic brines;
3. Investigate the effect of impurities and contaminants on the salt product formed by an EFC process.
4. Investigate the effect of impurities and contaminants on the ice product formed by an EFC process.
5. Investigate how operating temperatures affect the yield and purity of the final products formed during an EFC process.

The structure of the report is as follows: the report begins with an overall theory and literature review, in which all of the background material is covered. This is followed by the Experimental Methods for each of the objectives, then the Results and Discussion for each of the objectives. Finally, the

conclusions for each separate objective are set out in the Conclusions section. The report concludes with overall Recommendations.

3 THEORY AND LITERATURE REVIEW

3.1 Theory of crystallization

Crystallization can be defined as a phase change where a crystalline solid is obtained from the solution (Myerson, 2002). This can only be achieved in a supersaturated solution; that is a solution that has a concentration of the solute exceeding the equilibrium solute concentration. The thermodynamic driving force for crystallization is called supersaturation. Hence, the nucleation of particles and their subsequent growth are driven by the existing supersaturation in the solution (Loffelmann and Mersmann, 2002).

Supersaturation can be expressed in dimensionless form as (Myerson, 2002):

$$S = \frac{\mu - \mu^*}{RT} = \ln \frac{a}{a^*} \quad \textbf{(1)}$$

where

S	supersaturation, -
μ	actual chemical potential, J
μ^*	equilibrium chemical potential, J
R	Universal Gas Constant, 8.314 J $mol^{-1}K^{-1}$
T	temperature, K
a	actual activity, mol m^{-3}
a^*	equilibrium activity, mol m^{-3}

For cooling crystallization, the supersaturation can be expressed as a temperature difference:

$$S = T - T^* \quad \textbf{(2)}$$

Where

T	actual temperature, K
T^*	equilibrium temperature, K

3.1.1 Nucleation

A crystalline material can only develop if there are a critical number of nuclei in a solution. The nucleation process may either occur spontaneously or the system can be forced to nucleate. The process of nucleation in systems containing no previous crystalline matter is termed primary nucleation while the process of artificially inducing nucleation is known as secondary nucleation. In the primary nucleation system, many nuclei are formed at high supersaturation, resulting in small crystals.

The primary nucleation process can also be further subdivided into homogenous and heterogeneous nucleation. The homogenous nucleation process involves the spontaneous formation of crystals in the bulk solution while heterogeneous nucleation occurs on a solid surface typically because of impurities in the system (Mullin, 2001).

Secondary nucleation is dominant at low supersaturation where the supersaturation is consumed gradually. Thus, the control of supersaturation in the solution is possible for secondary nucleation systems. As a result, large crystals can be prepared (Tai et al., 2009). Seeds usually consist of crystalline material of the solute and the addition of these seed particles to a supersaturated solution is called seeding.

3.1.2 Crystal growth

Crystal growth is the enlargement of crystals caused by the deposition of matter on an existing surface in a supersaturated solution (Torsen, 2011). It involves the mass transfer of molecules to the crystal surface as well as the removal of the heat of crystallisation (Ayel, 2006).

Once a stable nucleus has been created in a solution, it is capable of growing into a crystal (Mullin, 2002). Crystal growth rates depend upon temperature; supersaturation (super cooling) and the nature of the fluid flow in the vicinity of the crystal surface (Jones, 2006). Fast crystal growth will result in high yields over a specific time interval. However, it has been found to be the most common cause of inclusion formation during crystallization processes (Mullin, 2002).

3.1.3 The solid-liquid interface

An interface is the physical boundary between two adjacent bulk phases (Eribil, 2006). In order for a new phase to appear, an interface must be formed (Mersmann, 2011). The solid-liquid interface is the most interesting area compared to the other regions of the system as the entire reaction takes place in this area (Genceli, 2009).

The heat of crystallization generated at the solid-liquid interface and the diffusion of solutes from the ice phase creates a temperature and concentration gradient (Mersmann, 2011). The temperature and concentration gradients affect the growth rate of the crystals and the amount of impurity inclusions (Ulrich, 2001). The structure of the interface may be smooth or rough depending on the level of supersaturation (Myerson, 2002) and the rate of removal of heat from the interface. It has been postulated that partial rejection of impurities at the crystal-solution interface causes the concentration of impurities in the interfacial region to increase above the value in bulk solution. Thus, with increasing growth rates, impurities can be rejected at a rate faster than they can diffuse into the bulk solution, resulting in an accumulation in the interfacial region (Myerson, 2002) as illustrated in Figure 1.

3.1.4 Morphology

Morphology relates to the physical form and structure of a material (Petzold, 2009). The morphology of a crystal is determined by internal and external factors i.e. growth parameters (Sato, 2001). In the case of ice, morphology means characterizing the structure at scales ranging from crystal lattice to supra-crystalline structures such as needles, plates and columns, and macro-structures such as floes and glaciers.

3.1.5 Impurity incorporation

Impurities are trapped in the crystals during growth (Ulrich, 2001) and this mechanism usually depends on crystal growth parameters. Mechanisms by which impurities can be incorporated into crystalline products include adsorption of impurities on crystal surfaces, solvent entrapment in cracks, crevices and agglomerates, as well as inclusion of pockets of liquid (Ulrich, 2011).

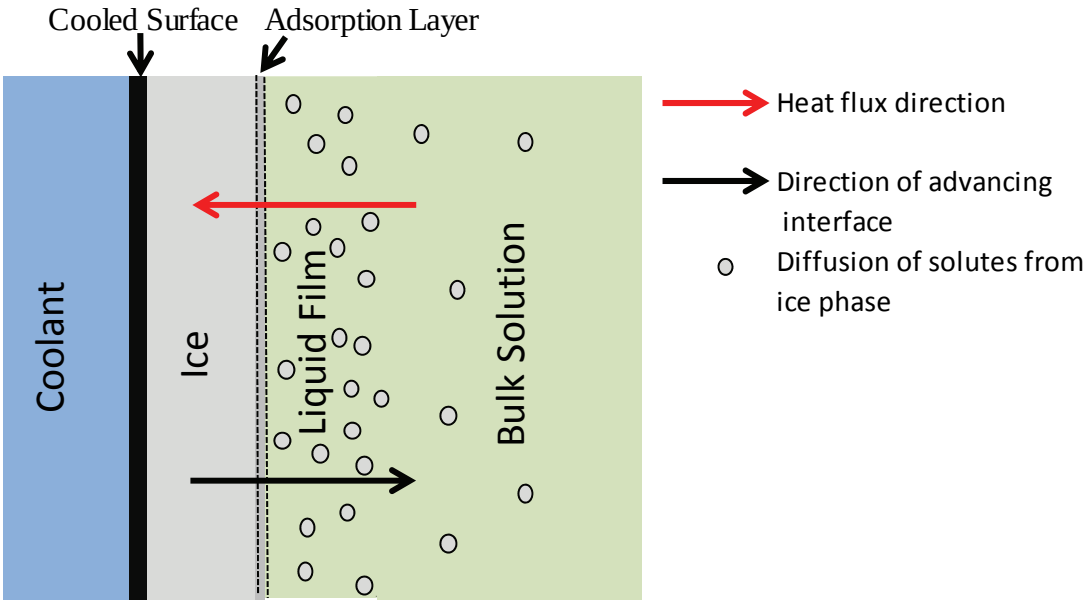

Figure 1: Ice Crystal: Solid-Liquid Interface (adapted from Myerson (2002))

3.1.6 Heat and mass transfer effects of ice growth

When an ice crystal begins to grow in an electrolyte solution, heat of crystallization is released into the system and solutes diffuse from the ice phase and accumulate at the solid-liquid interface. The heat and mass transfer fluxes will determine the characteristics of the crystals during the growth phase. Mass transfer fluxes during the phase change in the boundary layer affects the concentration and temperature at the solid-liquid interface, which then changes the freezing point and influences the purity of the ice formed (Chen, 1999). It is well known that the impurity component is captured in the growing solid layer of a crystal even for a simple eutectic system due to the unsteady and non-equilibrium phase transitions (Maeda, 2002). The spatial variation of solution concentration and temperature around the crystal provides information about the mechanisms of growth, the onset of instabilities and the relationship between growth conditions and crystal growth (Shlichta, 2008). For example, conditions like local supersaturation determine how the crystal would grow thereby affecting crystal morphology, a parameter that is frequently related to the purity of crystals (Mersmann, 2011).

3.1.7 The Metastable Zone and seeding

The metastable zone width is usually defined in terms of the maximum obtainable undercooling temperature. Figure 2 explains the definition of the MSZ using a phase diagram. A solution is initially at point **A** with a solute concentration of $\mathbf{C}_1$. Point **A**, the thermodynamic solubility limit, is reached as the solution is cooled to $\mathbf{T}^*$. Further cooling to **T** causes the solution to move along line **AB** into the metastable region until the metastable limit is reached at point **B**. In the metastable zone, between points **A** and **B**, crystallization will only occur in the presence of seeds. Spontaneous nucleation commences when the metastable limit is reached at point **B**.

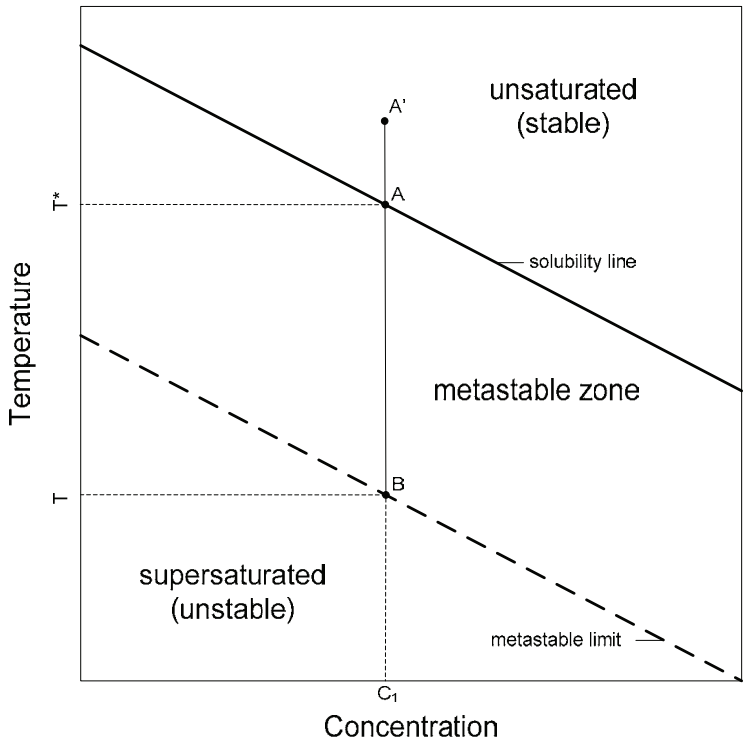

Figure 2: Phase diagram of a binary solid-liquid system showing the metastable region

The MSZ has been discussed by many authors (Sangwal, 2009; Nyvlt et al., 1970; Kubota, 2008) and, while many agree that the nucleation event is a stochastic process (Nyvlt, 1971), the MSZ is usually characterized using one experiment. The fact that nucleation is stochastic in nature implies that the MSZ would be different for repeat experiments at exactly the same conditions. It is only by analysing a number of experiments that an estimate can be made as to the actual width of the MSZ. Significant differences in nucleation temperatures during the spontaneous nucleation of ice have been reported by Chen et al. (1998). In their investigation into the crystallization of supercooled water, the researchers reported large variations (-3°C to -10°C) in the nucleation temperatures of ice.

The MSZ can be determined in one of two ways, namely the polythermal and the isothermal methods (Sangwal, 2009). In the polythermal method, the solution is cooled from the saturation temperature at a fixed cooling rate. The isothermal method involves rapidly cooling the solution to a predetermined temperature which is below the saturation (equilibrium) temperature of the component of interest. The solution is left at this temperature until spontaneous nucleation occurs (Sangwal, 2009). The time taken for spontaneous nucleation to occur at each temperature for a specific concentration of the component provides one data point towards determining the MSZ.

The key difference between these two methods is that in the polythermal method the supersaturation is constantly changing while in the isothermal method the supersaturation remains constant. Experimentally, the isothermal method takes much longer, especially if the specified supersaturation level is very low.

Table 1 tabulates the maximum undercooling, or MSZ, for a number of substances at cooling rates of 2, 5 and 20°/hour. A faster cooling rate results in a wider MSZ.

Table 1: Maximum undercooling for different components at various cooling rates (Myeron, 2002)

Substance	Saturated Solution Temperature (°C)	Maximum Undercooling Before Nucleation — Cooling Rate 2°C/hour	5°C/hour	20°C/hour
$Ba(NO_3)_2$	30.8	1.65	2.17	3.27
$CuSO_4 \cdot 5H_2O$	33.6	5.37	6.82	9.77
	60.4	0.930	1.30	2.16
$FeSO_4 \cdot 7H_2O$	30.0	0.890	1.21	1.93
	40.6	0.570	0.830	1.46
KBr	30.3	1.62	2.33	4.03
	61.0	1.69	2.41	4.11
KCl	29.8	1.62	1.86	2.30
	59.8	1.02	1.18	1.48
$MgSO_4 \cdot 7H_2O$	32.0	1.95	2.63	4.15
$NH_4Al(SO_4)_2 \cdot 12H_2O$	30.2	0.810	1.34	2.88
	63.0	1.19	1.95	4.13
$NaBr \cdot 2H_2O$	30.6	4.60	6.97	13.1

Figure 2 also shows the different seeding areas in the model binary solution. Two seeding approaches can be used to promote crystallization. The first involves the addition of seed material at a temperature just below the solubility temperature (Mullin, 2001). Subsequent cooling will result in crystallization occurring at some temperature below the solubility temperature.

The second approach involves cooling the solution until a temperature within the MSZ, at which stage the seed material is added. This approach usually leads to crystallization occurring at the moment the seed material is added.

3.2 Thermodynamic phase diagrams

A phase diagram indicates the equilibrium phases of a crystallization system present at a given temperature and concentration. The phase diagram is for conditions of thermodynamic equilibrium and therefore does not accurately describe the kinetics of a system.

3.2.1 Binary phase diagrams

A binary system is defined as a single salt dissolved in a solvent, typically water. Figure 3 is a theoretical binary phase diagram showing the different phases present and their corresponding conditions. The diagram is divided into different areas as follows:

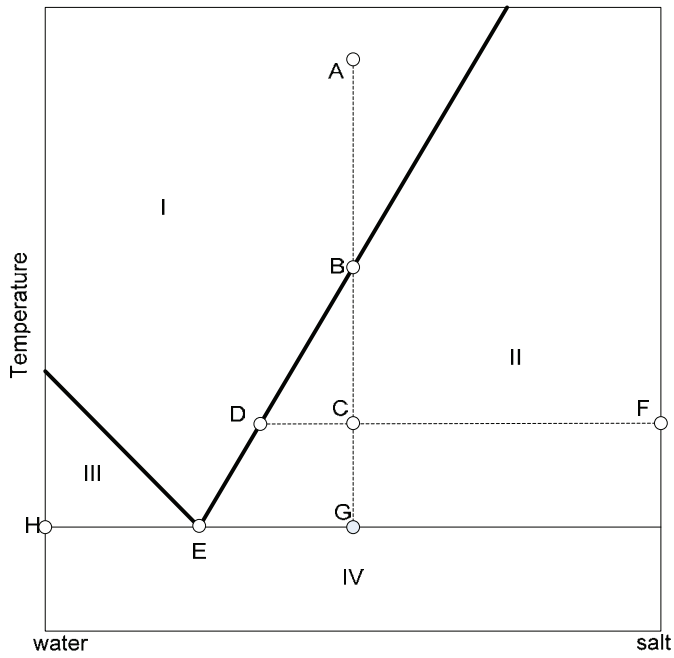

Area I – solution of salt in water

Area II – saturated solution and solid salt

Area III – saturated solution and ice

Area IV – mixture of solid salt and ice

Figure 3: Theoretical binary phase diagram (Nyvlt, 1971)

Cooling the solution from A to B results in the formation of salt crystals at B. Further cooling to point C leads to a situation where the pure solid phase is in equilibrium with a solution of composition D (Nyvlt, 1971).

The theoretical yields for each species are also given by the phase diagram. The relative weight ratios are given by lever rule:

$$\text{Weight of salt/weight complete system} = CD/DF \quad \textbf{(3)}$$

If the system is cooled further to G, then the salt will be in equilibrium with a saturated solution of composition E. At this point ice will also begin to form. The second solid phase, ice, at concentration H, will be in equilibrium with the system.

Figure 4 shows the effect of a temperature reduction on the yield of ice for different concentrations of sodium sulphate. The eutectic temperature is indicated by the dotted line in Figure 4 and describes the temperature at which $Na_2SO_4 \cdot 10H_2O$ begins to crystallize simultaneously with ice.

The highest yield of ice is obtained from the lowest concentration of sodium sulphate (1wt%). The temperature at which ice begins to crystallize (-0.4°C) is also the highest for a 1wt% solution. Also, more than 70% of the water needs to be removed in the form of ice (point **A**) before any salt will begin to crystallize while 48% (equivalent of point **B**) and 21% (equivalent of point **C**) of the water needs to be removed for concentrations of 2wt% and 3wt% sodium sulphate respectively. Each concentration curve also does not reach a 100% yield of ice. The reason for this is as a result of some of the water molecules being used to form the hydrates in the $Na_2SO_4 \cdot 10H_2O$ salt. Highly concentrated streams will therefore have a reduced yield of ice since more solvent would be needed to form the salt hydrates. The results shown in Figure 4 do not take into account the kinetics of the system. For example, a 1wt% solution would require more time to reach eutectic conditions compared to the more concentrated curves in Figure 4. The 1wt% solution is also likely to result in excessive ice scaling as well as salt-ice

separation issues as a result of the high solid content in the crystallizer compared to the other concentration levels.

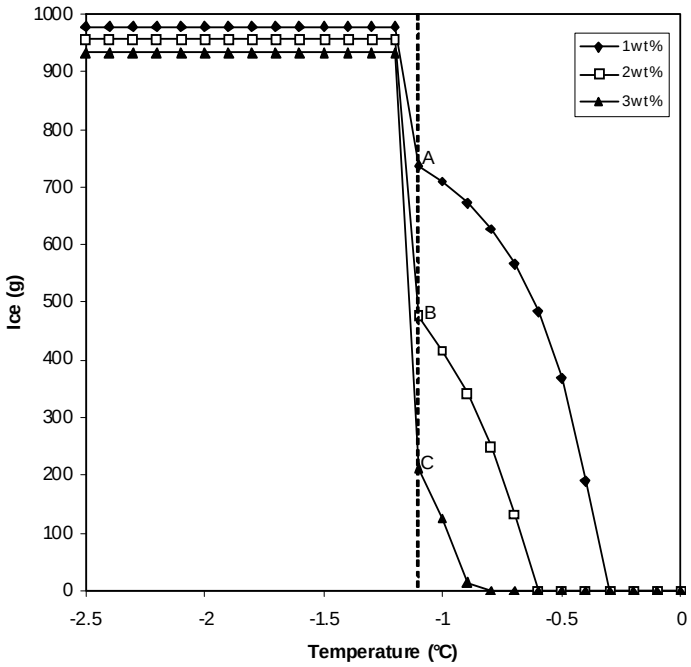

Figure 4: Effect of temperature reduction on yield of ice in a Na_2SO_4 system (OLI Stream Analyser, 2010)

3.2.2 Ternary phase diagrams

A ternary system, in this context, is defined as two salts, with a common ion, dissolved in water. The ternary phase diagram is usually plotted on an equilateral triangle as shown in Figure 5. Each apex of the equilateral triangle represents a pure component and each side of the triangle represents a binary system of the two corresponding components.

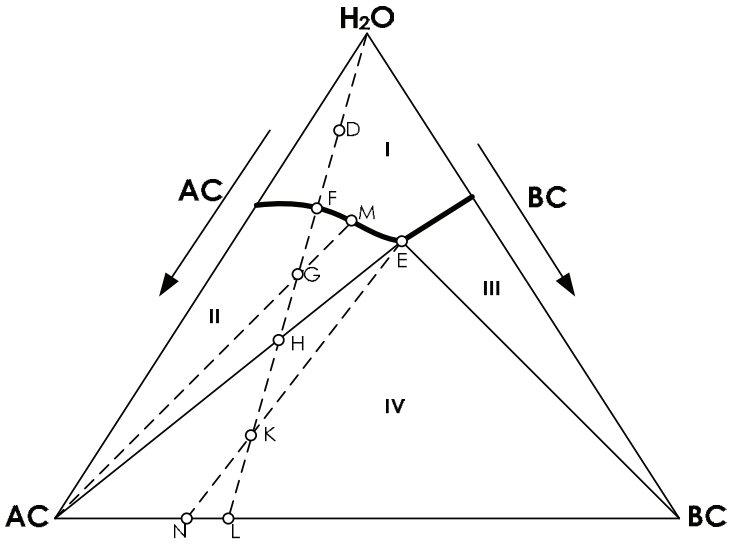

Figure 5: Theoretical ternary phase diagram (Nyvlt, 1971)

The equilateral triangle in Figure 5 shows the isothermal phase diagram of two salts, AC and BC, dissolved in water. The different areas of the ternary phase diagram are:

Area I – unsaturated aqueous solution of the salts
Area II – solid salt AC in solution
Area III – salt BC in solution
Area IV – both salts in a saturated solution of composition represented by E
Point E – ice, solid AC and solid BC

The interior of the triangle shows the thermodynamic equilibrium conditions for all three components at a specific temperature, called an isotherm. The lever rule can again be used to determine the weight ratios of each species (Nyvlt, 1971).

The lines separating regions **I** from **II** and **I** from **III** indicate the saturated solutions of salts AC and BC. Starting at point **D**, if water is removed, the composition change would occur along the line through **D** and the apex representing pure water. Once point **F** is reached, solid AC begins to crystallize. As more water is removed, point **G** is reached which has a saturated solution composition of **M** and is in equilibrium with pure salt AC.

The relative weight of salt AC at point **G** is given by:

$$\text{Relative weight of salt AC} = GM/ACM \quad \textbf{(4)}$$

With further removal of water, the system reaches point **H**. From point **H** onwards the composition of the equilibrium saturated solution moves along the curve FME until point **E**, the ternary eutectic point, is reached (Nyvlt, 1971). Further water removal will result in no composition change of the solution, but a mixture of salts AC and BC.

If the composition of the system is at point **K**, the region where salt AC and salt BC coexist with a saturated solution of composition E, then the relative weight ratio of the salt is given by:

$$\text{Relative weight of salt AC/ relative weight of salt BC} = (BCN)/(ACN) \quad \textbf{(5)}$$

A number of isothermal equilateral triangles can be used to construct a three dimensional phase diagram (Figure 6). The concentrations are measured along the sides of the base of the triangle while the temperature is measured vertically. The surface of Figure 6 shows contours representing constant temperatures (isotherms).

Another method of depicting a ternary phase diagram is shown in Figure 7. The diagram, however, does not show the water content. The salt fraction, sf, is defined as follows:

$$sf = \frac{[Na_2SO_4]}{[Na_2SO_4]+[MgSO_4]} \quad \textbf{(6)}$$

Where

$[Na_2SO_4]$ – molal concentration of anhydrous sodium sulphate (mol/kg H_2O)
$[MgSO_4]$ – molal concentration of anhydrous magnesium sulphate (mol/kg H_2O)

Thus a salt fraction of one refers to a pure binary Na_2SO_4-H_2O system while a salt fraction of zero refers to a binary $MgSO_4$-H_2O system.

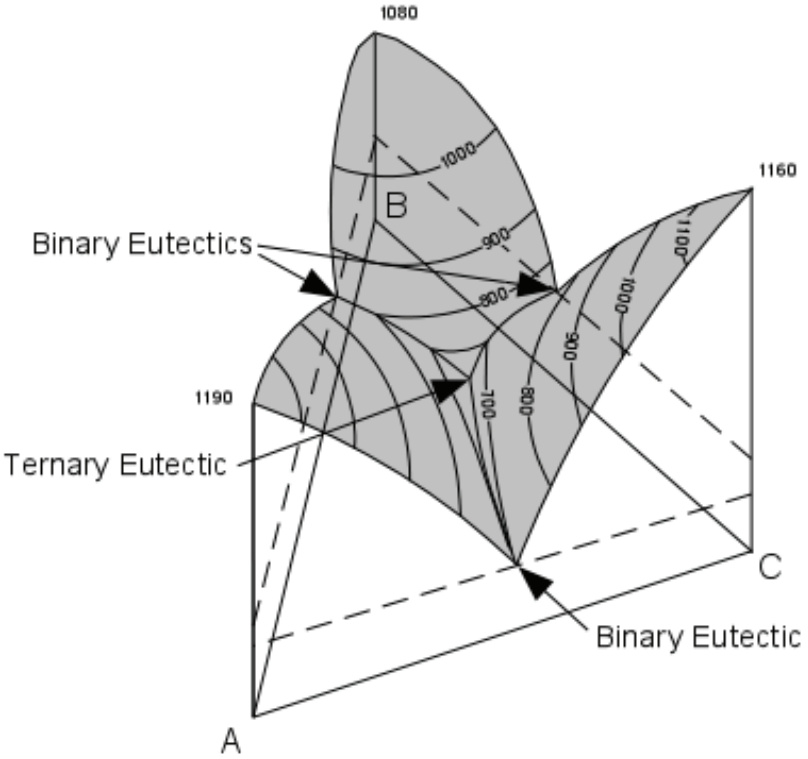

Figure 6: 3D Ternary phase diagram (Ternary Phase Diagrams, 2008)

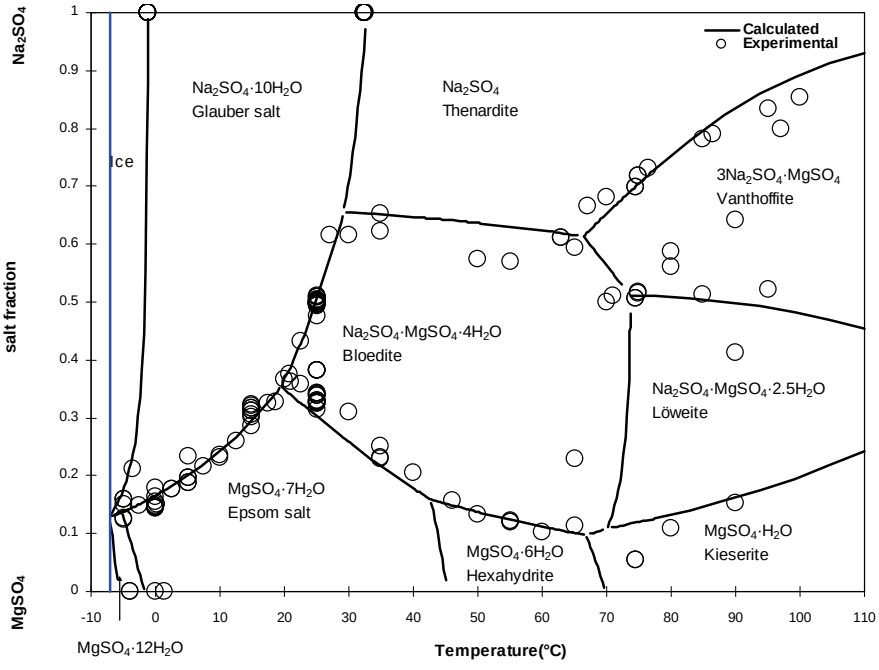

Figure 7: Ternary phase diagram for Na_2SO_4-$MgSO_4$-H_2O (Thomsen, 1997)

Phase diagrams or solubility data can also be used to determine if selective nucleation can be used as a solute separation technique for a particular system. However, this information alone does not guarantee the feasibility of this technique; a system also has to have the ability to sustain a significant level of

supersaturation without the occurrence of primary nucleation (Nyvlt, 1971). This can only be determined experimentally.

3.2.3 Quaternary phase diagrams

Quaternary systems (four different ions) can be depicted on a Jänecke projection. Figure 8 shows such a projection for a system with the following ions Na^+, NH_4^+, SO_4^{2-} and Cl^-. The water content is given as a weight percent on the grid line intersections.

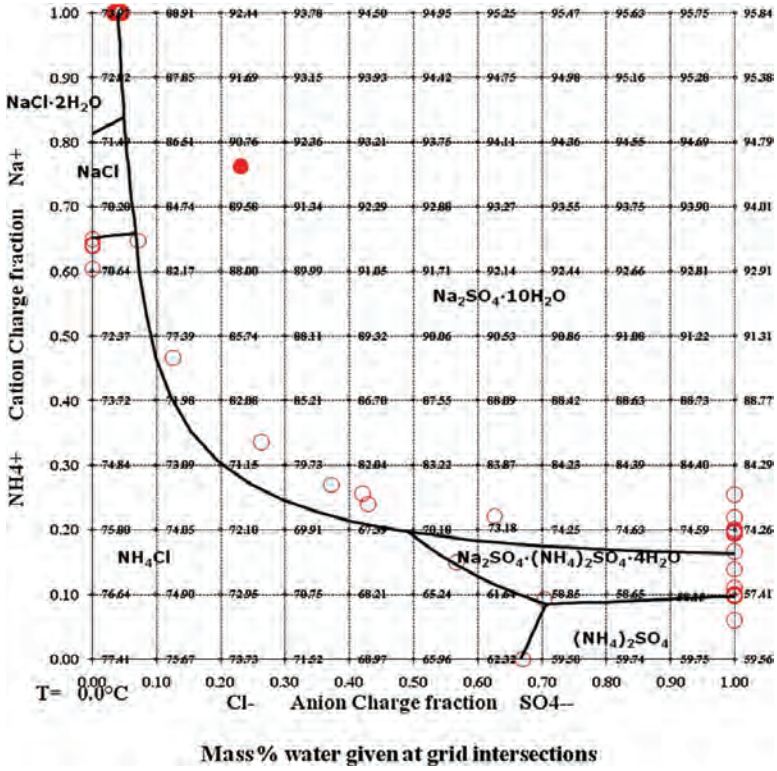

Figure 8: Jänecke projection of the Na^+:NH_4^+:Cl^-:SO_4^{2-} system at 0°C (Thomsen, 1997)

3.2.4 Thermodynamics of complex systems

It is important to take into account the accuracy of the thermodynamic simulating tool during modelling since this can significantly affect the results obtained. Figure 9 shows a binary sodium sulphate phase diagram as predicted by OLI and the extended UNIQUAC model. The trends for the phase equilibria predicted by each model are similar. The results obtained from each model also compare well with experimental solubility data for a binary sodium sulphate system (Thomsen, 1997). Although the results obtained from OLI are at higher temperatures than the results predicted by the extended UNIQUAC model.

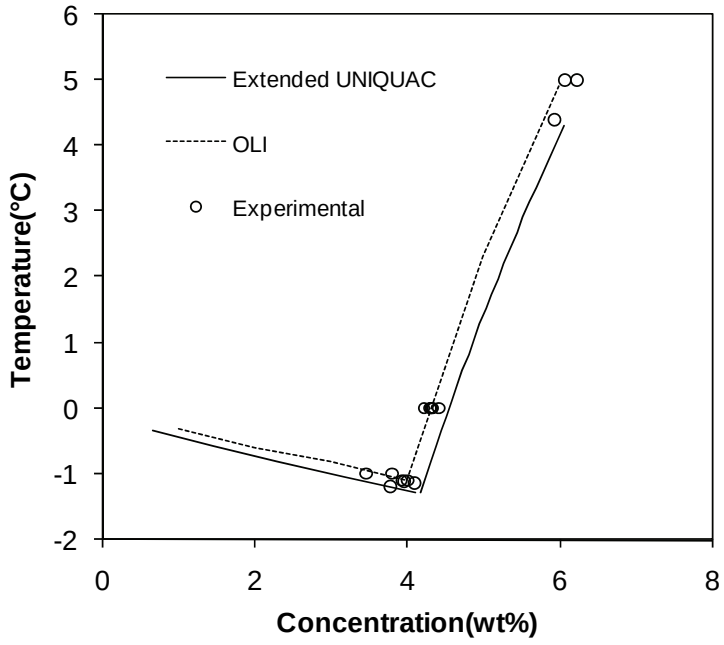

Figure 9: Thermodynamic modelling comparison (Thomsen, 1997; OLI Stream Analyzer, 2010)

3.3 The Eutectic Freeze Crystallization process

3.3.1 The history of Eutectic Freeze Crystallization

In 1952, the Organisation for European Economic Cooperation convened a meeting to discuss options for sea water desalting. This team, with delegates from Belgium, Denmark, England, France, Germany, The Netherlands and Sweden, and observers from Australia, South Africa, United States of America and the Rockefeller Foundation, concluded that a freezing method for sea water desalting was difficult and economically impractical (Wiegandt and von Berg, 1980). It was this conclusion that lead to a delay into the research of using freezing as a water treatment method. In fact, it was only in the 1970s that this research was conducted. To this day most people remain sceptical of freeze concentration as a water treatment option.

Stepakoff and co-workers first introduced EFC in the early 1970's as a separation technique (van der Ham, 1999) while Barduhn and Manudhane (1979) devised the first process. A decade later Swenne and co-workers (Vaessen, 2003) investigated using this technique for the production of sodium chloride. Direct cooling, as opposed to indirect cooling, was used by these three researchers (van der Ham, 1999).

Barduhn and Manudhane (1979) investigated the use of EFC with natural waters in 1979. They concluded that EFC would operate well at temperatures no lower than -25°C for natural waters containing the following ions: Na^+,K^+Ca^{2+},Mg^{2+},Cl^-,SO_4^{2-},HCO_3^- (Barduhn and Manudhane, 1979).

Nelson and Thompson (Vaessen, 2003) investigated the formation of salts during the freezing of sea water. About 80% of the water initially present was removed as ice before $Na_2SO_4 \cdot 10H_2O$ and $NaCl \cdot 2H_2O$ began to crystallize (Stepakoff et al., 1974).

In the late 1990s van der Ham (1999) started EFC research using indirect cooling as opposed to direct cooling (Vaessen, 2003). This research focused on the industrial application of the EFC concept and the realization of an economically efficient EFC process.

Presently EFC research is continuing at the Technical University of Delft and conducted at the University of Cape Town.

3.3.2 The advantages and disadvantages of Eutectic Freeze Crystallization

The concept of freezing a solution in order to separate water and solutes is not a new one. Many authors have described such a method as a means of separation (Wiegandt and von Berg, 1980; Vaessen, 2003; Johnson, 1976; Lorain et al., 2001). Eutectic Freeze Crystallization uses these concepts and focuses on a specific area of freeze crystallization, namely operating at the eutectic point of two components (ice and salt). By so doing a number of advantages can be achieved over conventional brine treatment methods, some of which are listed below (Randall et al., 2011):

- The process is not complicated by the addition of chemical compounds (Lorain et al., 2001);
- From a thermodynamic perspective, as the heat of vaporisation is six times higher than the heat of fusion (van der Ham, 1999), freezing the brine as a means of treating it is theoretically less energy intensive than an evaporative process;
- Impurities are excluded from the ice structure during the crystallization of ice (Halde, 1980);
- The ice crystals that are produced can be used for cold heat storage (Shirai, 1999);
- Gravitational separation of ice and salt is an added advantage during EFC since, at eutectic conditions, both products separate as a result of their density differences. Salt sinks to the bottom of the crystallizer while ice floats to the top (Genceli, 2008);
- Theoretically, a 100% yield can be obtained when operating at eutectic conditions (van der Ham, 1999);
- As the potential for corrosion is minimised due to the low operating temperatures (Johnson, 1976), cheaper materials of construction can be used;
- Freeze crystallization is already used extensively in concentrating fruit juices as well as purifying organic chemicals (Rahman et al., 2007).

The two significant disadvantages of EFC are the capital costs (two or three times those of distillation or evaporation systems (Rahman et al., 2007)) but this has recently been revised in a commercial study carried out by Proxa, a South African engineering company, and scale limitations, but these can be overcome as the technology develops (van der Ham, 1999). Industries are reluctant to accept a fundamentally new technique, especially when acceptable results are being obtained from old and proven techniques (Muller, 1976; as cited by Rahman et al., 2007). Wiegandt and Von Berg (1980) suggested that in the future people and universities would realise that a freeze crystallization process for the treatment of waste water would be achievable with sound concepts and engineering. Only when brine disposal has to be considered, the economic focus changes, since the cost of disposal may be as much as the cost of fresh water produced, thus making a technology such as EFC more attractive as a separation method (1979).

3.3.3 The operating principle

The operating principle of EFC can be described using a typical phase diagram for a binary aqueous solution as shown in Figure 10. The concentration of dissolved solids in waste waters is usually very low (Lorain et al., 2001) (<35 g/L), thus ice will generally crystallize first.

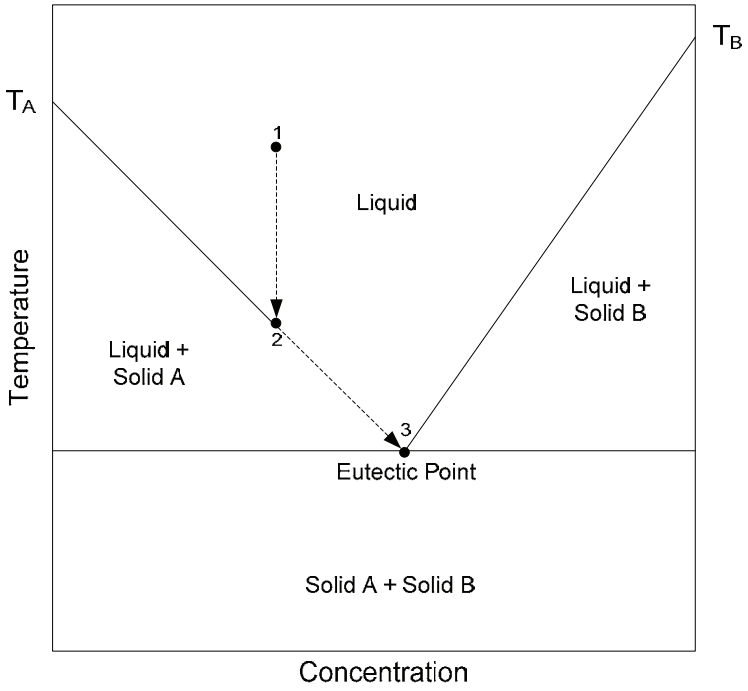

Figure 10: Typical phase diagram for an inorganic aqueous system

The phase diagram used to describe the EFC process therefore has the starting position on the left side of the eutectic point because this is the region where ice crystallizes first. In EFC, the unsaturated solution (1) is cooled until the first crystal of A forms (2). The eutectic point is reached if the solution is cooled more (3). At this point both solid A and solid B is formed (3). Similarly, for a solution with a higher starting concentration than the eutectic concentration, the crystallization of salt will occur first, followed by ice at the eutectic point.

3.4 Impurities in salts produced by EFC

The three different ways in which impurities can occur are through liquid inclusions, isomorphous inclusions and adhesions. Liquid inclusions are chambers of mother liquor that are entrapped by the growing crystals. These liquid inclusions contain whatever impurities existed in the mother liquor and that cannot be removed by washing. Isomorphous inclusions can be described as ionic substitutions or solid solutions. Sometimes when an impurity has a similar structure to one of the ions comprising the desired salt, it can occupy a place in the lattice of the crystal. Alternatively the impurity can be incorporated interstitially, where the impurity is located in the spaces between ions. Adhesions refer to substances that are adsorbed onto the surface of the crystal. They are seldom discussed as impurities but are sometimes mentioned in papers discussing their ability to alter the growth pattern of the crystal.

3.4.1 Isomorphous inclusions

Isomorphous impurities are mixed crystals or solid solutions that have undergone isomorphous substitution. Isomorphous substitution is characterised by the random replacement of an ion within the macro-component by an 'impurity' ion, or micro-component. These types of inclusions are influenced by a number of factors including chemical composition, solubility, interactions between particles and solvent, symmetry and parameters of the crystal lattice (Kirkova et al., 1996; Zhang et al., 1999). How these factors influence isomorphous substitution has not been conclusively determined from a sound theoretical perspective. However, findings indicate that most impurities found in crystalline products are as a result of these solid solutions as opposed to liquid inclusions (Zhang et al., 1999). This should not be interpreted as a blanket statement that applies to all systems however, but what must be noted is that in systems as complex and varied as industrial brines there is a significant probability that solid solutions could occur.

It is generally understood that crystallization is an effective purification process because of the tendency for growing crystals to reject foreign particles. This is related to the large energetic penalties incurred when the structure of the crystal lattice is disrupted (Myerson, 2002). That is to say, it is thermodynamically favourable for a growing crystal to reject particles that do not form part of the natural crystal structure, especially during fast crystal growth. However, during fast crystal growth, which is a molecular recognition process, it is possible for foreign substances to be integrated into the crystal lattice. The frequency of this occurrence can be considered to be related to both the degree of energetic disturbance that a foreign body in the lattice might cause and the concentration of the foreign body in the mother liquor. If a substance crystallizes from a solution containing a high concentration of a substance similar to one of the crystallizing substances, there is likely to be a significant extent of isomorphous substitution. These similarities refer to issues pertaining to molecular volume, ionic radii and steric interactions (Myerson, 2002). In a system as varied as industrial brine there is great potential for some of the dissolved substances to be similar enough to the crystallizing substances such that molecular recognition fails and foreign particles are incorporated.

i. Structural dependence of isomorphous inclusion

The more similar two crystalline structures are, the more likely they are to be interchangeable with one another. What is observed, however, is that the structure of the microcomponent adapts to suit that of the macro component (Kirkov et al., 1996). For example; $MgSO_4 \cdot 7H_2O$, $NiSO_4 \cdot 7H_2O$ and $ZnSO_4 \cdot 7H_2O$ have a rhombic structure, whereas $FeSO_4 \cdot 7H_2O$, $CoSO_4 \cdot 7H_2O$, $MnSO_4 \cdot 5H_2O$ have a monoclinic structure. Despite this however, these substances can form solid solutions by mutual substitution (Kirkova et al., 1996). Thus, it would seem that other factors are more important in determining isomorphous substitution than crystalline structure.

ii. Temperature dependence of isomorphous inclusion

When considering an impurity, the relative temperature dependence of the solubility of the impurity in the host and the solvent is a factor. The solubility of an impurity in the crystal, relative to its solubility in the mother liquor, may change with temperature. To achieve effective purification it is desirable that the impurity is freely soluble in the solvent at the operating temperature and insoluble in the host (Myerson, 2002).

iii. Effects of mass transfer on isomorphous inclusion

The amount of isomorphous impurity found in the product crystal is, amongst other things, dependent on the concentration of the impurity in the mother liquor relative to the concentration of the host in the mother liquor. Since crystallizing ions are assimilated and foreign substances are rejected at the face of the growing crystal, a situation arises in which the concentrations of the impurities are raised locally around the crystals (see Figure 11). This increases the likelihood of impurities being incorporated into the crystal. However, this occurrence is dependent on the width of the boundary layer around the crystals. In the case of a crystal left to grow in a non-agitated system the accumulation of impurities at the growing surface may be quite significant, resulting in measurable incorporation of impurities. In a vigorously agitated system, the effects of mass transfer limitations are less likely as the impurities never accumulate at the growth surface. A further result of this accumulation is that there is a heterogeneous distribution of impurities in the crystal. Thus, the concentration of impurities at the crystal surface increases and the concentration of impurities surrounding the crystal is constantly changing (Kirkova et al., 1996). If the impurity is being concentrated in the bulk, the concentration of the impurity within the crystal will increase radially from the centre out.

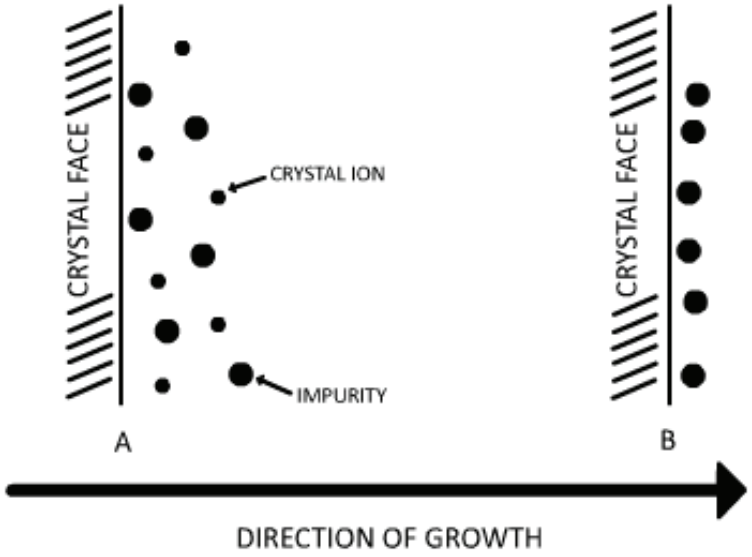

Figure 11: Accumulation of impurities crystal growth face (adapted from Myerson (2002))

iv. Impact of growth rate on isomorphous inclusions

During crystal growth, growth units are subject to various orienting forces before being completely incorporated into the lattice (Myerson, 2002). Inorganic, ionic crystals grow under the direction of strong aligning forces and organic crystals usually grow under weaker ones. Stronger forces allow the growth unit to be more quickly oriented such that it can be properly positioned into the lattice. During rapid growth however, these units can be incorporated before they are properly oriented, resulting in irregularities and dislocations in the crystal. These conditions can provide additional sites that promote the uptake of impurities. This is in keeping with the convention that slower growth results in purer crystals and faster growth more impure ones.

3.5 The Colour Schlieren Technique

The Colour Schlieren technique is a non-intrusive optical technique that measures changes in the refractive index of the solution. The changes in refractive index can be related to variations in density as a result of different concentrations and temperatures.

It is generally recognized that optical techniques are powerful tools to investigate heat and mass transfer in transparent fluids (Ambrosini, 2008). Since they are non-intrusive (Shlichta, 2008) they enable the analysis of test regions to be performed in the absence of instrument probes which could influence and disturb the process under research. Alvarez-Herrera and co-workers (2009) developed a procedure for full-field measurement of fluid flow temperature by using the Schlieren technique. Cork and co-workers (1991) reported local concentration of electrolyte in electro chemical deposition using Schlieren method while Bredikhin and co-workers (2000) used a technique based on optical Schlieren for an in situ investigation of growing crystal morphology under rapid growth conditions.

Image formation in a Schlieren system is due to the deflection of the light beam in a variable n-field towards a region of higher refractive index (Srivastava, 2004). The colour Schlieren images are representative of the changes in refractive index of the medium along the passage of light. These images carry information related to the first derivative of the refractive index of a transparent material which is related to its density and, in turn to temperature and concentration. Colour changes represent either the magnitude or the direction of an encountered density gradient. Quantitative information about the strength of a density gradient can be obtained from an adequately designed magnitude-indicating colour Schlieren system (Kleinea, 2006).

In order to recover quantitative information from a Schlieren image, one has to determine the deflected angle as a function of position in x-y plane that is normal to the beam.

Magnitude of deflection is given by:

$$d = f_c \tan\theta_{exit} \approx f_c \, \theta_{exit} \quad \textbf{(7)}$$

d is the magnitude of deflection at the plane of the filter and f_c is the focal length of decollimating lens. The approximation in this equation is roughly 1 part in 10^5 for most optical systems that are typically encountered (Greenberg, 1995). Therefore, the change in displacement from the centre of the filter is given by:

$$\Delta d = f_c \, \theta_r \quad \textbf{(8)}$$

Rearranging equation (2) and making the angle of refraction, θ_r, the subject of the formula becomes:

$$\theta_r = \frac{\Delta d}{f_c} \quad \textbf{(9)}$$

Using the principles of ray optics, the angle of refraction can be related to the refractive index n by

$$\theta_r = \int_0^L \frac{\partial n}{\partial r} \partial z \quad \textbf{(10)}$$

Where L is the thickness of the test region and Z is the axis in which light is travelling. Assuming a two dimensional field with $\frac{\partial n}{\partial r}$ constant at a given x**,** y position over the length L in the z direction,

$$\theta_r = \frac{\partial n}{\partial r} L \quad \textbf{(11)}$$

The measuring range (ε_{range}) of the colour Schlieren is the maximum deflection angle at which linear range of colour indicator(hue) is achieved (Gupta, 2010). The measuring range depends on the dimensions of the filter b_f, size of pinhole b_s through which the light passes and the focal length of the decollimating lens f_2

$$\varepsilon_{range} = \frac{b_f - b_s}{f_2} \quad \textbf{(12)}$$

4 EXPERIMENTAL STUDIES

4.1 OBJECTIVE 1: Establish the thermodynamic and kinetic factors governing the operation of a sequential EFC process

Since the brine analysis was crucial to both the thermodynamic and kinetic aspects of the Sequential EFC process, the first objective of this project was split into three key areas namely, *brine analysis*, *thermodynamic modelling* and the *kinetic aspects*.

4.1.1 Brine Analysis

The analysis of a brine is a step whose complexity is often overlooked. The majority of hypersaline brines contain multiple, interacting ionic species. Therefore it is important to be able to identify them all at an early stage of the Sequential EFC treatment process. A combination of standard water analysis techniques and wet chemistry can be used to characterize the brine. The brine samples used in this study were obtained from a reverse osmosis (RO) plant that was built to recover potable water from the waste water generated during coal mining.

i. Methodology for brine analysis

Two brine samples (**Brine 1** and **Brine 2**) from the RO plant were taken three months apart. A third brine (**Brine 2'**) was obtained by concentrating **Brine 2**. Conductivity and pH measurements were conducted on site to ensure accurate measurements. The pH, for example, can change within 24 hours of sampling (Pulles, 1993). The density was experimentally measured upon arrival of the brine samples at the laboratory. The samples were diluted with de-ionised water to prevent the crystallization of salts during the storage and transportation.

The following techniques were used to measure the ions present in the solution:

- Total Kjeldahl Nitrogen (TKN) to measure total organic nitrogen, especially ammonia,
- The Spectroquant® NOVA 60 A photometer to measure the nitrate (NO_3^-) concentration,
- Gran titration was used to measure the carbonate concentration,
- Inductively Coupled Plasma Mass Spectroscopy (ICP-MS) was used to measure the other cations and anions.

Figure 12 gives a summary of the methodology for the brine analysis.

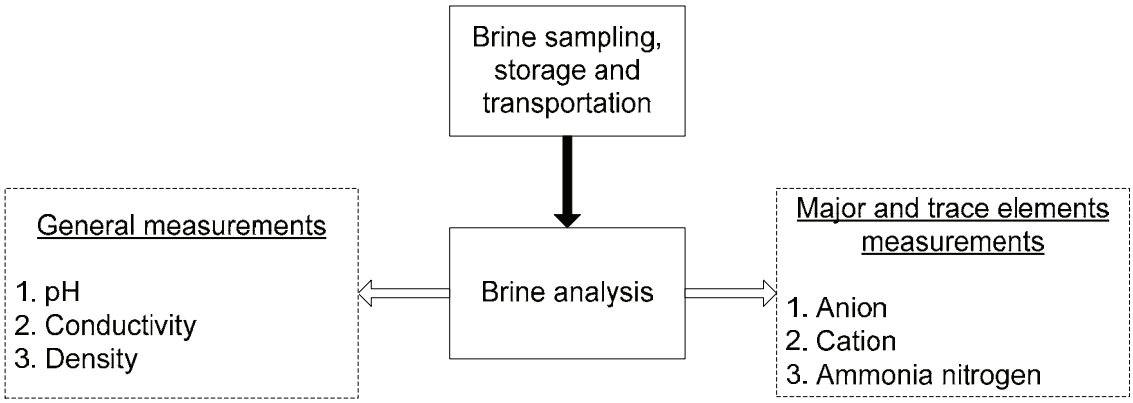

Figure 12: Brine analysis procedure (Zibi, 2010)

4.1.2 Thermodynamic modelling

Once the analysis of the brines has been attained, thermodynamic modelling can be used to predict the identities of the potential salts, the temperatures at which they will crystallize, as well as the potential yields of the various products.

i. Methodology for thermodynamic modelling

Figure 13 shows a summary of the thermodynamic modelling procedure using OLI Stream Analyser (2010). The blocks in bold are the particular names of the steps used by OLI during the modelling process. The **Water Analysis** option performs a charge balance that is then used to model the aqueous chemistry in the **Stream** option. The Mixed Solvent Electrolyte (MSE) model as well as the special $MgSO_4$ databank was used during the modelling process. The MSE model was used because it predicts electrolyte behaviour for a wide concentration range; from infinite dilution to molten salts. The addition of the $MgSO_4$ databank provided a more complete component list.

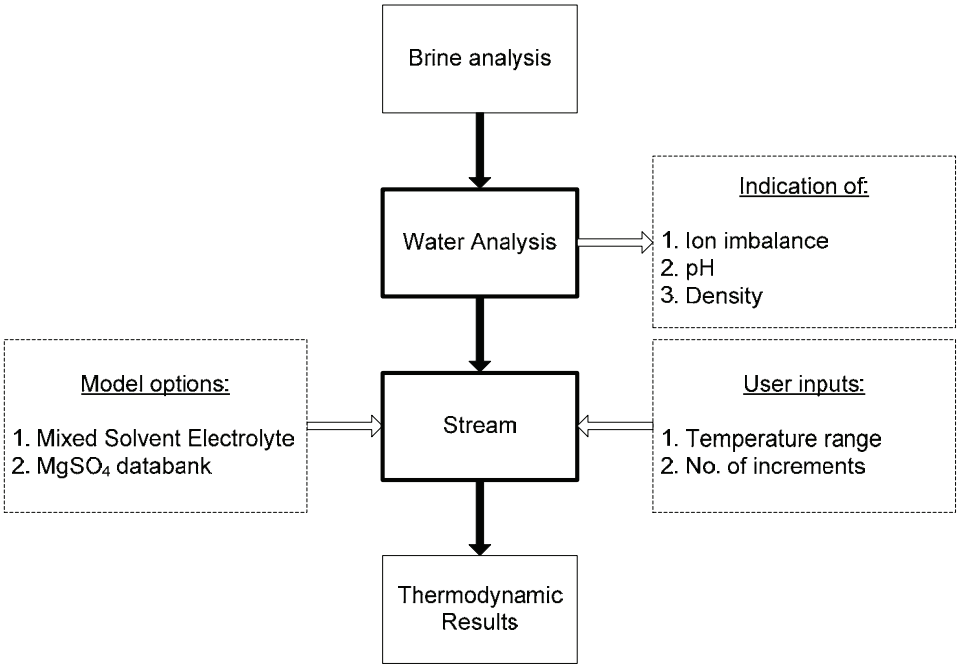

Figure 13: Thermodynamic modelling procedure

4.1.3 Kinetic aspects

i. Methodology for kinetic aspects

This section is the final step of the Sequential EFC process. It presents the experimental studies that investigated the sequential removal of calcium sulphate and sodium sulphate along with ice from brine samples obtained from a RO process.

The experimental aims for the sequential removal of salts presented in this section are given in Table 2.

Table 2: The aims of the experimental procedure for the sequential removal of salts during EFC

Part	Aim(s)	Experiment Name	Concentration		
A	• To demonstrate "proof of concept" of sequential EFC by reducing the volume of brine while at the same time producing potable water and pure salt(s), • To identify the salts that form, • To determine the purity of ice and salt(s) formed, • To carry out a mass balance for the EFC process.	A1, A2, A3…A17	Brine 1		
B	To produce different brine samples of varying concentrations for subsequent tests (Part H).	B1, B2, B3…B26	Brine 2		
C	To determine the mass deposition of calcium at 0°C and 22°C and for different brine concentrations.	C1	Brine 2	22	Temperature (°C)
		C2	Stage 1B (filtrate of C1)		
		C3	Stage 2B (filtrate of C2)		
		C4	Stage 3B (filtrate of C3)		
		C5	Brine 2	0	
		C6	Stage 1B (filtrate of C5)		
		C7	Stage 2B (filtrate of C6)		
		C8	Stage 3B (filtrate of C8)		
		C9	Brine 2 (24 hour period)		
D	To determine the operating conditions for the removal of calcium sulphate and ice under eutectic conditions.	D1	Brine 2		

Brine samples obtained from the RO plant were used in most of the experiments described in this section (the other experiments used synthetic streams). The same methodology was used for both brines and synthetic streams, unless otherwise stated.

ii. Solution preparation for objective 1

The brine samples were kept at 10°C and filtered using a Buchner funnel with filter paper of a 0.45µm pore size before use. The filtrates from experiments for **Brine 1** were kept at ~22°C while the filtrates from experiments for **Brine 2** were kept in a fridge at 3°C. The filtrates from Brine 2 were kept at 3°C to prevent salt from crystallizing out of solution. The brine samples for Part C were obtained by concentrating **Brine 2.** The filtrates from each stage of the concentrating procedure were used for the experiments. The **Stage B1** brine was obtained by removing 36.7% ice from **Brine 2**. The **Stage B2** brine was obtained by removing 52% ice from the feed to this stage (filtrate from **Stage B1**). Similarly, the **Stage B3** brine was obtained by removing 23.6% ice from the feed to this stage.

iii. Experimental setup for objective 1

The industrial brines (Parts A and Part B) experiments were performed in a 1.5L jacketed glass reactor. A Testo 175-177 temperature logging device was used to measure the solution temperature of the reactor. An IKA stirrer with variable speed control was used to provide adequate mixing with a 4-bladed rushton turbine impeller. The required level of cooling was achieved with a Lauda RE207 thermostatic unit that continuously circulated the coolant, Kryo40, through the jacket of the reactor. The setup, excluding the thermostatic unit, was kept in a freeze room at different operating conditions depending on the stage of the cascading concentration procedure (Figure 14 and Figure 15).

Filtration of the final products was conducted in the cold room maintained at the same set-point temperature as the thermostatic unit. A Buchner funnel connected to a 1L filtration flask was used to filter the ice product. A 300ml Millipore All-Glass filter holder connected to a vacuum pump was used to filter the salt for those experiments that produced salt. The pore size of the filter paper was 0.45µm.

For calcium mass deposition experiments (Part C), 200ml samples of varying concentrations were placed in a 250ml conical flask and sealed with Parafilm M laboratory film. A set of four solutions (C1 to C4) were agitated using a magnetic stirrer at a temperature of 22°C. The other four experiments (C5 to C8) were magnetically stirred whilst being kept at a constant temperature of 0°C in a freeze room. A seed mass of ~1.0 g $CaSO_4 \cdot 2H_2O$ was added to each conical flask.

iv. Experimental procedure for objective 1

The experiments for Part A and Part B were initiated by adding approximately 1250 g (except for experiment B1 which used a 3L crystallizer with a brine feed of 2585 g) of the brine that had been previously maintained at 10°C to the crystallizer. The thermostatic unit and set point of the freeze room were set to the same temperature and simultaneously adjusted depending on the stage of the cascading concentration procedure. These values were typically 1°C below the expected crystallizing temperature of the ice. For example, in the initial stream of **Brine 1**, ice crystallized at -0.5°C thus the thermostatic unit and freeze room were set at -1.5°C. The data logging of temperature and conductivity measurements were initiated upon addition of the solution to the crystallizer.

The contents of the reactor were then removed and placed in a 3L beaker and kept in the freeze room. The ice and salt were left to stand in the beaker and allowed to separate for ±10minutes following which the ice and its entrained brine were carefully separated from the salt and its entrained brine into separate beakers. The ice was then filtered under vacuum using a Buchner Funnel. The saturated salt solution was filtered with the 300ml Millipore setup.

Liquid samples of the feed, ice and the filtrate were analysed using ICP-MS to determine the concentration of the various cations and anions present. For experiments in which salt formed, the salt was dissolved in de-ionised water and the solution analysed using ICP-MS.

Figure 14 and Figure 15 show the cascading concentration procedures, as described by Baker (1967), which were employed during the experiments for Part A and Part B. The blocks show the experiment number as well as the identity of solid contents obtained from each experiment. This approach was adopted because a working volume of the same concentration as that obtained from the cascading concentration procedure could not be achieved with a single 1.5L crystallizer. In addition, it was found that a solid content of more than 30% ice during the co-crystallization with salt made the separation of ice and salt extremely difficult as the entire crystallizer was filled with ice from top to bottom. Thus, to avoid this, the concentrating procedure was spread over a number of experiments.

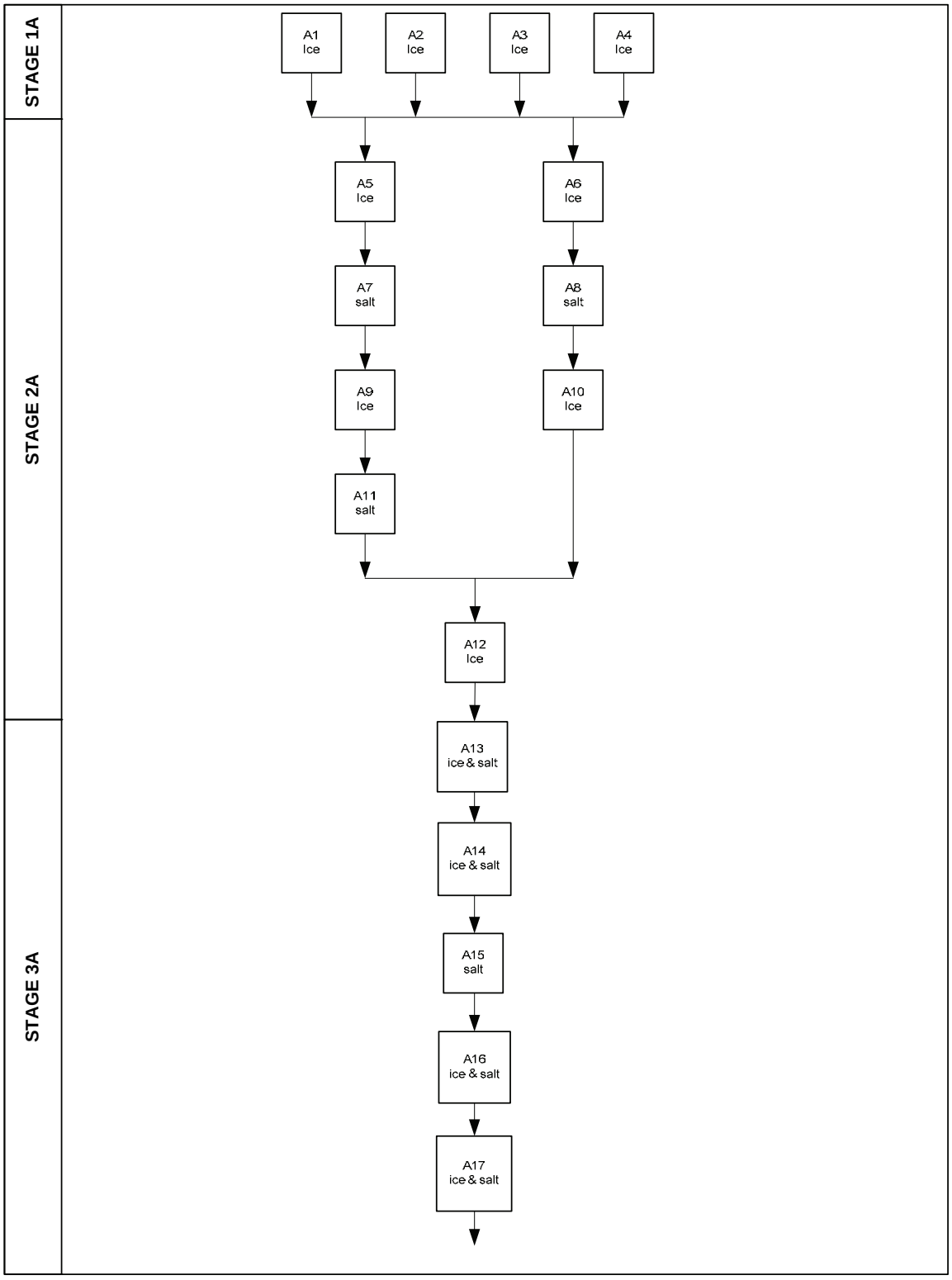

Figure 14: Cascading concentration procedure for Brine 1 (Randall et al., 2011)

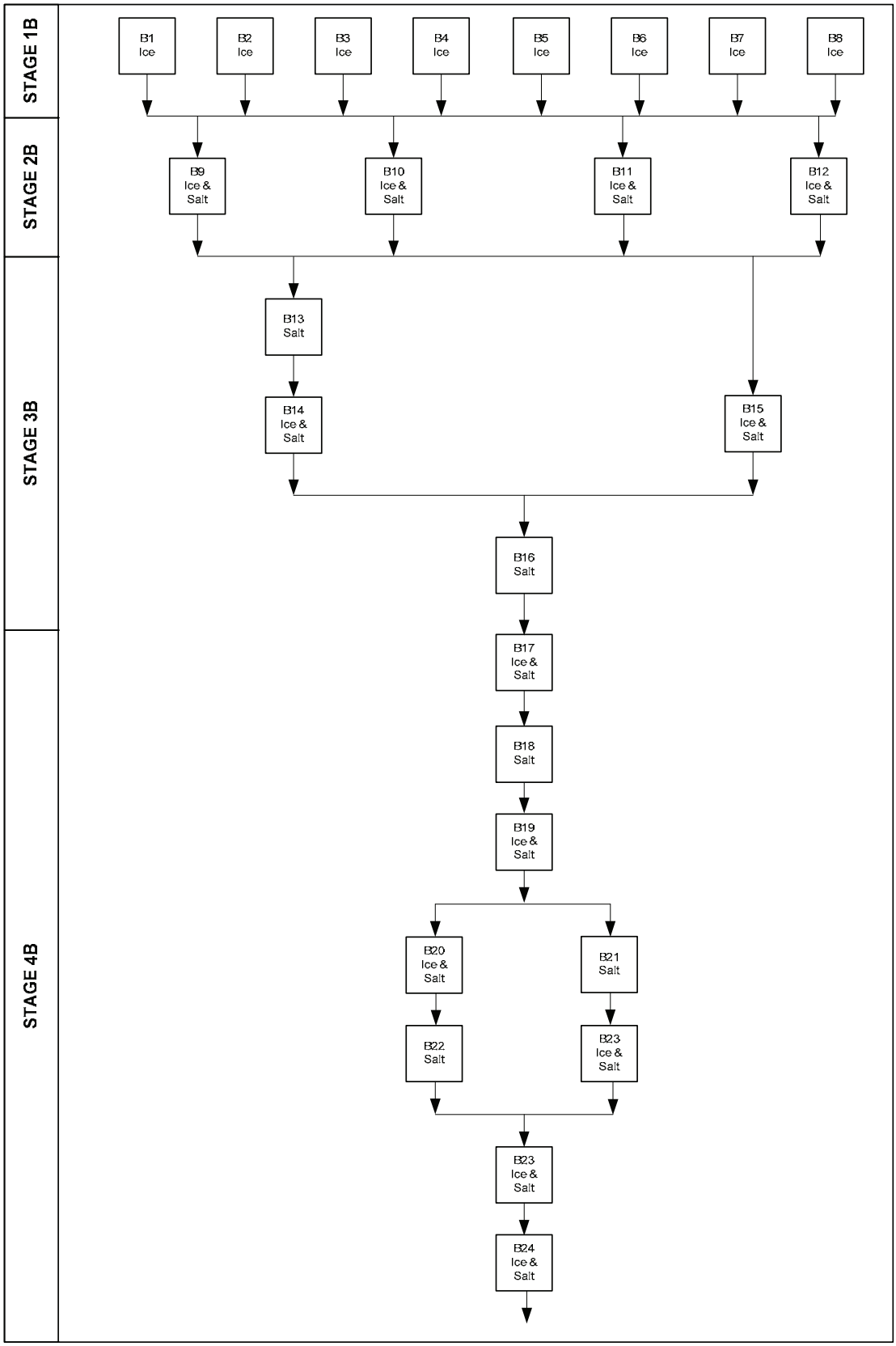

Figure 15: Cascading concentration procedure for Brine 2 (Randall et al., 2011)

4.2 OBJECTIVE 2: Establish how the treatment of real brines differs from that of synthetic brines

This objective investigated the validity of using a synthetic brine to represent a real brine. The synthetic brine makeup was based on the composition of the original brine. Salts corresponding to the equivalent molar concentrations of the respective ions were used to make the synthetic brine. The nucleation temperature at which ice and salt (eutectic conditions) formed was used to compare the accuracy of the synthetic brine.

4.2.1 Solution preparation

The synthetic brine was prepared from 99% pure chemicals (Merck) (see Table 3). The $CaSO_4 \cdot 2H_2O$ mass in Table 3 is based on a supersaturated concentration and therefore this amount of calcium sulphate cannot fully dissolve. Therefore, the actual amount of calcium sulphate used to make up the synthetic was 1.9305 g/L (saturated) and not 2.9214 g/L (supersaturated).

Table 3: Synthetic brine composition

Component	Mass g/L
Na_2SO_4	38.7626
$MgSO_4$	1.7196
$CaSO_4 \cdot 2H_2O$	2.9214
K_2SO_4	6.7381
$NaHCO_3$	1.0119
NaCl	4.3862
$(NH_4)_2SO_4$	1.2132

4.2.2 Experimental setup

The experiments were performed in a 1.5 L jacketed glass crystallizer. A Testo 175-177 temperature-logging device was used to measure the solution temperature in the crystallizer. An IKA stirrer with variable speed control was used to provide adequate mixing with a 4-bladed rushton turbine impeller. The required level of cooling was achieved with a Lauda RE207 thermostatic unit that continuously circulated the coolant, Kryo40, through the jacket of the reactor. The setup, excluding the thermostatic unit, was kept in a freeze room kept at -2°C.

4.2.3 Experimental procedure

The experiment was initiated by adding approximately 1250 g of the synthetic brine to the crystallizer. The thermostatic unit and setpoint of the freeze room were set to the same temperature (-2°C). The data logging of temperature measurements was initiated upon addition of the solution to the crystallizer. The solution was cooled until -1.4°C, at which stage ~1 g $Na_2SO_4 \cdot 10H_2O$ seed crystals were added to the solution. The experiment run was approximately 4 hours. Liquid samples were taken at the start of the experiment, after 30minutes and after 1, 2, 3 and 4 hours. These liquid samples were analysed for the Na^+ ion concentration using AAS.

4.3 OBJECTIVE 3: Investigate the effect of impurities and contaminants on the salt product formed by an EFC process.

This objective investigated the nature of the impurities in the salt product formed during an EFC process. Two aspects relating specifically to selenium in a sodium sulphate salt are investigated. The

first aspect focuses on establishing the form of the selenium impurity, which is most likely to be in the oxidised form (selenite (4^+ oxidation state) and selenate (6^+ oxidation state)). The second aspect focuses on the relationship between NaCl, Na_2SO_4, Na_2SeO_4 and selenium inclusions in the salt product.

4.3.1 Nature of the selenium impurity in the salt

i. Solution preparation for investigating the nature of the selenium impurity

A standard solution containing 90 g/l NaCl and 110 g/l Na_2SO_4 was made. To maximise repeatability, a sufficiently large batch was made up to supply all the individual beaker tests. Separate solutions containing 150 g/l Na_2SeO_4 and 150 g/l Na_2SeO_3 were also made in sufficiently large quantities. All solutions were made with 18 MΩ.cm water.

ii. Experimental setup for investigating the nature of the selenium impurity

The experiment consisted of 30 separate beaker tests in which a standardised solution containing sodium sulphate and sodium chloride was doped with varying amounts of sodium selenate and sodium selenite. Five different selenate and selenite concentrations were investigated, each repeated three times. The concentrations of sodium chloride and sodium sulphate in the synthetic test brine were the same as those in the original industrial brine, 90 g/l and 108 g/l respectively. The selenite and selenite concentrations can be found in Table 4.

The beakers were placed on magnetic stirrers in a large freezer room, set at -4°C. For reasons of space and practicality, six samples were investigated at a time. Filtration of the product salt occurred inside the freezer room (similar setup as mentioned in section 4.3.1).

Table 4: Concentrations of sodium selenite or sodium selenate in beaker tests

Batch	Concentration (g/l)
1	1.00
2	1.30
3	1.60
4	1.90
5	2.20

iii. Experimental procedure for investigating the nature of the selenium impurity

The separate beakers were cooled to -4°C in order to crystallise the sodium sulphate. The crystals were then filtered and dried in an oven and analysed using ICP-OES for sulphur and selenium. Figure 16 shows a graphical representation of the experimental setup.

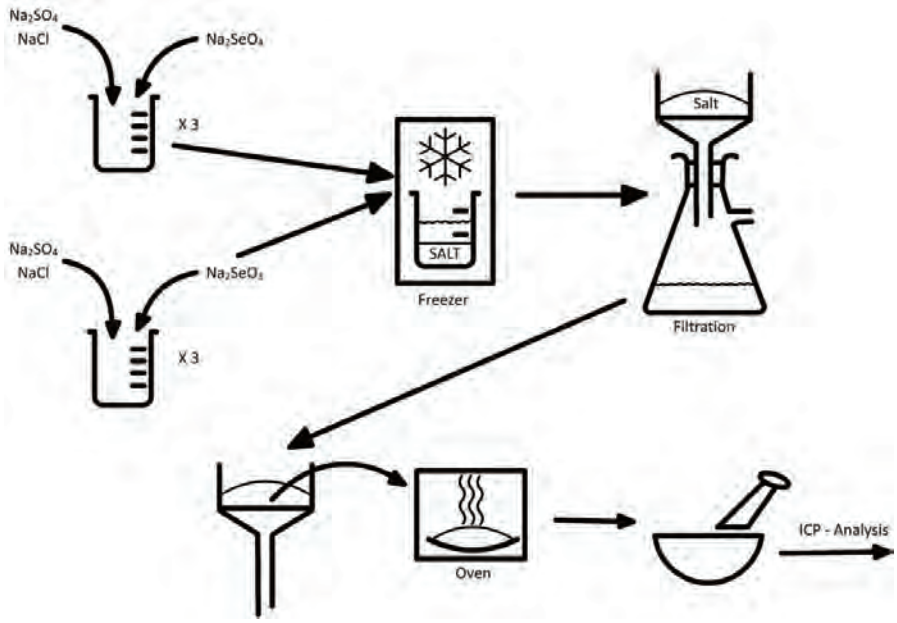

Figure 16: Experimental procedure for determining nature of selenium impurity

4.3.2 Relationship between NaCl, Na_2SO_4, Na_2SeO_4 and selenium inclusions in the salt product

The purpose of this experiment was to determine the impact sodium chloride has on the nature of the selenium impurity in the sodium sulphate product. The experiment offers a better understanding about what contributes to impurities in real brines.

i. Solution preparation for investigating inclusion relationship

Standard solutions of NaCl, Na_2SO_4 and Na_2SeO_4 were made using purified water of 18 MΩ.cm. The concentrations of the solution can be found in Table 5. The concentrations of the standard solutions were initially high so that the necessary concentrations could be achieved in the brine once all the solutions were combined. The drawback of high concentrations is that any measurement errors in the following stages of the experiment are amplified. This must be considered during the experimental procedure and extra care must be taken. For example, issues like drips from pipettes can have an appreciable impact on the concentrations. As such, any spills or extra drops cannot be overlooked.

The values in the 'g/l' column of Table 5 are the final concentrations of the salts in each synthetic brine sample. The values in the 'ml standard added to 200 ml sample' represent the volumes of standard solution added to each beaker to achieve the concentrations required in the 'g/l' column. The concentrations were chosen to approximate the range one would find in similar brines to the industrial brine, yet still offer enough latitude in the data points to establish trends. The standard solutions were:

- NaCl – 300 g/l
- Na_2SO_4 – 170 g/l
- Na_2SeO_4 – 150 g/l

Table 5: NaCl, Na_2SO_4 and Na_2SeO_4 experimental concentrations

Sample	g/l			ml standard added to 200 ml sample		
	Na_2SeO_4	Na_2SO_4	NaCl	Na_2SeO_4	Na_2SO_4	NaCl
1	1.20	108.00	10.00	1.59	127	7
2	2.39	108.00	10.00	3.19	127	7
3	3.59	108.00	10.00	4.78	127	7
4	4.78	108.00	10.00	6.38	127	7
5	5.98	108.00	10.00	7.97	127	7
6	7.18	108.00	10.00	9.57	127	7
7	1.20	108.00	50.00	1.59	127	33
8	2.39	108.00	50.00	3.19	127	33
9	3.59	108.00	50.00	4.78	127	33
10	4.78	108.00	50.00	6.38	127	33
11	5.98	108.00	50.00	7.97	127	33
12	7.18	108.00	50.00	9.57	127	33
13	1.20	108.00	90.00	1.59	127	60
14	2.39	108.00	90.00	3.19	127	60
15	3.59	108.00	90.00	4.78	127	60
16	4.78	108.00	90.00	6.38	127	60
17	5.98	108.00	90.00	7.97	127	60
18	7.18	108.00	90.00	9.57	127	60
19	1.20	30.00	90.00	1.59	35	60
20	2.39	30.00	90.00	3.19	35	60
21	3.59	30.00	90.00	4.78	35	60
22	4.78	30.00	90.00	6.38	35	60
23	5.98	30.00	90.00	7.97	35	60
24	7.18	30.00	90.00	9.57	35	60
25	1.20	50.00	90.00	1.59	59	60
26	2.39	50.00	90.00	3.19	59	60
27	3.59	50.00	90.00	4.78	59	60
28	4.78	50.00	90.00	6.38	59	60
29	5.98	50.00	90.00	7.97	59	60
30	7.18	50.00	90.00	9.57	59	60
31	1.20	80.00	90.00	1.59	94	60
32	2.39	80.00	90.00	3.19	94	60
33	3.59	80.00	90.00	4.78	94	60
34	4.78	80.00	90.00	6.38	94	60
35	5.98	80.00	90.00	7.97	94	60
36	7.18	80.00	90.00	9.57	94	60

ii. Experimental setup for investigating inclusion relationship

The setup for this experiment consisted of six beakers and six magnetic stirrers placed in the freezer room at -3.5°C. When placed in the freezer, all the samples cooled at the same rate, and as such the crystal growth rate was assumed to be the same for all samples. Filtration was carried out in the freezer room.

iii. Experimental procedure for investigating inclusion relationship

The 200 ml beakers were placed in freezer at -3.5°C stirred by magnetic stirrers and sodium sulphate decahydrate was allowed to crystallise. The samples were left in the freezer until no further crystallization occurred. The crystals of each sample were filtered thoroughly, but not washed. This was to prevent error from sample to sample resulting from inconsistent washing. The filtered crystals were

placed in an oven and dried at 35°C. At this temperature the sodium sulphate decahydrate melted. The water in the melt was driven off and the salt recrystallized in the anhydrous form. The anhydrous salt was ground in a pestle and mortar and sent to an external laboratory for analysis by ICP-OES. Figure 17 shows a graphical representation of the experimental setup.

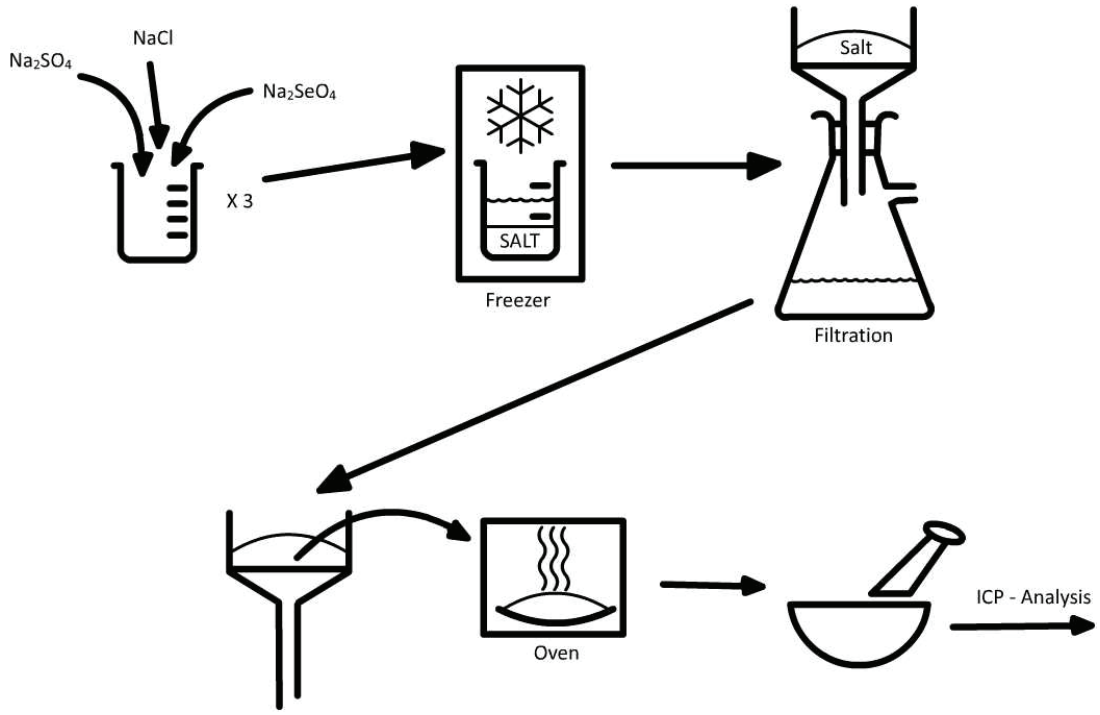

Figure 17: Experimental procedure for the investigation of the relationship between Na_2SO_4, NaCl and Na_2SeO_4

4.4 OBJECTIVE 4: Investigate the effect of impurities and contaminants on the ice product formed by an EFC process

This objective aimed to investigate the mechanisms affecting the purity of ice formed in an EFC process. The four possible mechanisms are:

1. Entrapment of the salt crystals within the bulk ice: it is expected that the trapped salt can be removed from the bulk ice by implementing agitation in a vessel with a large settling surface area,
2. Mother liquor (brine) inclusions in the ice crystal due to the growth morphology of the ice,
3. Entrainment of brine: this is external to the crystal itself and can be eliminated by washing the bulk ice produce,
4. Isomorphous substitution: this occurs when impurity molecules substitute into the crystal lattice itself. Because ice molecules (H_2O) are some of the smallest molecules in the periodic table, it is highly unlikely that impurity molecules will be able to substitute into the ice crystal lattice without causing enormous strain. For example, the atomic radius of the sodium ion is 180 pm, compared to the atomic radius of hydrogen (25 pm) and oxygen (60 pm).

For mechanism (1), salt entrapment, the removal of the trapped salt crystals within the bulk ice region depends on efficient ice-salt separation. On the other hand, for mechanism (2), these can be better understood by investigation the fundamentals of ice crystallization. The entrainment of brine (mechanism 3) can be overcome by washing the bulk ice with cooled water while isomporphous substitution (mechanism 4) will not be investigated in this study as it is unlikely to occur. This objective

therefore focuses on three key areas namely, *factors affecting ice-salt separation* and *fundamental studies of ice crystallization* and *ice washing*.

4.4.1 Factors affecting ice-salt separation

The factors that affect ice-salt separation are degree of agitation of the bulk ice solution and settling surface area. These experiments aim to investigate these factors.

i. Solution preparation

A 5wt% binary solution of Na_2SO_4-H_2O was used as the test case. Weighed quantities of analytical grade (> 99wt%) Na_2SO_4 was dissolved in 1 kg of ultra pure water using a magnetic stirrer for 20 minutes to obtain a homogeneous solution.

ii. Experimental setup

Batch test studies were carried out in a 1.5 L jacketed, glass crystallizer. Agitation was achieved using an IKA RW 20 digital overhead stirrer connected to a 4-bladed impeller. The agitation rate was changed depending on the experiment being conducted. Cooling was achieved using a Lauda Proline RP845 cooling unit, which circulated the coolant, Kryo 45, through the walls of the crystallizer. A Testo 175-177 temperature-logging device was used to measure the solution temperature of the crystallizer.

For the agitation experiments, a paddle impeller was used to agitate the bulk ice at 50 rpm.

For the surface area experiments, three additional settling vessels of varying sizes (183 cm^2, 236 cm^2 and 650 cm^2) were used.

iii. Experimental procedure for testing the effect of agitation on ice-salt separation

The synthetic Na_2SO_4 solution was transferred to the crystallizer and maintained at a temperature of 20˚C for 30 min. Thereafter the solution was cooled isothermally to -2˚C. Once the solution reached -0.4˚C, 1 g salt ($Na_2SO_4 \cdot 10H_2O$) was added followed by 1 g ice seeds at -1˚C. The crystals were allowed to grow for 2 hours minutes after salt nucleation. A gentle agitation rate, 50 rpm, was used to agitate the bulk ice for 10 minutes with the paddle impeller situated in the ice region only. The vessel was placed in a temperature-controlled environment at -1.2˚C. The solution contents were thereafter filtered and the mass of ice, salt and remaining mother liquor was recorded. The ice was allowed to melt and samples were sent for analysis.

iv. Experimental procedure for testing the effect of settling surface area on ice-salt separation

The synthetic solution was transferred to a 1L crystallizer where the solution was cooled isothermally to -2˚C. Salt seed crystals of 1 g were added to the solution at -0.4˚C followed by the addition of 1 g ice seed crystals at -1.0˚C. The experiment was run for 2 hours and the timing was started with the addition of the Na_2SO_4 to the crystallizer. After the 2 hours, the contents of the crystallizer were transferred to another vessel (183 cm^2, 236 cm^2 and 650 cm^2 vessel) containing a 4.2wt% binary solution of Na_2SO_4 that had been chilled to just below 0˚C. The vessel was placed in a -1.2˚C environment where the ice and salt crystals were then allowed to separate out for 10 minutes, after which the ice crystals and salt crystals were filtered out separately. The crystals were filtered out in approximately 3 minutes, with the

3 minutes starting once all the contents of the crystallizer had been placed into the Buchner funnel. The ice crystals were then melted and samples sent for analysis in order to determine the purity.

v. Analytical techniques

Atomic Absorption Spectroscopy (AAS) was used to analyse the concentration of Na^+ ions in the aqueous phase. The purity of the ice crystals could be determined from the concentration of Na^+ ions present in the melted ice.

4.4.2 Fundamental studies of ice crystallization

Because ice crystallization is a special case of cooling crystallization, that is cooling crystallization from the melt, the factors governing ice crystallization are more complex than those governing the salt crystallization process. Firstly, the crystallizing component (ice) is the solvent (water) and secondly, the operating temperature is close to the melting temperature of the main component. This means that the crystal growth processes for ice are different to those of salts, and thus the possible mechanisms for impurity incorporation into the ice crystals are different. Therefore, these experiments focus on a non-intrusive method to investigate the interaction of the growing ice crystal with its environment. The non-intrusive method has the advantage of generating in-situ data without the need for sampling and without the need to disturb the system.

i. Solution preparation

Binary salt solutions were prepared by dissolving measured amount of $MgSO_4$ salts into de-ionised water. When the experiments started running, the room was darkened by switching off the lights to improve the quality of images captured.

ii. Apparatus and instrumentation

The experimental setup used in this work is similar to the one used by Gupta and co-workers (2010). This technique is used because of sensitivity (Shlichta, 2008) and of clarity of images (Srivastava, 2004). A halogen cold white light source (REVOX SLG-50S 250 watts) was connected to a 400μm pinhole with fibre optical cable for obtaining a point light source. The pinhole was placed 115.5 mm from the first lens of 99 mm diameter that collimates the light onto the test cell. The test cell was placed 125.5mm away from the collimating and located at the focus of the decollimating lens of 278.5 mm focal length and 149.5 diameter. A colour filter of 5mm in radius was placed in front of the decollimating lens at its focal point. The images will be captured using CMOS (640 by 480 pixels) camera connected to a computer. In order to obtain and enhance clear images, a diaphragm placed between the filter and the CMOS camera. An adjustable objective lens was also added to the CMOS camera for better resolution and focusing of images. The CMOS camera was connected to a PC with Point Grey software where video images were displayed and recorded. A schematic diagram of the experimental set up is presented in Figure 18.

Parallelism and straightness of the optical lenses are crucial for generation of meaningful images hence considerable precaution was taken in this regard by placing all optical equipment on a straight rail

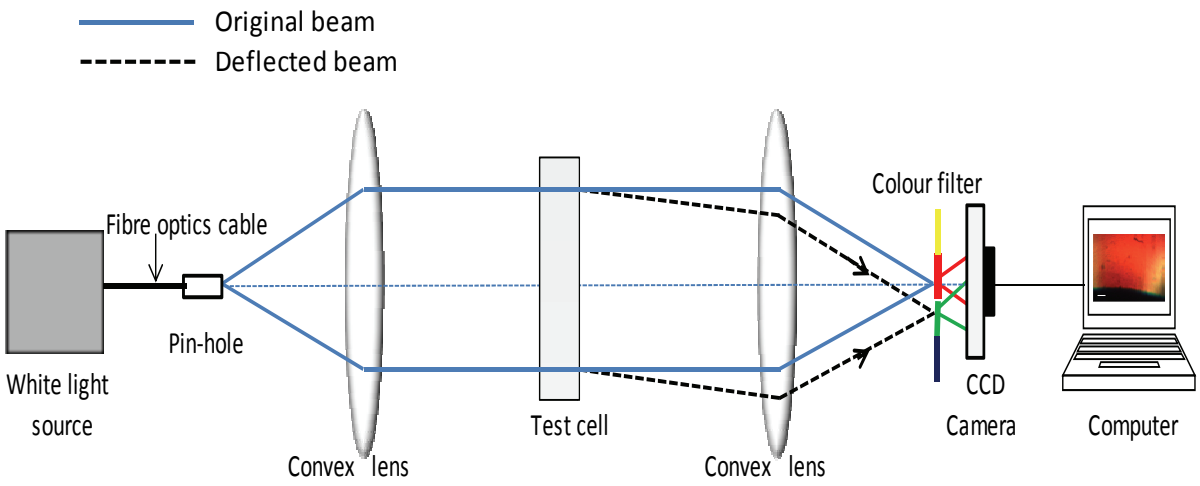

Figure 18: Colour Schlieren deflectometry setup

Figure 19 shows a test cell made of Plexiglas. It is used as a crystallizer and consists of two compartments separated by a 1 mm thick stainless steel, which acts as a heat exchanger. Cooling was achieved by pumping the coolant (Kryo 40) into the cooling chamber through the coolant inlet tube. The coolant was pumped back to the cooling unit through coolant outlet. In order to reduce the pressure at which the coolant was pumped, the coolant was pumped from the cooling unit using a peristaltic pump (Watson Marlow 505S). Crystallization took place in the test chamber above the cooling chamber. A measured amount of solution was injected into the cell using one of the top access tubes of the cell. During cooling, condensation was avoided by continuously blowing air on both sides of the cell. Temperature readings were measured using probes and recorded using a Testo 177-T4 data logger with an accuracy of ±0.3 °C.

All vibrating equipment, such as the pumps and the chiller, were placed away from the platform where the Schlieren equipment was setup. This was to avoid external disturbances and vibrations that would introduce unsteadiness in the flow field of the test cell.

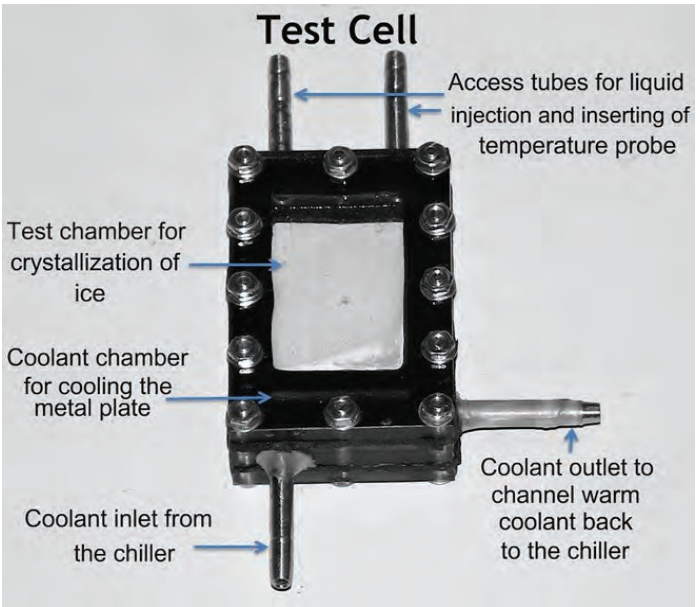

Figure 19: Test cell

iii. Colour filter calibration

A 2-D axisysmetric colour filter with radial hue distribution was designed using Matlab (Mathworks) and developed onto a strip of photographic film. Hue values instead of red-green-blue (RGB) values were used to generate the filter as recommended by Greenberg and co-workers (2011). This colour scale is used because each colour is unique and numerically identified as a hue, independent of dilution by white light (saturation) or its brightness (intensity).

To maximise sensitivity, the colours on the filter varied continuously to ensure that refracted light passed through a unique colour based on the refraction angle.

4.4.3 Ice washing

A similar setup and procedure to the one outlined in *4.4.1 Factors affecting ice-salt separation* was used for the washing of the ice product. The brine used in Objective 1 (Brine 1) was used for these experiments. The concentration of salts in the brine was low and this ensured that ice formed during the experimental run since these experiments only focused on mother liquor entrainment and not the entrapment of salt crystals within the bulk ice product. The ice was washed with 50 mL cooled deionised water maintained at approximately 0°C and filtered under vacuum using a Buchner funnel.

4.5 OBJECTIVE 5: Investigate how operating temperatures affect the yield and purity of the final products formed during an EFC process

This objective looks at the effect of operating temperature on yield and purity of the products formed during an EFC process.

4.5.1 Investigation into the effect of operating temperature on the yield and purity in the Eutectic Freeze Crystallization of an alkaline wastewater brine

The aim of these experiments was to conduct a cooling crystallization process at various set-point temperatures, including the eutectic temperature. In these experiments, recovery and purity of salt and (where applicable) ice would be determined. Table 6 shows a summary of these experiments.

Table 6: Summary of experiments.

Operating temperatures investigated	Expected products	Measured variables
1°C	$Na_2CO_3 \cdot 10H_2O$	Recovery and purity of products
-4°C	$Na_2CO_3 \cdot 10H_2O$	
-9°C	$Na_2CO_3 \cdot 10H_2O$ and ice	
-11°C	$Na_2CO_3 \cdot 10H_2O$ and ice	

i. Solution preparation

The raw brine was sourced from a PGM plant and is characterised by its high alkalinity. This arises from high concentrations of the carbonate anion. Sodium ion concentrations were determined using a Varian FS240 Atomic Absorption Spectrometer, anion concentrations were determined using a DX-

120 Chromatograph and carbonate and bicarbonate ion concentrations were determined using a 702 Metrohm Titrino for titration by HCl.

ii. Experimental setup

The experiments were performed in a 2 L jacketed glass reactor. A Mettler-Toledo multi-purpose probe was used to measure the solution temperature and conductivity of the reactor. A stirrer with variable speed control was used to provide adequate mixing with a 4-blade impeller, set to a speed of approximately 250 rpm. Cooling was achieved with a thermostatic unit using Kryo40 as a coolant. All experiments were conducted within a temperature controlled cold room, with a temperature set-point equal to that of the thermostatic unit.

Filtration was completed in the cold room. A ceramic Buchner funnel connected to a 1 L filtration flask was used to filter the ice. A 300 mL Micropore glass funnel was used to filter the salt product. The pore size of this filter paper was 0.45μm.

iii. Experimental procedure

Each experiment was started by adding approximately 1 L of pre-filtered brine to the jacketed crystallizer. The thermostatic unit was set at a temperature approximately 1°C below the desired temperature to account for heat losses to the environment and inefficiencies in heat transfer. The choice of operating temperatures (see Table 6) were investigated based on predicted temperatures by OLI Stream Analyzer. The data logging of temperature and conductivity measurements was initiated upon addition of the solution to the crystallizer.

Approximately 1 g of $Na_2CO_3 \cdot H_2O$ was used to seed at 1°C. For the relevant experiments, the solution was seeded with ice at -9.7°C (the eutectic). The system was left to equilibrate and grow. After 2 hours, the contents of the reactor were allowed to settle and separate. When ice was present, approximately 10 min was allocated for separation between the ice and salt phases. Ice was removed first into a separate beaker, if present, with some brine entrainment. The ice was filtered using the Buchner funnel and vacuum flask, and washed with methanol stored at the cold room temperature. The salt was then filtered using the Micropore filter and also washed using methanol.

Both ice and salt samples were taken. The feed brine, the filtrate from both filtration steps and the mother liquor (without wash solvent contamination) were also sampled and sent for analysis of ion concentrations.

RESULTS AND DISCUSSION

4.6 OBJECTIVE 1

4.6.1 Brine analysis

Table 7 shows the results obtained from the analysis of the two RO brine samples (**Brine 1** and **Brine 2**). The conductivity and density of the samples were similar while the pH was different (6.56 for **Brine 1** and 7.28 for **Brine 2**). A more comprehensive list of components was measured in an earlier study that allowed for this more refined list of components to be established.

The dominant cations (Na^+, K^+, Ca^{2+}) and anions (SO^{2-}, Cl^-) give an indication of the possible identities of the salts that could crystallize under EFC conditions. The salts will probably be sodium, potassium and calcium sulphate or chloride salts. However, this does not necessarily mean these salts will form under EFC conditions. It is only by conducting a thermodynamic modelling exercise and experimental work that the identity of the salts can be predicted and confirmed.

The concentration of anhydrous sodium sulphate is less than 2 wt% for both brines and this is lower than the eutectic concentration (4.2 wt%; Thomsen, 1997) of a binary sodium sulphate system. This indicates that ice is expected to crystallize before any salt crystallization. The presence of other components can affect the eutectic temperature of either ice or salt (Lewis et al., 2008). Although the crystallization temperature of ice will be different, the sequence of the crystallizing components (ice and salts) is unlikely to be affected.

The concentration of individual ions does vary between each brine, but without an observable trend. This variation in the concentrations of cations and anions for the two brine samples is unlikely to affect the operation of the EFC process since the system will adjust or move to a new eutectic point where the crystallization of two components can still occur. The concentrations of various cations and anions are only useful for the thermodynamic modelling step if the ion imbalance is within an acceptable range (<10%; Carvalho, 2008). If the ion imbalance is too high then the accuracy of the analysis and hence the actual component concentrations can be questioned. The ion imbalance, shown in Table 7, was 5.8% for **Brine 1** and 6.3% for **Brine 2**. This was deemed acceptable considering the complex nature of the brines.

Table 8 gives an indication of how dilute the brine samples are. The salts making up the synthetic brine in Table 8 are calculated based on the brine analysis shown in Table 7.

Table 8 gives a purely theoretical indication of the amount of salts necessary for a synthetic brine so that every possible ion is accounted for. However, because there is a charge imbalance, a dominant ion needs to be added to ensure a balance is achieved. The dominant ion in both instances was the sulphate ion.

Table 7: Brine analysis results for two different brine samples

Brine 1			
Temperature	°C	22	
Conductivity	mS/cm	22.2	
pH		6.6	
Density	g/cm^3	1.019	
	Concentration	Molality	
	mg/L	mmol/L	meq/L
Na^+	6718	292	292
K^+	1808	46.3	46.3
Ca^{2+}	1338	33.4	66.8
Mg^{2+}	75.0	3.08	6.17
NH_4^+	41.5	2.30	2.30
Sr^{2+}	*	*	*
SO_4^{2-}	16050	167	334
Cl^-	955	26.9	26.9
NO_3^-	398	6.43	6.43
HCO_3^-	61.2	1.00	1.00
F^-	*	*	*
Total Cation	meq/L	414	
Total Anion	meq/L	369	
Imbalance	%	5.8	

*ions not measured

Brine 2			
Temperature	°C	22	
Conductivity	mS/cm	19.3	
pH		7.28	
Density	g/cm^3	1.02	
	Concentration	Molality	
	mg/L	mmol/L	meq/L
Na^+	5796	252	252
K^+	3871	99	99
Ca^{2+}	1058	26.4	52.8
Mg^{2+}	170	7.01	14.0
NH_4^+	66.4	4.74	4.74
Sr^{2+}	11.9	0.136	0.272
SO_4^{2-}	15600	162	324
Cl^-	1504	42.4	42.4
NO_3^-	167	2.70	2.70
HCO_3^-	151	2.48	2.48
F^-	13.6	0.714	0.714
PO_4^{3-}	4.70	0.050	0.149
Total Cation	meq/L	423	
Total Anion	meq/L	373	
Imbalance	%	6.3	

Table 8: Synthetic brine makeup based on ion concentrations

	Brine 1	Brine 2
	g/L	g/L
Na_2SO_4	**18.77**	**14.72**
$CaSO_4$	**4.545**	**3.593**
K_2SO_4	**3.470**	**7.585**
NaCl	**1.574**	**2.479**
KNO_3	**0.650**	**1.208**
$MgSO_4$	**0.371**	**0.843**
$(NH4)_2SO_4$	**0.304**	**0.627**
$NaHCO_3$	**0.084**	**0.208**
Total	**29.77**	**31.26**

Note: Excess sulphate ions added to ensure there was an ion balance.

Table 8 also indicates that both brine samples were dilute when compared with sea water which generally has about 35 g/L dissolved solids. In addition, **Brine 1** was slightly more dilute than **Brine 2** (29.77 g/L and 31.26 g/L respectively). The reason for the low concentration of dissolved solids can be attributed to the source of the brine. The brine was obtained from an RO plant and, although RO does concentrate a water stream significantly, it can only concentrate it up to the level of the component with the lowest solubility, in this instance calcium sulphate. For example, the solubility of anhydrous $CaSO_4$ at 25°C is 2.1 g/L (Thomsen, 1997) while the solubility of Na_2SO_4, also anhydrous, is more than a hundred times higher (215 g/L at 25°C; Thomsen, 1997). The remaining component concentrations in the stream will therefore remain low. The other components would have a much higher final concentration if there was no calcium present in the water stream and if the stream was then passed through an RO plant.

i The concentrated brine

Brine 2 was concentrated by removing ~70% of the water, resulting in **Brine 2'**. The analysis of this concentrated brine is shown in Table 9.

The brine became significantly concentrated, as indicated by the increase in the ion concentrations compared to those of the original **Brine 2**. The ion imbalance for this brine was low, with a value of 2.4%. The dominant sulphate anion was chosen in order to ensure an ion balance. This was used to make up the synthetic brine. The brines were also very dilute with a total dissolved content of 29.77 g/L for **Brine 1** and 31.26 g/L for **Brine 2**.

Table 9: Concentrated brine analysis.

Brine 2'			
Temperature	°C	20	
Conductivity	mS/cm	39.23	
pH		8.3	
Density	g/cm^3	1.042	
	Concentration	Molality	
	mg/L	mmol/L	meq/L
Na^+	14200	618	618
K^+	4351	111	111
Ca^{2+}	2927	73.0	146
Mg^{2+}	347	14.3	28.6
NH_4^+	331	18.4	18.4
Sr^{2+}	41.2	0.470	0.940
SO_4^{2-}	41400	431	862
Cl^-	2115	59.7	60
NO_3^-	2105	34.0	34.0
HCO_3^-	735	12.0	12.0
F^-	3.200	0.168	0.168
PO_4^{3-}	4.200	0.044	0.133
Total Cation	meq/L	923	
Total Anion	meq/L	968	
Imbalance	%	2.41	

4.6.2 Thermodynamic modelling

i Brine 1 and Brine 2

Figure 20 shows the recovery of water and various salts and ions as the temperature of **Brine 1** is decreased from 25°C to -25°C. The salt and ion recoveries are plotted on the primary y-axis, and the water recovery on the secondary y-axis. Each data point in Figure 20 represents an equilibrium condition. The mass of a component crystallizing from the solution is therefore as a result of the system reaching a new equilibrium condition. Table 10 shows the nucleation temperatures of the various components as predicted by the OLI thermodynamic modelling procedure.

The model predicts that the system is already saturated with respect to $CaSO_4 \cdot 2H_2O$ at 25°C. It also predicts that water (in the form of ice) will begin to crystallize at -0.8°C followed by $Na_2SO_4 \cdot 10H_2O$ at -1.5°C. A double salt, $K_2SO_4 \cdot CaSO_4 \cdot 1H_2O$, begins to crystallize at -2.2°C followed by KCl at a lower temperature of -19.6°C.

The Ca^{2+} recovery is 65% at 25°C and increases to above 77% once ice begins to crystallize at -0.8°C. The Na^{+} recovery increases during the crystallization of $Na_2SO_4 \cdot 10H_2O$ with 92% of it being recovered by -5°C. The recovery of Na^{+} reaches 99% at -25°C. The majority of ions are recovered at -5°C. For example, Ca^{2+} recovery is 99% while the recovery of Na^{+}, K^{+} and the SO_4^{2-} ions are 92%, 74% and 97% respectively. No chloride is recovered at this temperature. The chloride ion reaches a recovery of 16% at -20°C as a result of the start of KCl crystallization at -19.6°C.

In terms of water recovery, ice begins to crystallize out at -0.8°C and a 95% recovery is achieved at -5°C. The recovery of ice continues to increase until it reaches a constant value of 97% at -21°C.

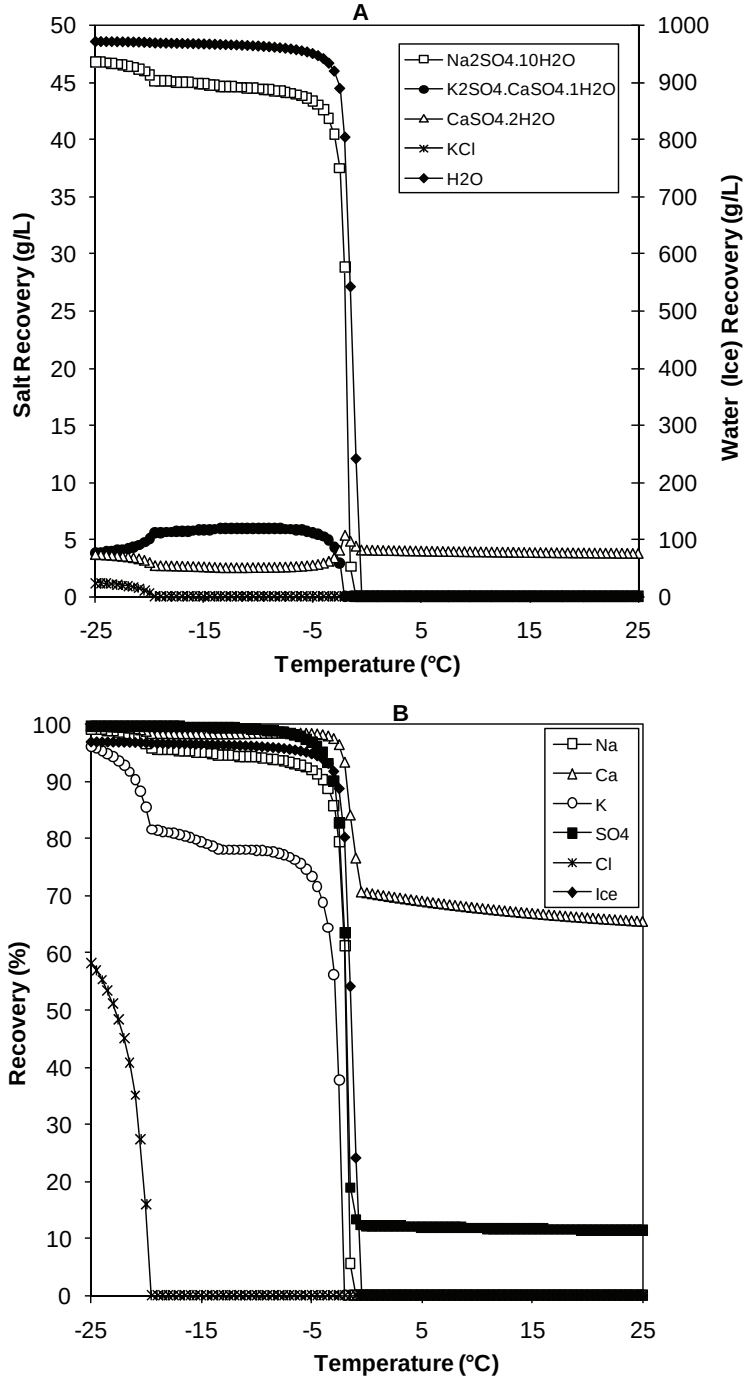

Figure 20: Effect of temperature reduction on salts and water recovery for Brine 1 (salts (A) and ions (B))

Table 10: Solid nucleation temperatures for Brine 1 and Brine 2

	Brine 1	Brine 2
	Temperature °C	
H_2O	-0.8	-0.9
$CaSO_4 \cdot 2H_2O$	saturated	saturated
$Na_2SO_4 \cdot 10H_2O$	-1.5	-1.9
$K_2SO_4 \cdot CaSO_4 \cdot 1H_2O$	-2.2	-2.1
KCl	-19.6	-16.6

The thermodynamic modelling results indicate that four major components crystallize from **Brine 1** in a narrow temperature interval of 1.4°C. Figure 21 is a zoomed in section of Figure 20 showing the narrow temperature range (-0.8°C to -2.2°C).

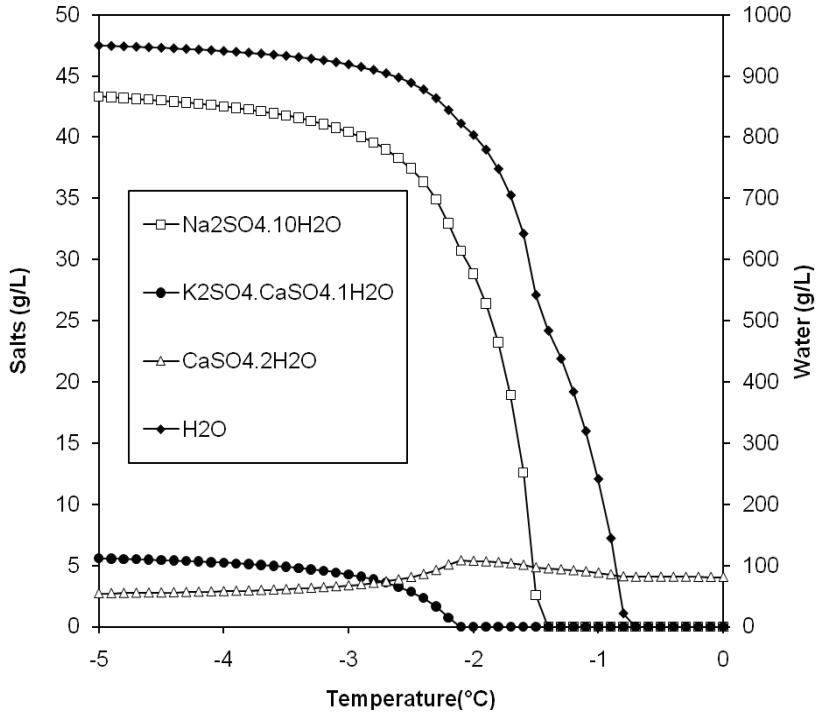

Figure 21: Effect of temperature reduction in the temperature range 0°C to -5°C for Brine 1

Three of these four components are salts and therefore, according to the thermodynamics, salt contamination is likely to occur if the temperature is not precisely controlled. The reason for the possibility of salt contamination is based on the fact that the EFC process works on the utilization of the density difference between salt and ice. The process is not effective if two or more salts crystallize at EFC conditions since the salts, having similar densities, would sink to the bottom of the crystallizer, making separation difficult. The purity of the salts formed would therefore ultimately be affected.

However, these results are based on thermodynamic predictions and do not consider the use of kinetics and process manipulations, such as selective seeding, that could be adopted in order to prevent salt contamination.

The thermodynamic modelling results for **Brine 2** (Figure 24) are similar to those obtained for **Brine 1**. The same salts crystallize out, even though there is a difference in ion concentrations between the brines. However, the crystallizing temperatures and amounts are different. Table 10 shows that both brines have ice crystallizing at similar temperatures (-0.8°C and -0.9°C). This is not surprising, considering that both brines have similar concentrations of total dissolved solids (30 g/L and 31 g/L) and hence approximately the same amount of water. The thermodynamic modelling also indicates that both brines were saturated with respect to $CaSO_4 \cdot 2H_2O$ at 25°C. The crystallizing temperature of $Na_2SO_4 \cdot 10H_2O$ in **Brine 2** is -1.9°C while it is -1.5°C for **Brine 1**. As expected, the sodium ion concentration affects the nucleation temperature of $Na_2SO_4 \cdot 10H_2O$. For example, **Brine 1** had a Na^+ concentration of 6718mg/L and a crystallization temperature of -1.5°C. On the other hand, the Na^+ concentration and the crystallization temperature of **Brine 2** was 5796 mg/L and -1.9°C respectively. There is also a direct correlation between the concentration and the crystallization temperature. A low Na^+ concentration results in a low crystallization temperature for $Na_2SO_4 \cdot 10H_2O$.

The double salt, $K_2SO_4 \cdot CaSO_4 \cdot 1H_2O$, crystallizes at similar temperatures for both brines (-2.2°C for **Brine 1** and -2.1°C for **Brine 2**). Potassium chloride crystallizes at -19.6°C for **Brine 1** and -16.6°C for **Brine 2**. A comparison of the chloride ion concentration (955 mg/L for **Brine 1** and 1504 mg/L for **Brine 2**) shows that once again the lowest concentration of a specific ion results in the lowest crystallization temperature. This indicates that, for certain ions, there is a direct correlation between the concentration of that ion and the crystallization temperature of its corresponding salt.

ii Concentrated brine 2'

The thermodynamic modelling for **Brine 2'** is based on the results obtained from the experimental concentrating procedure and the analysis of this stream. It is not based on merely removing water in the thermodynamic model. Figure 22 shows two options for the thermodynamic procedure for obtaining a concentrated brine. The concentrated brine in this section was obtained using option 1. Option 2 is based on a theoretical approach because there is no experimental section. Water (ice) and salts are "removed" from the thermodynamic model resulting in a theoretical concentrated brine (**Brine 2***). This brine is then used in thermodynamic model.

The thermodynamic model can therefore predict how a stream concentration will change based on the theoretical removal of specific components (option 2). However, it is the experimental work that gives a more realistic result (option 1). This is the option that was used in this work.

Figure 23 shows the thermodynamic modelling results for the concentrated brine (**Brine 2'**).

The model predicts that the solution is saturated with respect to $CaSO_4 \cdot 2H_2O$ but the concentration is low (0.76 g/L) when compared to the other concentrations of salts formed so calcium sulphate is not presented in Figure 23. Sodium sulphate ($Na_2SO_4 \cdot 10H_2O$) begins to crystallize at -0.8°C before any ice crystallization, indicating that the stream is significantly concentrated in sodium. Ice only begins to crystallize at -1.7°C. The double salt begins to crystallize at -2.4°C followed by KCl at -20.4°C

The recovery of salts for the concentrated brine (**Brine 2'**) is the same as that of **Brine 2** but the individual ion amounts are different because some of the ions would have already been experimentally removed, for example calcium and sodium. The overall ion removal at -5°C (69%) is similar to that of **Brine 2** at -5°C (71%).

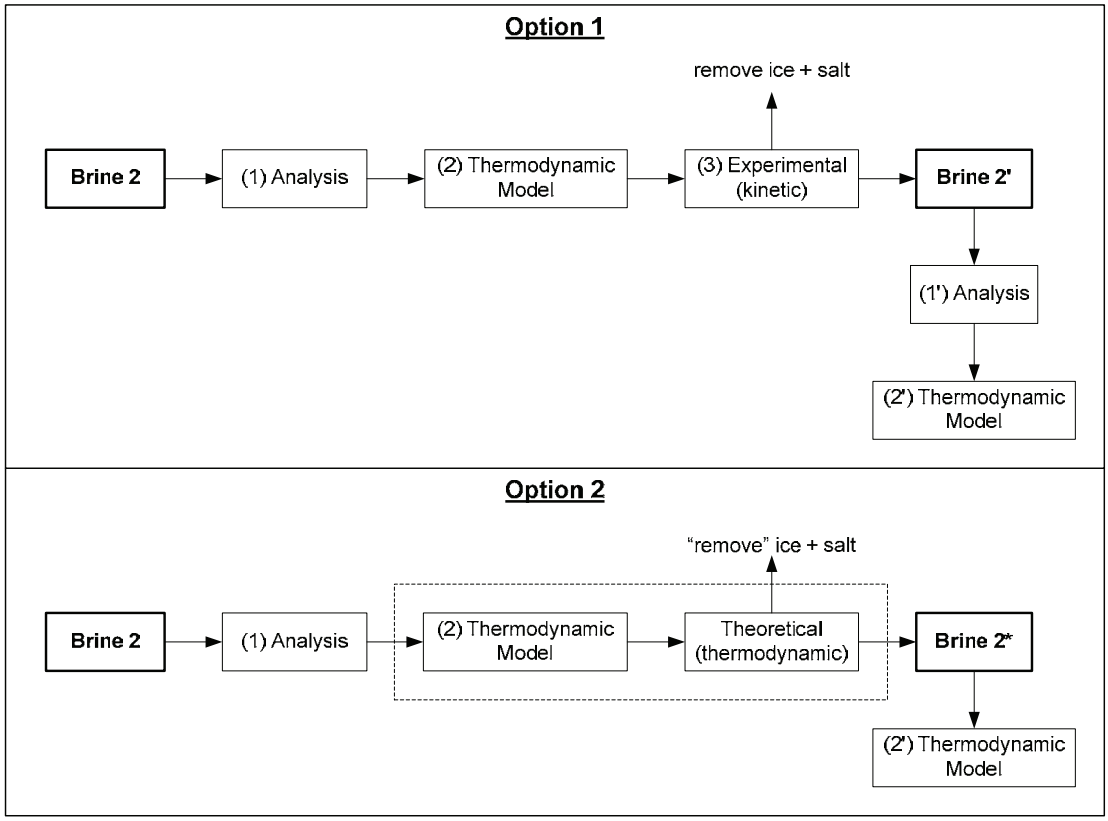

Figure 22: Two different options for obtaining a concentrated brine

The results obtained from the thermodynamic modelling of two similar brine samples indicate that the same salts crystallize out of the two brines but that their crystallization temperatures are different. There is a correlation between the cation and anion concentration of the salt and the crystallization temperature of the corresponding salt. For example, the brine with the lowest Na^+ concentration resulted in the lowest crystallization temperature of $Na_2SO_4 \cdot 10H_2O$. Similarly, the brine with the lowest Cl^- concentration resulted in the lowest crystallization temperature of KCl. This was as a result of the characteristic properties of the system.

In addition, the results indicate that it would be best to operate a freeze crystallizer at -5°C since this was the highest temperature that resulted in a high overall ion recovery (85% for **Brine 1** and 71% for **Brine 2**). The proposed brine treatment process should include a pre-concentration stage and two EFC stages for the removal of ice-$CaSO_4 \cdot 2H_2O$ and ice-$Na_2SO_4 \cdot 10H_2O$. This could improve the purity of $Na_2SO_4 \cdot 10H_2O$ formed in the ice-$Na_2SO_4 \cdot 10H_2O$ removal stage.

The concentrated brine (**Brine 2'**) resulted in the crystallization of $Na_2SO_4 \cdot 10H_2O$ before ice. The overall ion recovery for this brine (69%) was similar to the value calculated for **Brine 2** (71%).

Thermodynamic modelling provides the first indication of what could be expected during an EFC process but, because these thermodynamic results are calculated for equilibrium conditions, the results under real operating conditions need to be verified.

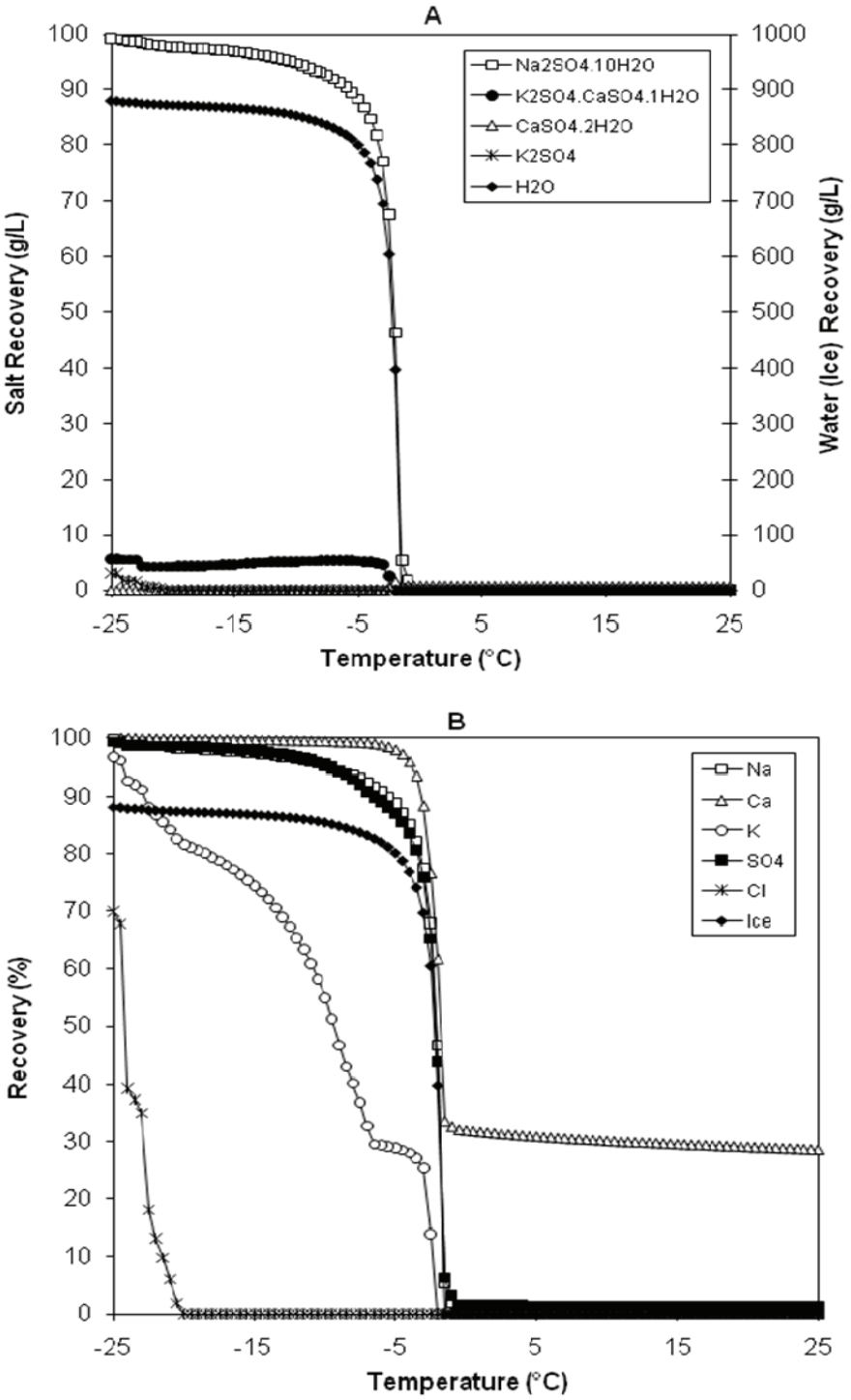

Figure 23: Effect of temperature reduction on salt and water recovery for Brine 2'

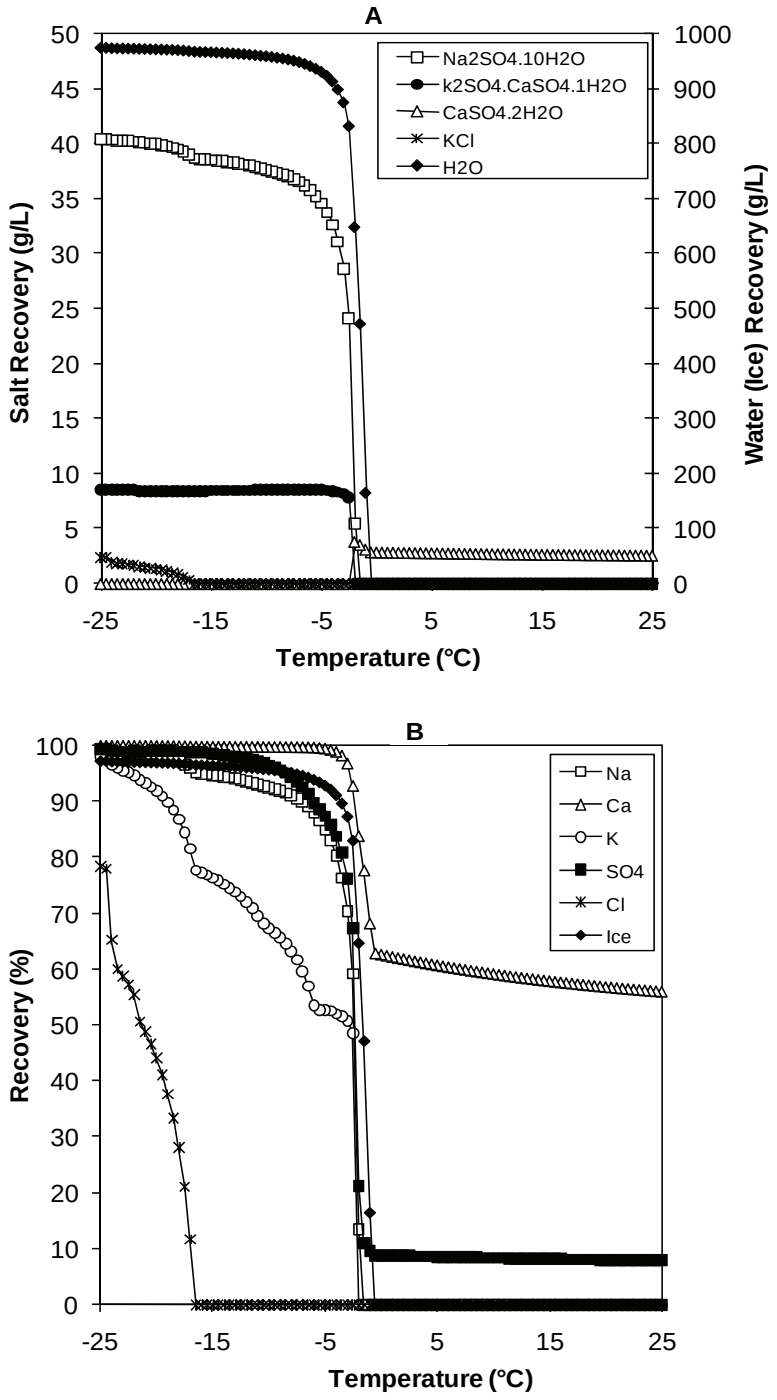

Figure 24: Effect of temperature reduction on salt and water recovery for Brine 2 (salts (A) and ions (B))

In order to further explore the observed correlation, a simplified ternary system based on the analysis of the brine was investigated. The nucleation temperature of $Na_2SO_4 \cdot 10H_2O$ in the ternary Na_2SO_4-K_2SO_4-H_2O system was obtained by modelling the system for a range of concentrations using OLI. Figure 25 shows the results obtained from the modelling exercise.

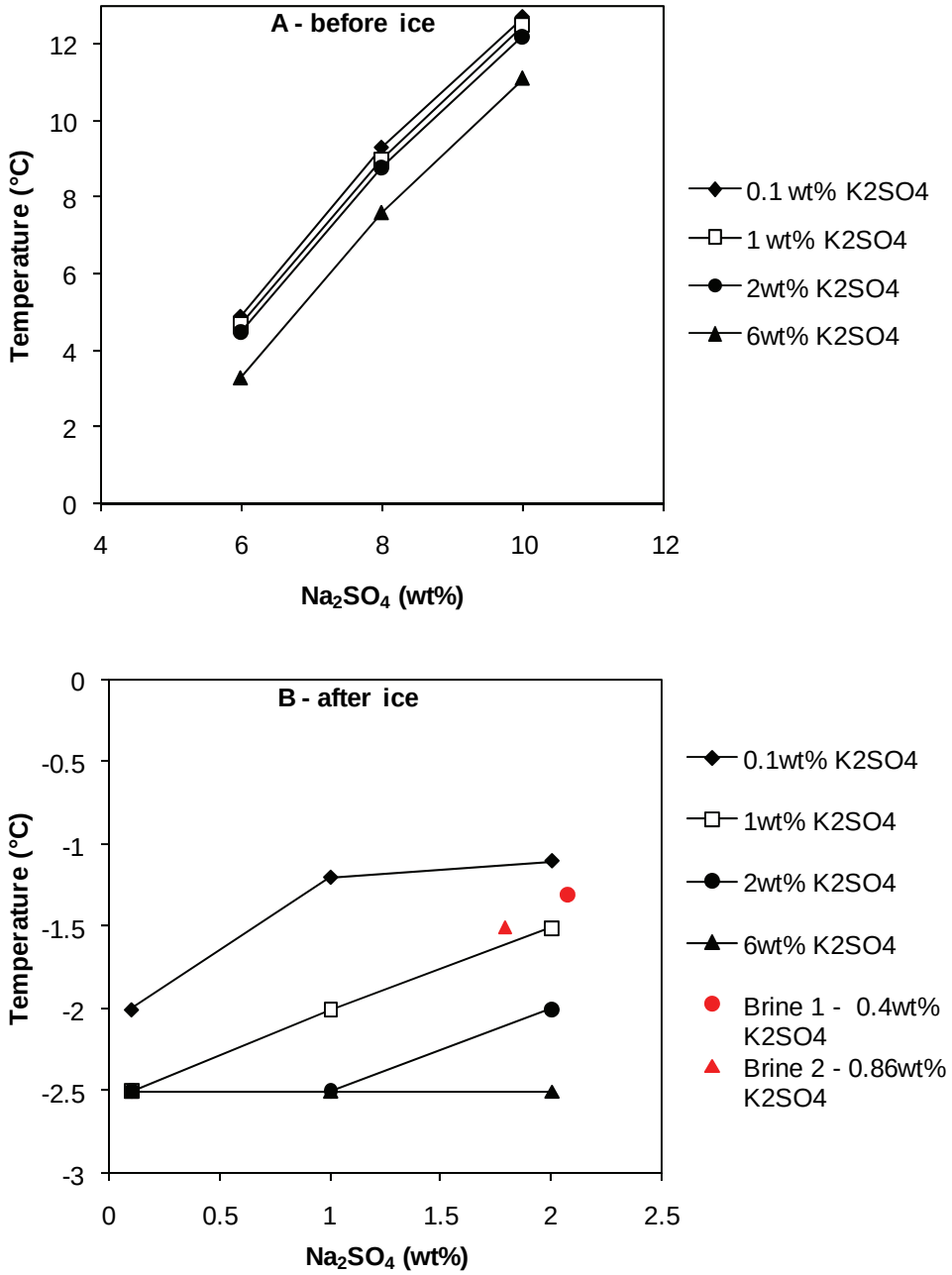

Figure 25: $Na_2SO_4 \cdot 10H_2O$ nucleation temperatures for varying concentrations in the ternary Na_2SO_4-K_2SO_4-H_2O system (before ice crystallization (A) and after ice crystallization (B))

The results from the thermodynamic modelling (Figure 25) indicate that, for concentrations that result in the crystallization of $Na_2SO_4 \cdot 10H_2O$ before ice crystallization (Figure 25 A), as the crystallization progresses, the crystallization temperature of $Na_2SO_4 \cdot 10H_2O$ increases as the concentration of the Na_2SO_4 solute increases. The opposite is true for the crystallization of $Na_2SO_4 \cdot 10H_2O$ after the crystallization of ice (Figure 25 B). As the crystallization progresses, the crystallization temperature of $Na_2SO_4 \cdot 10H_2O$ decreases, the concentration of Na_2SO_4 decreases and the concentration of the non-crystallizing component (K_2SO_4) increases. In addition, the system approaches the ternary eutectic temperature at -2.5°C for this system. A concentration of 6wt% K_2SO_4 and a range of Na_2SO_4 concentrations (0.1wt% to 2wt%) results in the ternary eutectic conditions being reached with the crystallization of ice, K_2SO_4 and $Na_2SO_4 \cdot 10H_2O$. The corresponding brine concentrations, relating to Na_2SO_4 and K_2SO_4 only, are also shown in Figure 25. The crystallization temperatures of

$Na_2SO_4 \cdot 10H_2O$ for the brines in Figure 25 occur at different temperatures to that of the actual brine modelling since Figure 25 is an approximation of the brine using only the Na^+, K^+ and SO_4^{2-} ions while excluding the other ions of the brine.

Thus, the nucleation temperature of a salt does decrease with a decreasing concentration of its corresponding solute in solution but only after the crystallization of ice. The trend is as a result of the characteristic properties of the system and depends on the components present in the system. A system with a number of components, such as a brine, will result in a complex interaction of ions but the same observed trend as seen in this simplified system.

The initial recovery of calcium is 60% for **Brine 2** while it is 65% for **Brine 1**. A 71% recovery of all ions is achieved at an operating temperature of -5°C for **Brine 2** compared to 85% for **Brine 1**. The same overall recovery (90%) for the brines is achieved at -20°C.

From this information, it is apparent that the amount of $Na_2SO_4 \cdot 10H_2O$ that could potentially be removed from the stream is far in excess of any other salt and therefore any process should ultimately aim to produce this salt. The other salts can be produced but because these salts are present in smaller quantities, it may not be economically viable to have a separate crystallizer merely to produce them.
The information also shows that a freeze crystallizer operating at -5°C could theoretically be used to recover both $Na_2SO_4 \cdot 10H_2O$ and ice, with the sodium salt being denser than water and thus being recovered at the bottom of the reactor. In addition, ice, being less dense than water, can be recovered at the top of the reactor. However, the thermodynamic modelling also shows that:

- the water recovery is far in excess of that of the salt, and it will be necessary to pre-concentrate the brine to remove the excess water since the high solid (ice) content would make the separation of ice and salt difficult and

- the presence of the solid $CaSO_4 \cdot 2H_2O$ at ambient temperatures could potentially contaminate the recovered $Na_2SO_4 \cdot 10H_2O$. The thermodynamic modelling also predicts the formation of a double salt, $K_2SO_4 \cdot CaSO_4 \cdot 2H_2O$, at -2.2°C (**Brine 1)** and -2.1°C (**Brine 2**) that could also potentially contaminate the recovered $Na_2SO_4 \cdot 10H_2O$.

The brine treatment process should include a series of three stages, the first being a pre-concentration step, the second being an ice-$CaSO_4 \cdot 2H_2O$ recovery step and the third being an ice-$Na_2SO_4 \cdot 10H_2O$ recovery step. The removal of $CaSO_4 \cdot 2H_2O$ in the second stage would serve two functions in that this stage would further concentrate the brine (and hence produce more ice) and the crystallizer would also remove $CaSO_4 \cdot 2H_2O$. The removal of calcium sulphate in stage 2 would prevent the salt contamination of $Na_2SO_4 \cdot 10H_2O$ in stage 3. The removal of calcium sulphate could be neglected if sodium sulphate crystallized before calcium sulphate (only 2.7 g/L $CaSO_4 \cdot 2H_2O$ formed at -5°C compared to 43 g $Na_2SO_4 \cdot 10H_2O$ at -5°C). Thus, the only reason for removing calcium sulphate would be to prevent $Na_2SO_4 \cdot 10H_2O$ contamination.

4.6.3 Kinetic Aspects

i Part A – Brine 1 volume reduction and product purity

Once ice crystallization was initiated, by the addition of the ice seeds, the solution temperature increased suddenly due to the release of the heat of fusion. The constant solution temperature (equilibrium temperature) reached after the sudden increase in solution temperature was always the

same for a fixed concentration. Thus, the equilibrium nucleation temperature for experiments **A1** to **A4** was constant at -0.5°C. This temperature consequently defined the minimum operating temperature necessary to commence the crystallization process for that specific concentration.

For experiments **A7** and **A8**, the crystallization of calcium sulphate occurred after leaving the filtrates from previous experiments (**A5** and **A6**) to stand for 24 hours. This was due to the slow crystallization of calcium sulphate and its inverse solubility (Ramsdell and Partridge, 1929). This was verified by leaving the filtrate obtained from experiment **A9** in the laboratory at a temperature of 22°C whilst the filtrate from experiment **A10** was kept in the freeze room at 5°C for 24 hours. From this test, it was found that experiment **A9** resulted in the crystallization of calcium sulphate while experiment **A10** did not. This provided the basis for investigating this phenomenon further by conducting separate experiments to determine the mass deposition of calcium at different temperatures and concentrations. **Brine 2** and its different concentrations were used for this investigation.

The results obtained from the cascading concentration procedure are shown in Figure 26. Pure calcium sulphate (98.0%) and pure sodium sulphate (96.4%) were produced along with potable water. The salt products were not washed and thus the purity is expected to increase further with washing. On a mass basis, a 97% reduction in the initial feed was obtained. However, calcium sulphate was not produced under EFC conditions since it did not crystallize along with ice but rather it crystallized within 24 hours. **Brine 2** was used to investigate if EFC conditions could be achieved with the crystallization of calcium sulphate and ice.

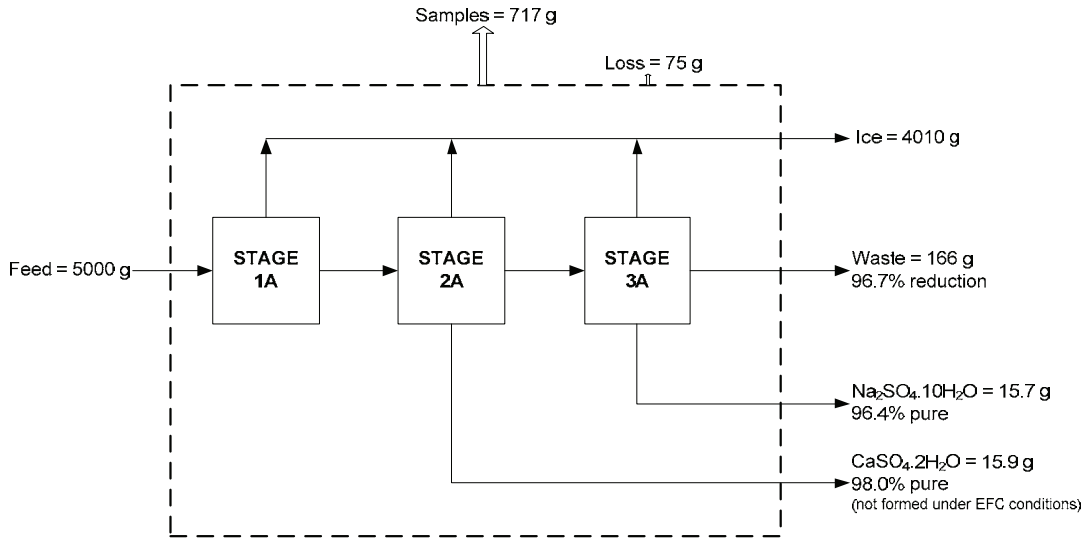

Figure 26: Mass balance for Brine 1 (Randall et al., 2010)

The loss calculated during the cascading concentration procedure for **Brine 1** was due primarily to the amount of liquid removed for sampling. Approximately 30 ml of solution was removed after each experiment which resulted in a loss of about 14% of the feed towards sampling. Other minor losses due to evaporation and human error only amounted to about 1.5% of the experiment feed not being accounted for.

Figure 27 shows the conversion of waste (brine) to viable products (ice and salts) at different stages of the cascading concentration procedure. Each stage of the cascading procedure is also a series of reproduced experiments. For example, experiments A1 to A4 were identical, and thus gave some confidence in the reproducibility of the procedure. Experiments **A1** to **A4** resulted in the highest single

conversion (54%) of the brine to ice. The overall conversion of waste to products for **Stage 1A** was 71% ice only since this stage was a pre-concentration stage with no salt crystallization occurring. The conversion increased marginally when salt crystallization occurred. The waste conversion for **Stage 2A** was 85% and 96% for **Stage 3A**. There was thus a lower increase in waste conversion from **Stage 2A** to **Stage 3A** (85% to 96%) compared to the waste conversion from **Stage 1A** to **Stage 2A** (71% to 85%) due to the majority of the ice forming in **Stage 1A**. Therefore the total salt and water recovery from stages **1A** to **3A** was 96%.

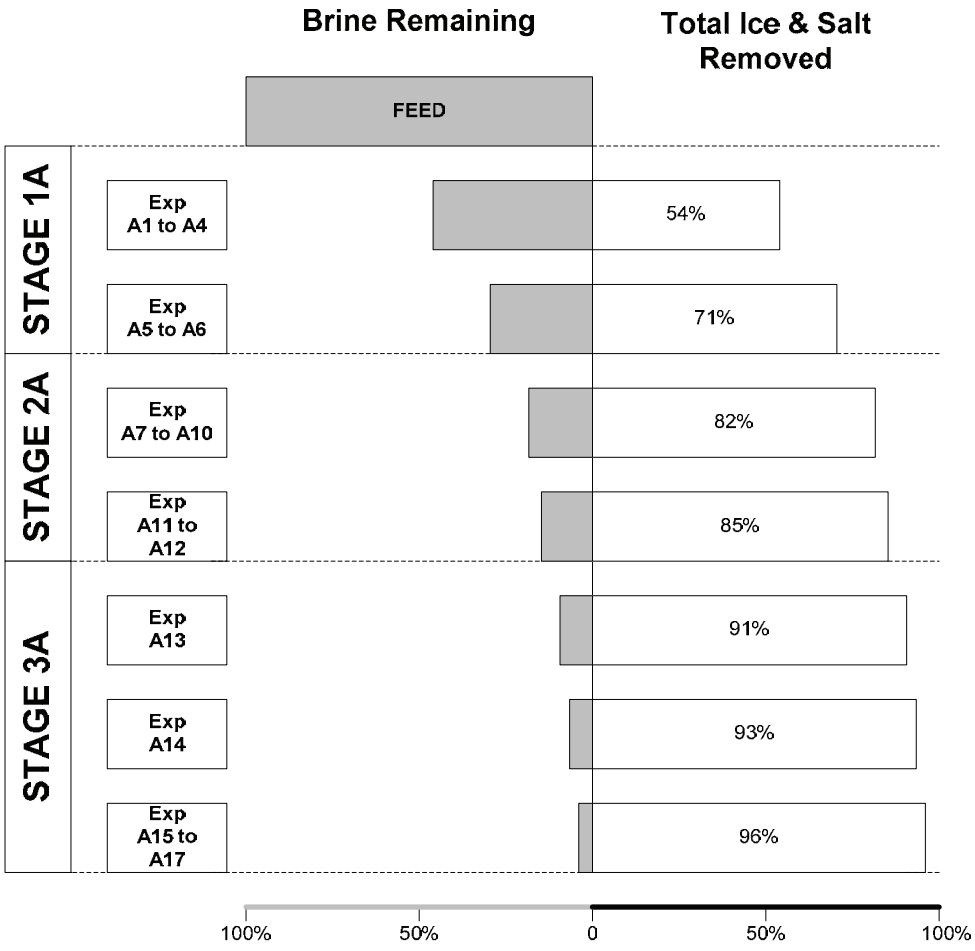

Figure 27: Waste conversion for different steps in the cascading concentration procedure for Brine 1 (Randall et al., 2010)

Figure 28 shows an overall mass balance for the treatment of waste water using different treatment methods. It includes the HiPRO process, GypSLIM process, as well as the proposed EFC process. The HiPRO process recovers 99% of potable water from the waste stream and produces a 1% waste stream. About 40% of this waste stream is solid waste that can be converted into valuable products using the GypSLIM process (Figure 28). The remaining 60% of this waste stream can be treated using EFC.

The EFC process could in theory add a further 120 m^3/d (0.5%) of potable water to the plant. A production of 476 kg/d $CaSO_4 \cdot 2H_2O$ and 471 kg/d $Na_2SO_4 \cdot 10H_2O$ would also be obtained. Whilst the additional amount of water recovered using EFC may appear relatively low, considering that the amount of water currently produced using the HiPRO process is 25 000 m^3/d, the primary emphasis should be on waste minimization and conversion of all possible waste products to useful ones (in this case calcium sulphate and sodium sulphate) rather than having to dispose of them at an

additional cost. The bar on the right of Figure 28 shows the overall conversion of the feed stream (waste) to valuable products. The product stream is 99.6% water, 0.286% pure individual salts and a 0.138% waste stream. Figure 28 also shows that only a combination of different technologies is capable of attaining a near zero waste discharge.

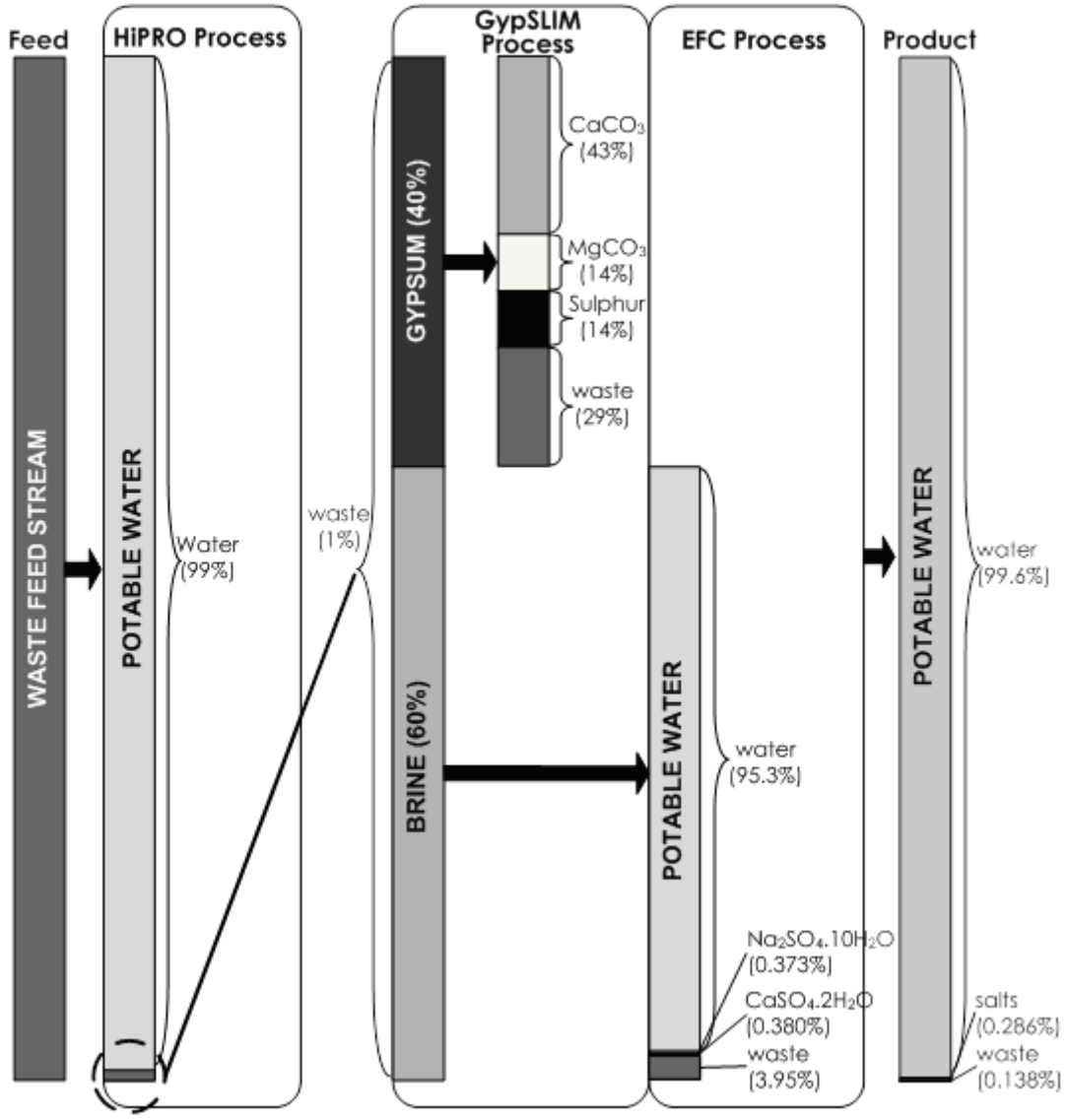

Figure 28: Overall mass balance for a combination of treatment methods (Randall et al., 2010)

As can be seen, novel technologies such as EFC can offer a sustainable method for the treatment of brines in accordance with the necessity for current water treatment processes to reduce the volume and extent of water pollution. There also needs to be a paradigm shift that focuses on new approaches that include wise investments and technological innovation that not only seeks to obtain treated water but also treats and converts the solid waste products into useful ones (Corcoran et al., 2010).

ii Part B – Cascading concentrating method for Brine 2

A similar cascading concentration procedure to that of **Brine 1** was conducted for **Brine 2**. The cascading concentrating procedure for **Brine 2** only produced ice in the first stage. The procedure produced ice and sodium sulphate (97.5% pure) in **Stage 2B**. The filtrate of **Stage 2B** was highly concentrated and as a result calcium sulphate crystallized out overnight at 3°C. More ice and sodium sulphate was produced in **Stage 3B**.

Figure 29 gives a summary of the components formed in the first three stages. The salt formed in the subsequent experiments (**Stage 4B**) had a low purity (<89% sodium sulphate purity; reaching a 12% sodium sulphate purity for experiment **B25**) and for this reason only the first three stages were considered.

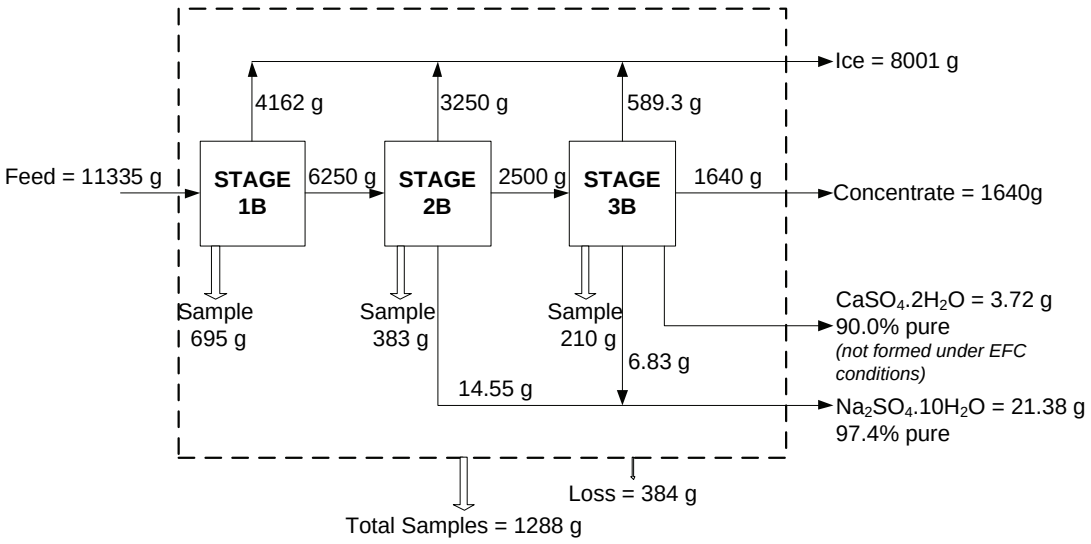

Figure 29: Mass balance for Brine 2

iii Part C – Calcium mass deposition from Brine 2

The potential problem with the calcium sulphate being present at saturation, as predicted by the preceding thermodynamic modelling is describe in this section.

Seeding can promote the growth or mass deposition of a specific component. For example, if $CaSO_4 \cdot 2H_2O$ seeds are added to a supersaturated calcium solution, the calcium ions crystallize out of solution in order to form more calcium sulphate. This process continues until a new equilibrium is reached. Therefore, a lower aqueous calcium concentration indicates that $CaSO_4 \cdot 2H_2O$ crystallized out of solution. Figure 30 shows the amount of calcium remaining in solution for experiments **B1** to **B9**. The initial calcium concentration in **Brine 2** (**B1**) at 22°C was ~1 g/L. The calcium concentration increased to a peak of 2.2 g/L after 1 day and subsequently decreased to 0.80 g/L after 7 days. The initial aqueous calcium concentration increase in the original **Brine 2** stream was due to dissolution of the seed material, indicating that the original brine sample was initially unsaturated. The subsequent decrease in the aqueous calcium concentration of the original after 1 day to a concentration of 0.75 g/L indicated that the solution was no longer supersaturated. The initial aqueous calcium concentration for **Stage B3** was lower than **Stage B2** even though **Stage B3** was slightly (23.6% ice removal from the feed to the stage) more concentrated. This was due to the crystallization of $CaSO_4 \cdot 2H_2O$ overnight at 3°C resulting in a lower aqueous calcium concentration.

The aqueous ion concentrations for **Stage B1**, **Stage B2** and **Stage B3** (experiments **B1** to **B4**) at 22°C all reached the same concentration after 3 days. The final calcium concentration after 7 days was 0.79±0.29 g/L at 22°C (A) and 0.67±0.01 g/L at 0°C (B). This indicates that more calcium sulphate crystallized out at a lower temperature.

However, this might require a longer residence time. Therefore, in an attempt to reduce this time, a separate experiment (**B9**) was conducted for a period of 24 hours in order to determine the calcium concentration profile for this time period.

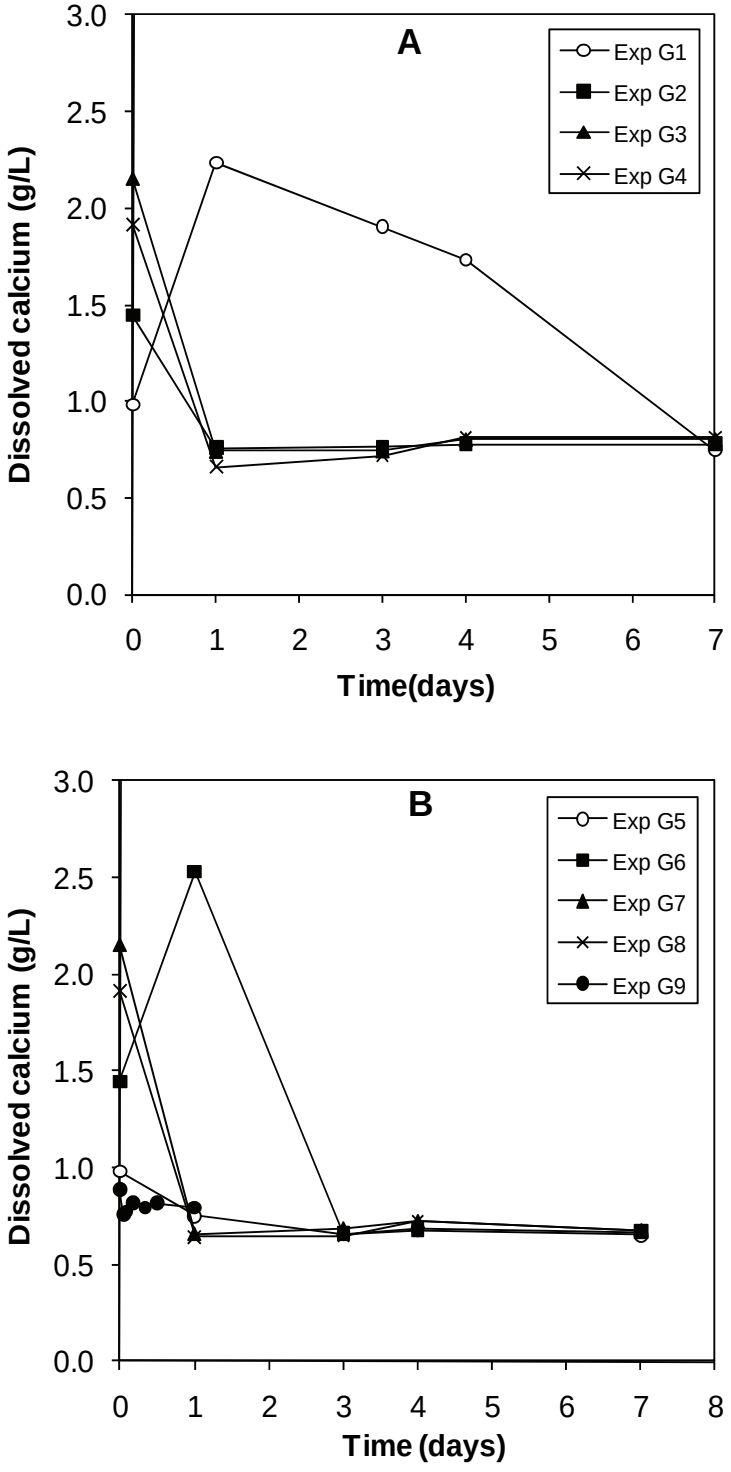

Figure 30: Changing aqueous calcium concentrations for different concentrations of Brine 2 at 22°C (A) and 0°C (B) (Experiments G1 to G9).

Figure 30 also shows the aqueous calcium concentration for the 24 hour period (Experiment **B9**). The initial calcium concentration for experiment **B9** was lower (0.89 g/L) than experiment **B5** (0.98 g/L). This is due to some of the calcium sulphate crystallizing out between the two experiments which were

one week apart. The aqueous calcium concentration decreased to a minimum of 0.76 g/L after 1 hour and subsequently increased and stabilized at 0.82 g/L from 4 hours onwards. The final value (0.80 g/L) after 1 day was slightly different to the values obtained for experiments **B1** to **B4** (~0.75 g/L).

iv Part D – The crystallization of $CaSO_4 \cdot 2H_2O$ and ice

The results obtained from the cascading concentrating procedure for **Brine 1** indicated that sodium sulphate formed in **Stage 2A** and **Stage 3A** with little or no calcium sulphate formed during ice crystallization (eutectic conditions). However, calcium sulphate did crystallize out of the filtrate when left overnight, indicating that the solution was supersaturated with respect to calcium sulphate. A separate experiment using the original **Brine 2** sample was conducted to investigate whether the calcium sulphate could crystallize out with ice during **Stage A1**. For this, calcium sulphate and ice seeding was utilized in order to achieve eutectic conditions with this brine sample.

Figure 31 shows the results obtained during the crystallization of ice and calcium sulphate under EFC conditions. The initial solution (at 0°C) was seeded with 1 g $CaSO_4 \cdot 2H_2O$ and cooled to -1°C. The solution temperature was kept constant for two hours at -1°C with no spontaneous ice crystallization occurring. Ice seeds (~1 g) were then added (after 2 hours) to the solution, resulting in the onset of ice crystallization. Due to the heat of fusion, the temperature of the solution increased to -0.5°C, followed by a slight decrease to -0.6°C and remained at this temperature for the remainder of the experiment. The aqueous calcium concentration increased during ice crystallization as a result of the stream becoming more concentrated. The calcium concentration reached a peak of 0.85 g/L after a further one hour and decreased to a low of 0.68 g/L after 5 hours. The amount of ice formed during the 3 hours of ice crystallization was ~20% of the feed.

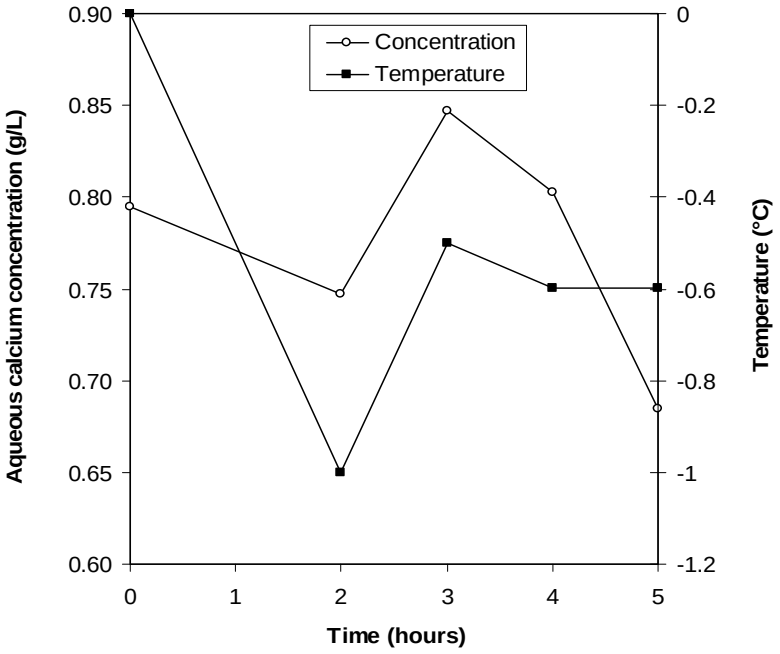

Figure 31: Aqueous calcium concentration and temperature change over time

The results presented in Figure 31 indicate that calcium sulphate can crystallize along with ice during the pre-concentration step, provided the stream is seeded with $CaSO_4 \cdot 2H_2O$. The concentration levels of aqueous calcium after three hours of EFC operation are slightly higher (0.68 g/L) compared to the concentration levels during calcium sulphate seeding at 0°C (0.67 g/L). However, the calcium

concentration reduction at 0°C with calcium sulphate seeding was obtained after a much longer period (1 week) compared to the three hours of EFC operation.

The feasibility of using EFC as a brine treatment method was experimentally verified at laboratory scale. The results showed that a 97% waste conversion (by mass) to viable products (pure water and salts) could be achieved. Pure calcium sulphate (98.0% purity) and pure sodium sulphate (96.4% purity) were produced along with potable water.

The results also showed that calcium sulphate could be removed under EFC conditions by means of seeding with $CaSO_4 \cdot 2H_2O$ and ice. The removal of calcium sulphate under EFC conditions also resulted in a similar calcium ion concentration to that obtained after 1 week (0.68 g/L compared to 0.67 g/L).

4.7 OBJECTIVE 2

Table 11 shows a comparison between the actual brine and the synthetic brine. The conductivity, pH, density and eutectic temperature compare well for the actual brine and the synthetic brine. The values predicted using the thermodynamic modelling software does not compare as well. The ion imbalance from the analysis for the real brine, on which the synthetic brine is based, was less than 3%. Therefore, the results in Table 11 show that, in this instance, a synthetic brine can approximate an actual brine, provided the key parameters (conductivity, pH, density and eutectic temperature) match and the ion imbalance is low.

Table 11: Comparison between a real brine and a synthetic brine

		Brine	Synthetic	OLI
Conductivity	mS/cm	40.86	39.23	-
pH	-	8.1	8.3	7.35
Density	g/cm3	1.041	1.042	1.049
Eutectic Temperature ($Na_2SO_4 \cdot 10H_2O$ and ice)	°C	-1.5	-1.5	-1.7
Imbalance	%	2.75	0	0

Note: all measurements were taken or simulated at 20°C.

The fact that the synthetic stream had less calcium sulphate than the real brine also did not affect the temperature at which ice and salt formed. This was probably due to the low concentration of calcium present in the brine compared to the other major components. Therefore, the synthetic brine was used to investigate the crystallization of sodium sulphate and ice under EFC conditions with a reduced calcium concentration. Figure 32 shows the concentration profile for the aqueous Na^+ ion as well as the temperature profile. The solution, initially at 10°C, had a Na^+ concentration of 12.3 g/L. The solution was cooled until -1.4°C, at which stage ~1 g $Na_2SO_4 \cdot 10H_2O$ seed crystals were added to the solution.

This addition of seed material resulted in a decrease in the aqueous sodium ion concentration to a concentration of 11.3 g/L after ~30 minutes. The temperature of the solution increased gradually to a maximum of -0.8°C, after which it continued to decrease until it stabilised at -1.5°C. This temperature increase was a result of the release of the heat of crystallization during the crystallization of $Na_2SO_4 \cdot 10H_2O$. Ice seed crystals (~1 g) were added after one hour. The addition of these ice seeds resulted in an eventual sodium concentration increase after 2 hours. The sodium ion concentration reached a final concentration of 12.1 g/L after 4 hours. The temperature of the solution did not increase with the addition of ice seeds because the seeds were added at the ice equilibrium temperature

(-1.5°C). Therefore, this experiment established that the eutectic temperature for this system was -1.5°C, as this was the temperature at which both ice and $Na_2SO_4 \cdot 10H_2O$ existed.

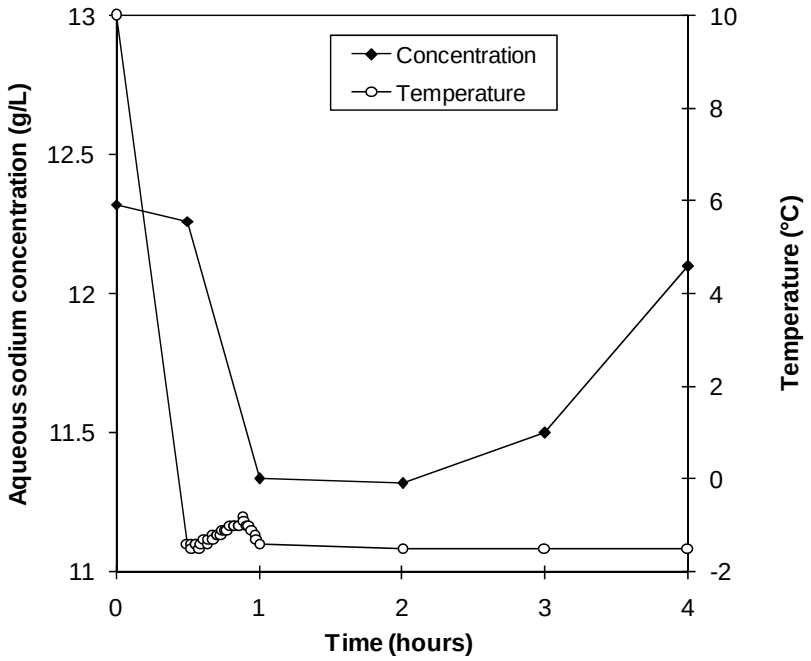

Figure 32: Aqueous sodium concentration and temperature change over time for a synthetic brine

In summary, the same nucleation temperature was achieved with both the synthetic brine and the real brine. The salt formed under EFC conditions was identified as $Na_2SO_4 \cdot 10H_2O$ with a purity of 97.5% after no washing.

4.8 OBJECTIVE 3

4.8.1 The nature of the selenium impurity

Figure 33 shows that selenate is incorporated preferentially over selenite. Additionally, the selenate values are comparable to the results from the actual brine tests, whereas the selenite values are not. In the actual brine, a concentration of roughly 108 g/l of sodium sulphate, 90 g/l sodium chloride and 775 mg/l selenium produced an impurity of 2-3 g/kg of selenium in the sodium sulphate product salt.

Though this result was not exactly matched in the experiment, it can be seen that the selenate concentrations are the same order of magnitude as those found in the industrial brine. The discrepancies could possibly be attributed to a difference in the crystallization rate. The faster the rate of crystallization, the less accurate molecular recognition becomes. Accelerated growth increases the likelihood of selenate and sulphate ions being indistinguishable from each other from a crystallization point of view. This would result in a greater inclusion of selenate ions than at lower crystallization rates and correspondingly a higher selenium impurity.

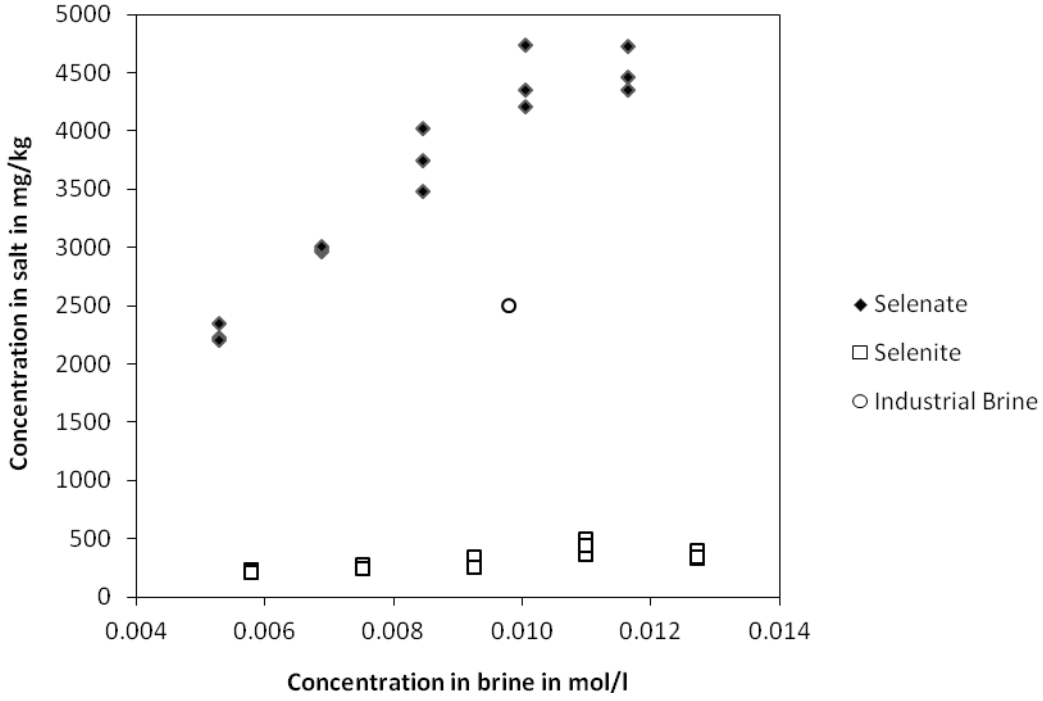

Figure 33: Comparison between uptake of selenate and selenite by sodium sulphate product

The selenium uptake in the case of the industrial brine was not replicated by the experimental brines. The solution containing only selenate resulted in selenium incorporation greater than that seen in the industrial brine, and vice versa for the solution containing only selenite. Though this can possibly be attributed to the differing crystallization rates between the industrial brine and the synthetic brine, it is also possible that the industrial brine contains selenium in both the selenate and selenite forms. Both selenate and selenite contribute to the total selenium concentration reported in the brine, but only the selenate has a significant impact on the purity of the product. In this way the selenium impurity in the sodium sulphate could be manipulated by changing the concentrations of sodium selenate and sodium selenite without changing the total selenium concentration.

Because selenate results in a much greater impurity uptake than selenite, it can be concluded that, in terms of inclusion, the selenate ion is of greatest interest. For this reason the selenium in the synthetic brines of further experiments will be in the form of selenate ions, contributed as sodium selenate.

4.8.2 Relationship between NaCl, Na_2SO_4, Na_2SeO_4 and selenium inclusions in the salt product

Figure 34 shows the impact of NaCl on the inclusion of selenium in the product sodium sulphate salt. The horizontal axis displays the concentration of sodium selenate in the mother liquor. The vertical axis represents the mass of selenium detected in the product salt. The legend to the right describes the concentrations of NaCl and Na_2SO_4 in g/l of the mother liquor. For example, the first entry reads 30 and 90. This means that the mother liquor had a sodium sulphate concentration of 30 g/l and a sodium chloride concentration of 90 g/l.

The results indicate that the relationship between selenium in the mother liquor and selenium in the product salt is linear for each brine composition. This can be seen in the trend that all data increase constantly in the y axis from left to right. This is expected since it is probable that an increase in the

concentration of a substance in the mother liquor will correspondingly result in an increased presence of that substance in the product salt.

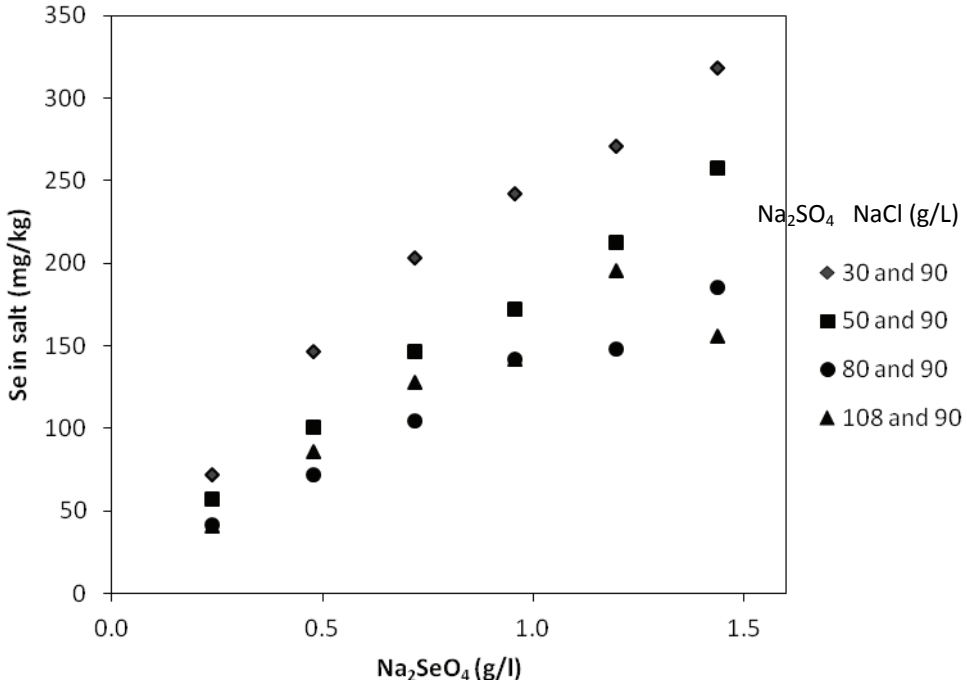

Figure 34: Effect of NaCl on the inclusion of selenium in product sodium sulphate salt

Additionally, it can be seen that an increase in the concentration of sodium chloride relative to sodium sulphate and sodium selenate results in an increased amount of selenium in the product salt. This is potentially due to the increased concentration of sodium ions promoting the uptake of selenium in the sodium sulphate salt. It is possible that the selenium is crystallizing in small amounts along with the sodium sulphate in the form of sodium selenate. If this is the case, the increased presence of sodium ions from the sodium chloride could result in the common ion effect playing a role in the selenium inclusion. In this case, one salt must be more affected by the presence of the common ion more than the other.

The common sodium ion serves to decrease the solubility of sodium sulphate. Thus, for a fixed cooling rate, the rate of crystallization will increase with the addition of sodium chloride. As has already been theorised, an increased crystallization rate could result in an increased selenium uptake. This occurs because, at faster crystallization rates, the molecular recognition process is more prone to failure. That is to say; the growing sodium sulphate crystal is more likely to mistake a selenate ion for a sulphate ion under conditions of rapid growth.

Another possible reason for the increased incorporation of selenium is the altered ionic strength of the mother liquor. As sodium chloride is added, not only is the concentration of sodium ions increasing, but the ionic strength of the solution is also increasing. This may impact on the solubility of sodium sulphate and sodium selenate in such a way as to promote the uptake of selenium.

4.9 OBJECTIVE 4

4.9.1 Factors affecting ice-salt separation

Effect of agitation on ice-salt separation and ice purity

Before this aim could be investigated, the repeatability of results obtained from the experimental setup was investigated. The repeatability for the production of product crystals, which included both ice and salt, was tested and the average mass yield was found to be 15.11% ±1.03%. The accuracy of this value indicates that the experiments are reproducible and that similar amounts of crystals are formed in repeat experiments.

Once the repeatability of the experimental setup and procedure was confirmed, the actual experiments focusing on the effect of agitation on the purity of the bulk ice produced could be investigated. Figure 35 shows the effect of agitation on the yield of ice and salt formed in an EFC process. There is no significant change in the yield of ice between experiments with agitation and experiments without agitation. However, the yield of salt ($Na_2SO_4 \cdot 10H_2O$) increases by a factor of 2.7 with agitation, showing that agitation releases some of the trapped salt incorporated within the bulk ice product thus improving the purity of ice. The agitation of the bulk ice suspends both the ice and trapped salt crystals thus allowing for easier gravitational separation to occur with the ice floating to the top of the crystallizer and the salt sinking to the bottom of the crystallizer.

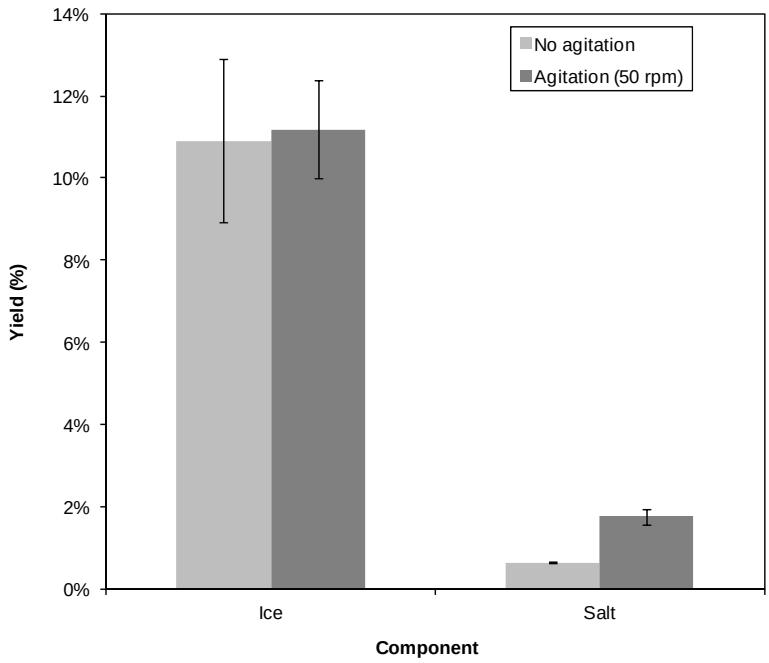

Figure 35: Yield of salt and ice for with and without agitation

Effect of vessel surface area on ice-salt separation and purity of ice

This section aims to determine the effect of increasing the surface area of a settling vessel on the purity of ice crystals formed under EFC conditions since a larger surface area should increase the voidage or reduce the contact points between the ice crystals and thus result in the release of more trapped salt. This would lead greater ice purity.

The difference in the settling rate of ice and salt obtained from repeat experiments in the settling vessels meant that there were significant errors when trying to separate and filter the ice and salt, as can be seen in Figure 36 and Figure 37. The errors were mainly due to the fact that, in some experiments, ice and salt both settled at the bottom of the vessel as shown in Figure 36. This was due to the salt crystals becoming entrapped in the ice, causing the ice to settle to the bottom of the vessel with the salt instead of floating to the top of the vessel. This observation confirms the importance of investigating the processes of ice growth in the EFC process, in order to ensure that the ice does, indeed, float to the top of the crystallizer.

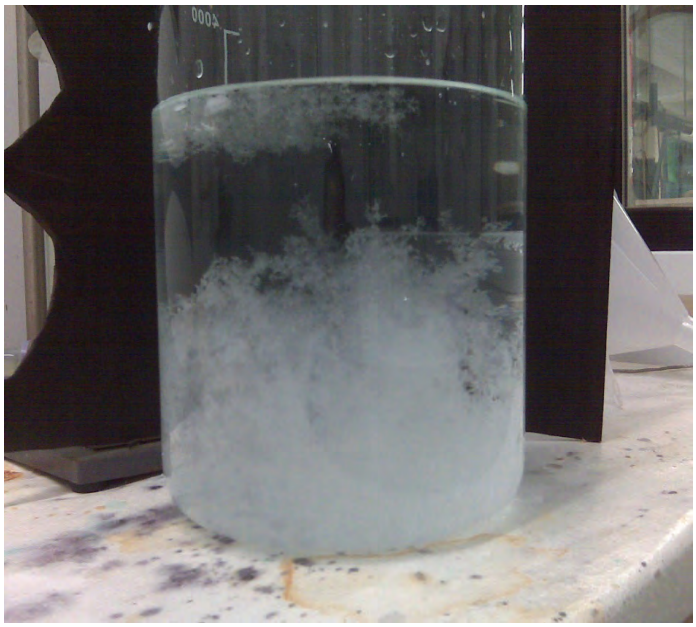

Figure 36: Ice and salt mixture at the bottom of the settling vessel

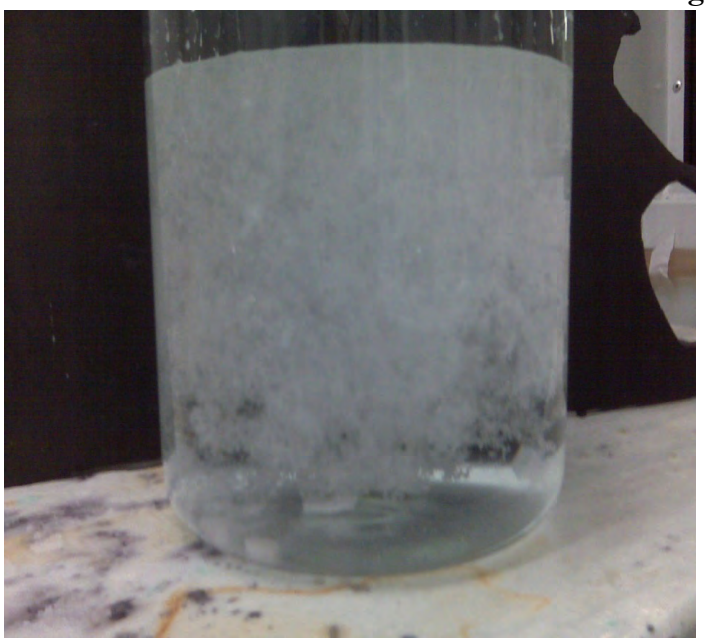

Figure 37: Ice and trapped salt at the top of the settling vessel.

This phenomenon made it difficult to distinguish accurately between ice and salt, and to recover all the ice from the experiment. As a result, some of the ice may not have been removed from the vessel and, in some cases a proportion of the salt may have been removed together with the ice. The removal of the ice and the salt from the settling vessel in Figure 37 is much easier due to the floating of the ice at

the top of the vessel. However, in this instance some salt was trapped with the ice product and thus the purity of the ice product was affected.

Figure 38 shows the effect of settling surface area on the concentration of sodium in the product ice formed under EFC conditions. Comparing the experimental results for the crystallizer and the other larger surface area vessels, a significant decrease in sodium concentration is observed. However, the concentrations for the 183, 236 and 650 cm^2 are relatively constant. This can be explained using the random loose packing theory which indicates that the packing of spheres is quantifiable. For example, the loosest way to pack spheres (random loose packing) will always give a density of ~55 per cent while the most compact way to pack spheres (random close packing) results in a maximum density of ~64 per cent (Song et al., 2008). The maximum random close packing density can be achieved by "agitating" the spheres. This same theory applies to the bulk ice, even though the ice crystals are not spheres. A larger settling surface area (smaller ice bed height) results in a closer and similar bed packing regardless of the ice bed height thus resulting in similar ice purities.

The initial concentration decrease between the results from the crystallizer (103 cm^2 settling surface area) and the larger surface area vessels (183, 236 and 650 cm^2) is because of a slight agitation as a result of the transfer of the contents from the crystallizer to another, larger vessel. This is the only difference between these experiments. Therefore, it can be seen that agitation improves the purity of ice, even if the agitation is minimal.

The ice collected from the crystallizer experiment has a higher concentration of Na^+ ions when compared to the larger surface area vessels. This is because the ice product for these experiments was not added to another vessel but instead the contents were collected directly from the crystallizer and hence there was no "extra" agitation. It is hypothesized that a combination of agitation and an increased settling surface area will result in an improved purity of ice. However, this needs to be investigated further.

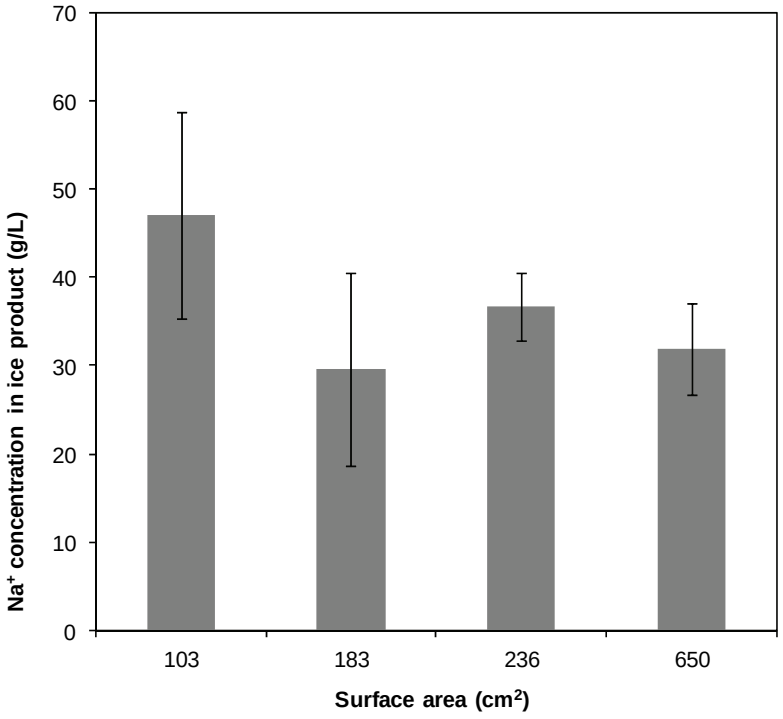

Figure 38: Sodium concentration in ice as a function of the surface area of a settling vessel. Error bars indicate the results of repeated experiments.

Another aspect to consider during these experiments is that of the yield of ice and salt, since ideally there should be no loss in product when purifying ice. The bars in Figure 39 show that the surface area of a settling vessel has little effect on the order of magnitude and maximum and minimum yields for ice and salt formed during the experiments. However, the error associated with these experiments is significant and is different to the initial experiments which had an error of 15.11% ±1.03%. This is due the occurrence of inadequate separation with some experiments thus resulting in varying amounts of ice.

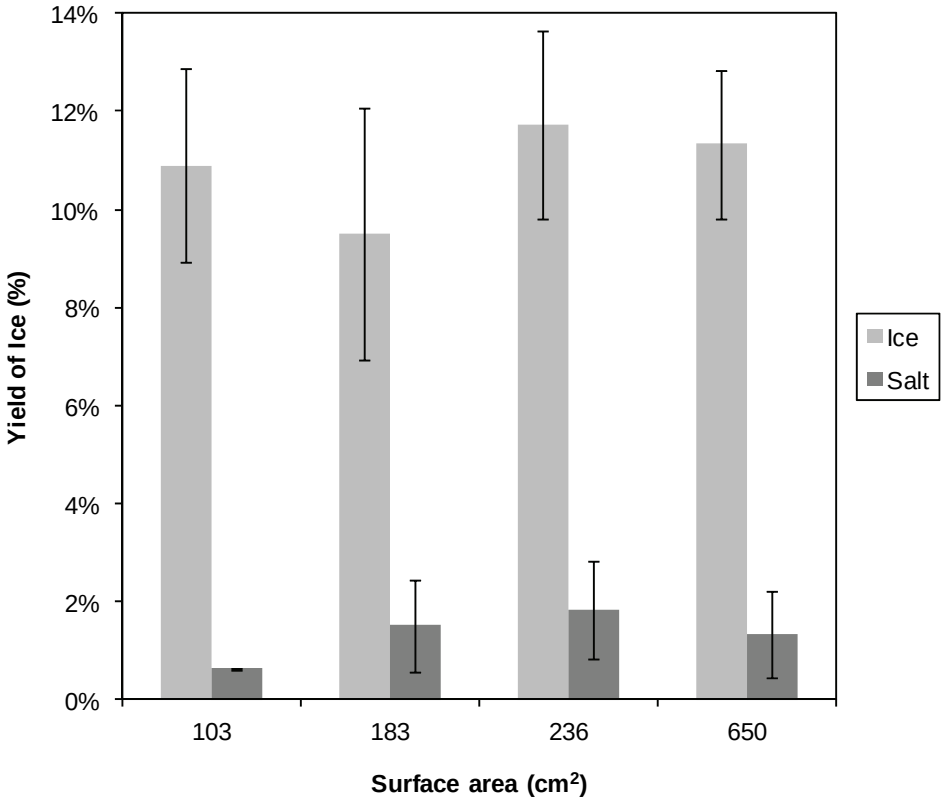

Figure 39: Yield of ice crystals as a function of varying vessel surface areas. Error bars indicate the results of repeated experiments.

The continuous removal of small amounts of ice during a period of approximately 8 minutes was also likely to be a reason for this error since this resulted in a greater loss of ice because of human error. Also, although the experiments were conducted in a temperature controlled environment, the temperature of the cold room fluctuated by approximately 2.3°C and the room went through defrost cycles (dotted rectangle in Figure 40) which resulted in even larger temperature fluctuations in the room. These temperature fluctuations affected the filtration temperature and thus, during some experiments, the ice product melted. This provided an additional contributing factor to this large error.

The yield of salt obtained from the 183, 256 and 650 cm^2 vessel experiments was higher than that of the crystallizer (103 cm^2) due to the slight agitation received from the addition of the contents to the larger surface area vessels.

The difficulties encountered with the removal of ice and salt from the vessels was the main reason for the large observed errors. The errors for the salt are particularly large because of the difficulty in removing the salt from the vessel and also because the amount of salt is far less that the amount of ice formed, meaning that small salt losses resulted in an amplified error. This is not the case for the

crystallizer, simply because in these experiments the ice product was floating at the top as shown in Figure 37.

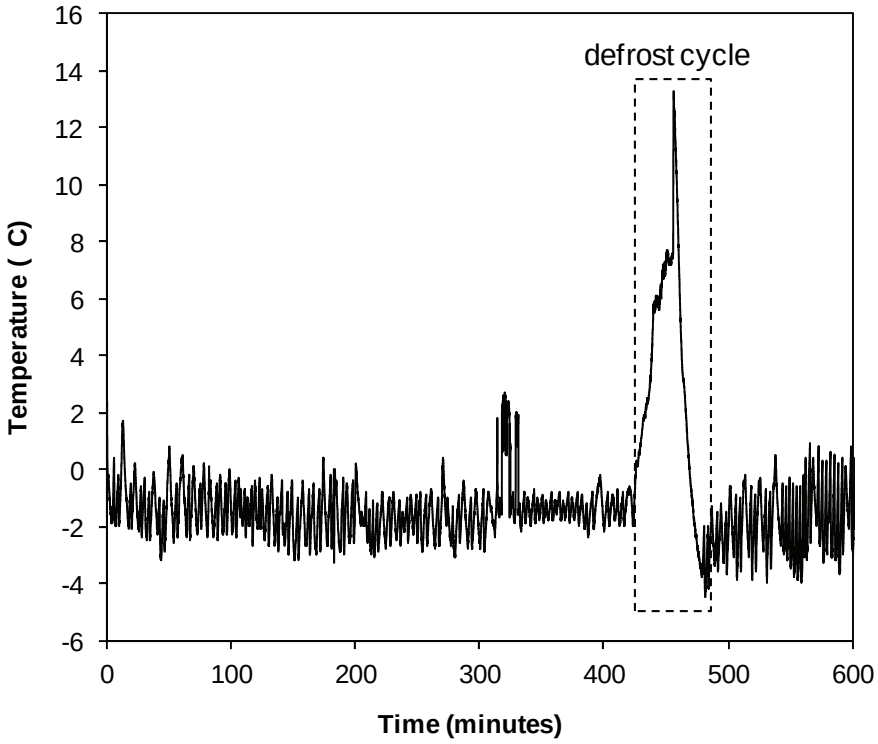

Figure 40: Cold room temperature fluctuations

Regardless, these experiments show that an increased settling surface area, as well as agitation of the ice-salt mixture, can result in a purer ice product. The accuracy of the results is likely to be improved if the separation process incorporates both agitation and a larger settling surface area in one piece of equipment together with better temperature control. The automation of the separation process would also likely improve the accuracy of the results.

In summary, it can be seen that the purity of the ice depends on efficient ice-salt separation. The ice product traps salt crystals thus resulting in low purity ice. The agitation of the ice product improves the purity of ice by removing any trapped salt. Also, the increase in settling surface area does have an effect on the ice purity but it is not as significant. However, it is thought that this is as result of the settling vessel having no agitation mechanism. Therefore, a settling vessel with a greater surface area and agitation is likely to result in a purer ice product.

4.9.2 Fundamental ice crystallization

Filter calibration

In order to obtain quantitative data i.e. convert image colour to refraction angle, the colour filter was calibrated. The refraction angle at any point in the Schlieren image was quantified by first identifying the location within the base image that had the same pixel intensity as the point of interest using Matlab. This was done by capturing the full image of the filter from which a transmissivity function was generated and used for calculation of refractive index

Figure 41 shows the full image of the filter with the corresponding transmissivity from which the quantitative analysis is done.

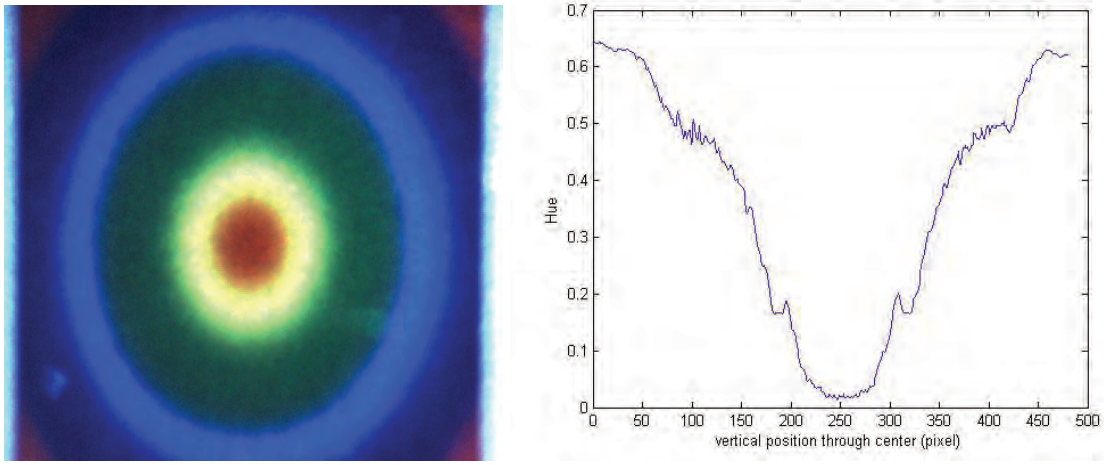

Figure 41: Image of 2-D axisymmetric colour filter and the corresponding transmissivity function

The orientation of the cell and direction of ice growth in the images obtained for data analysis is shown in figure 8.Since the centre of the filter is red, all base images (raw) are red as deflection of light at the through the test region is zero. The ice grown from solution was opaque hence the Schlieren images were dark as light could not pass through. Figure 42 shows the opaque ice displayed as dark part of the Schlieren images.

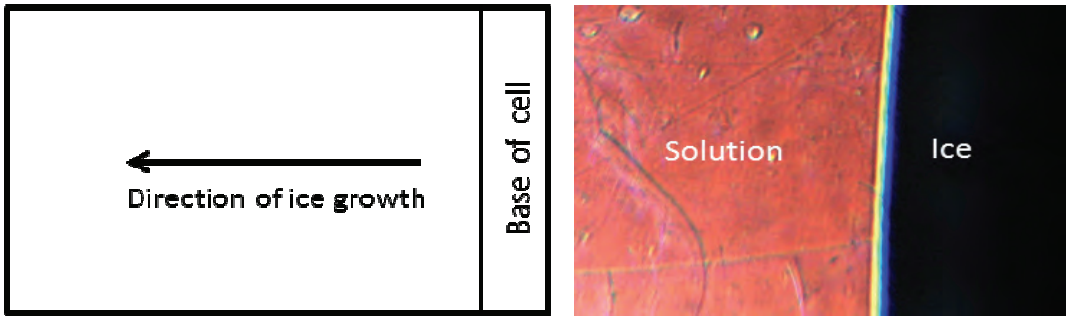

Figure 42: Image of ice growing in solution as captured by a CMOS camera

In all experiments, two systems were considered namely pure water, where a change in refractive index was due to temperature, and a salt solution where variations in refractive index were due to the coupled effect of both temperature and concentration.

Growth of ice and morphology

Ice was crystallized from both pure water and salt solution ($MgSO_4$ 10wt%). Ice crystals exhibited morphological instability in both systems. Dendrites were observed at the early stages of growth after nucleation and before melting. After dissolution of the dendrites, ice growth was smooth. The formation of dendrites was caused by high supersaturation of the supercooled solutions.

Dendritic growth is generally acknowledged to be controlled by a diffusion limited process. From Figure 43 and Figure 44, it can be seen that the dendrites in pure water were more spread out than in those in salt solution (Figure 45 shows a zoomed in section of the salt solution showing dendrites, although smaller in size). For ice growing in pure water, the growth rate of dendrites was controlled by

the diffusion of latent heat from the advancing solid-liquid interface as the ice grew towards regions (cold) of high supersaturation.

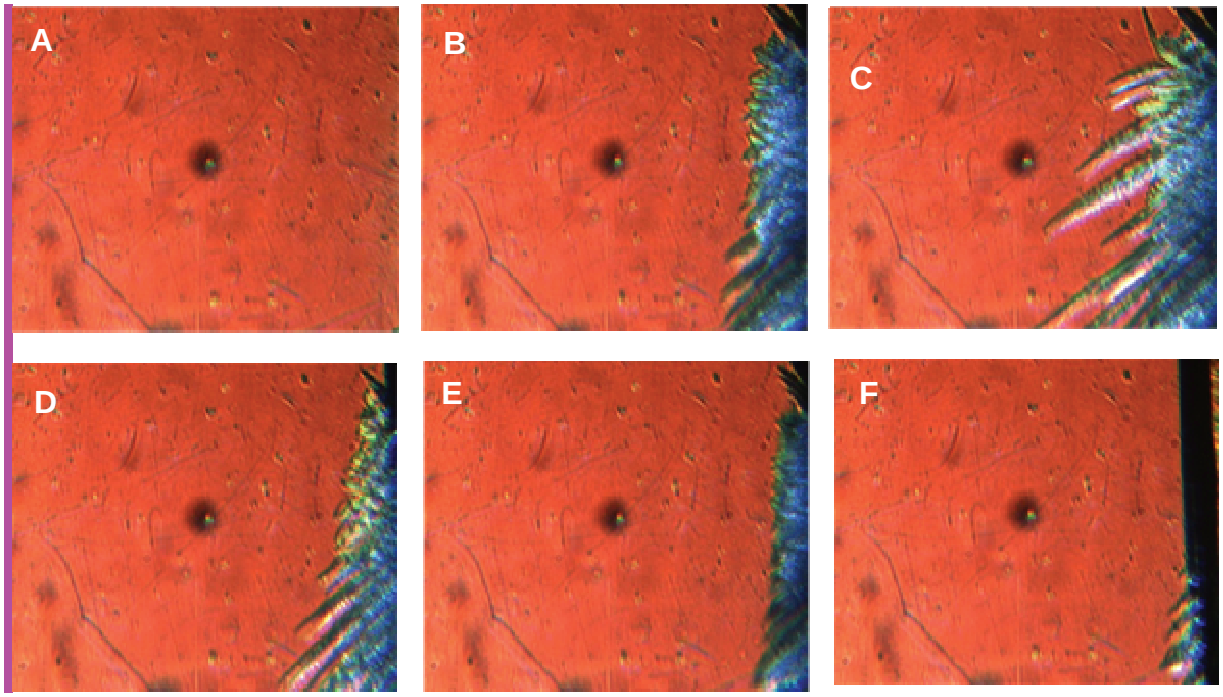

Figure 43: Morphological instability of ice in pure water: base image (A), sequential appearance of dendrites (B&C), receding dendrites (D-F).

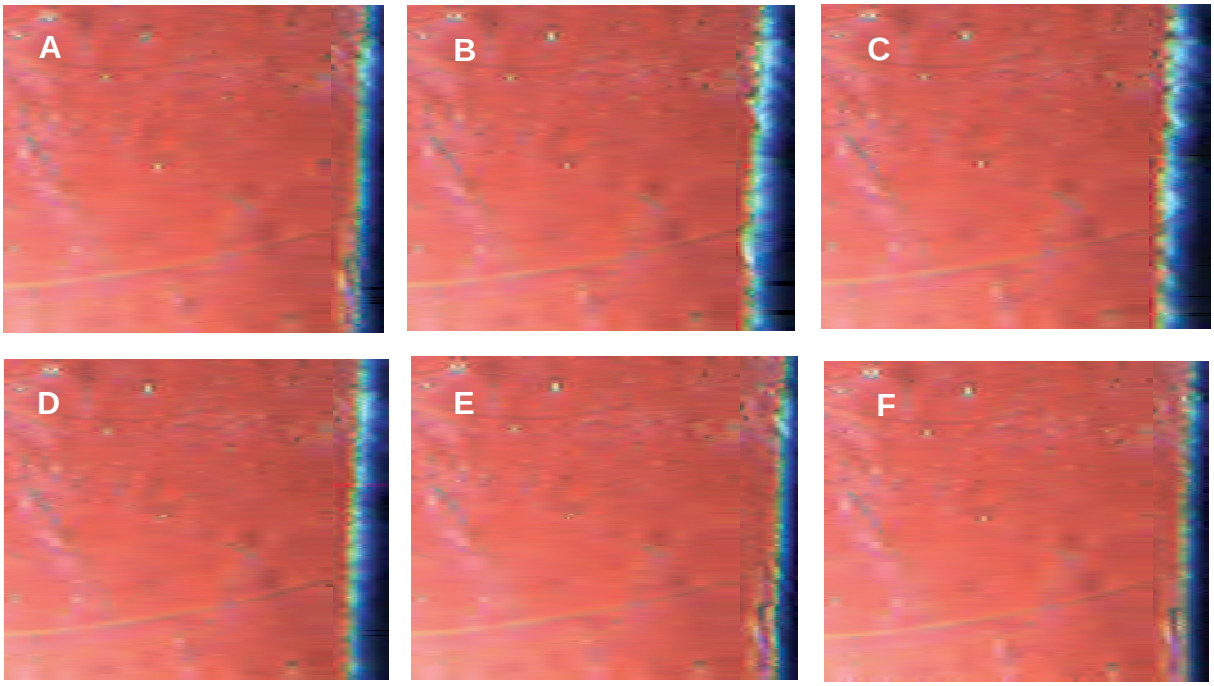

Figure 44: Morphological instability of ice in a 10wt% $MgSO_4$ solution: base image (A), sequential appearance of dendrites (B&C), receding dendrites (D-F).

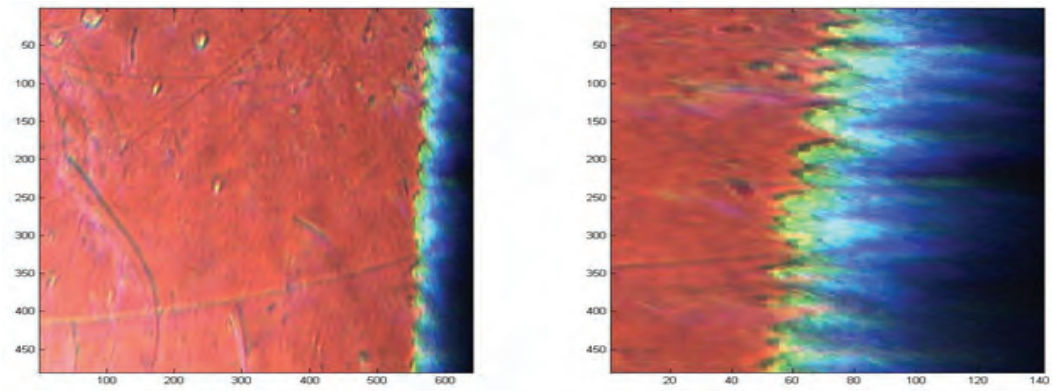

Figure 45: Zoomed in section of ice growing in a 10wt% $MgSO_4$ solution showing smaller dendrites.

Unlike dendrites in pure water, propagation of dendrites in salt solution is influenced by both the release of latent heat and the diffusion of solutes from the ice. The solutes rejected from the ice accumulate at the surrounding interfacial region and slows the diffusion of heat away from the ice into the bulk solution thereby slowing the dendritic growth. It has been reported that impurities can be trapped between dendritic ice crystals thus resulting in poor quality water (Shirai, 1999).

Concentration and temperature gradients

During crystal growth, temperature and concentration gradients are present in the bulk solution and in the interfacial region around the crystal due to heat and/or mass diffusion which influences the growth of a crystal. These gradients are related to the change in refractive index. The change in refractive index is represented by the colour change in the images. Figure 46 shows the variations in the refractive index represented by a colour scale as indicated on the colour bar with a certain colour corresponding to a magnitude of change in refractive index. It can be seen in the figure that across the interfacial region, refractive index gradient changes as a result of diffusion of both heat and solutes. The values corresponding with the solid phase and the noise in the bulk phase are meaningless and not regarded.

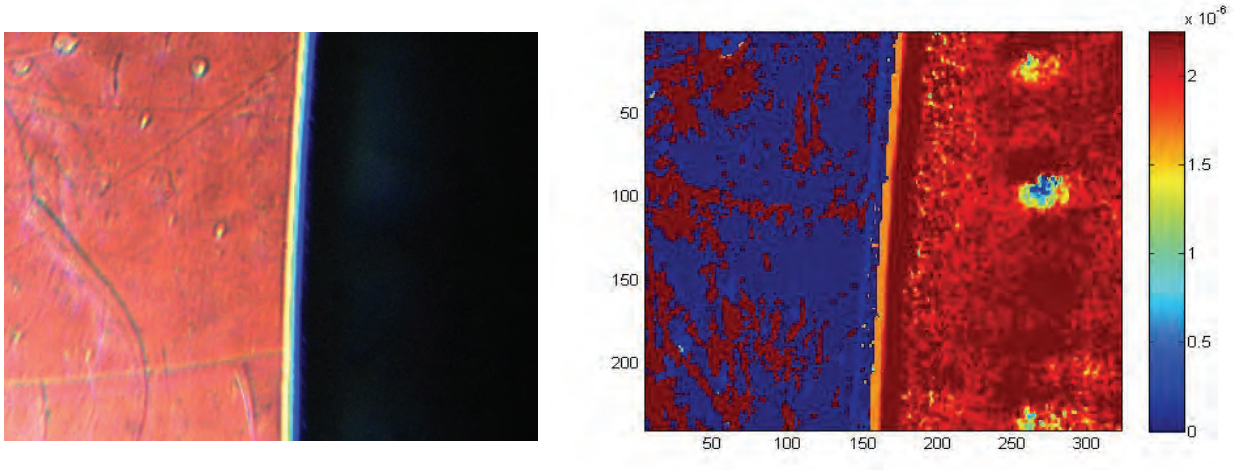

Figure 46: Ice growing in 10wt% $MgSO_4$

With the variation in refractive index, the temperature and concentration gradients can be calculated. Part of future work is to decouple temperature and concentration for ice growing in solution. This is

because colour Schlieren deflectometry is limited to either temperature or concentration measurement. Decoupling will involve the incorporation of another technique such as the use of thermochromic liquid crystals which can be used to measure temperature.

Thickness of boundary layer

The thickness of the boundary layer is given by the diffusion distance and it depends on the growth rate, in the case of crystallization, and on the rate of dissolution in the case of melting. Figure 47 shows the variation of boundary layer thickness with time of ice growing in a 10wt% $MgSO_4$ solution and pure water respectively. It can be seen that the boundary layer of ice growing in solution is thicker than ice growing in de-ionised water. This is could be because the boundary layer of ice growing in solution is characterised by both mass (solute) and heat diffusion from the solid phase into the bulk solution whereas ice growing in pure water, the boundary layer is only influenced by heat diffusion.

The average thickness of boundary layer of ice in solution between the times 525 to 1572 seconds after nucleation was 0.309 mm and that of ice in de-ionised water was 0.096 mm.

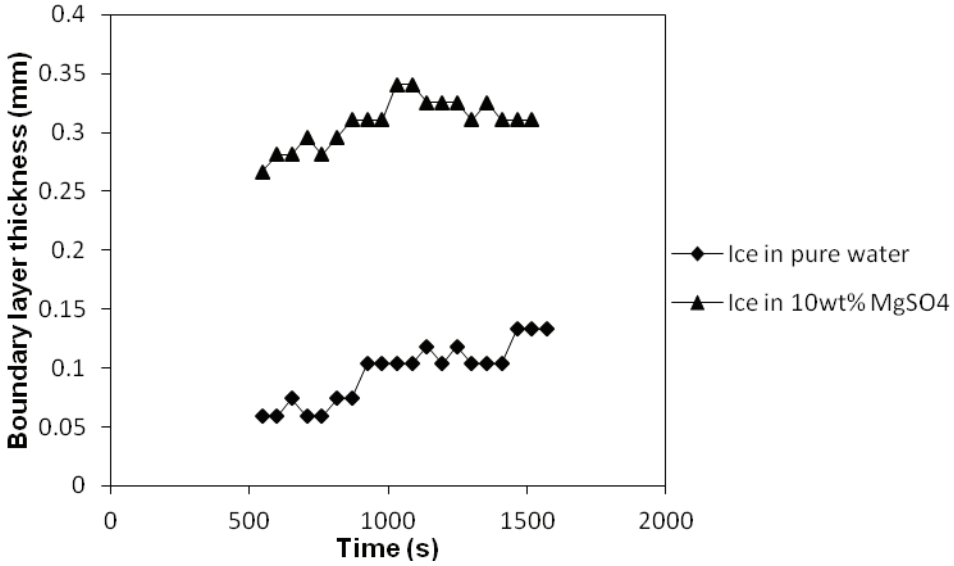

Figure 47: Thickness of boundary layer of ice growing in a 10wt% $MgSO_4$ solution and pure water

However, when compared to ice melting in solution of the same concentration (10wt% $MgSO_4$), the thickness of the boundary layer of ice growing in solution was smaller. Figure 48 shows the thickness of the boundary layer during melting of ice increasing sharply from 0.074 to 0.429 mm in 360 seconds as the system is heated up. When ice forms in pure water, latent heat of crystallization is released from the ice phase into the surrounding liquid. However, when it forms from a salt solution, not only is the latent heat of crystallization released but the solute diffuses away from the growing ice into the solution. The difference in boundary layer thickness can also be attributed to the coupled effect of both heat and solute diffusion in the case of growing ice solution compared to ice growing in pure water which was affected by heat diffusion only. For ice growing in a salt solution, it means that if the migration of solute from the ice interface into the bulk solution is slower than the crystal growth rate, solute will accumulate in the interfacial region within the boundary layer. This will subsequently result in solute incorporation into the growing ice crystal, ultimately affecting the purity of ice.

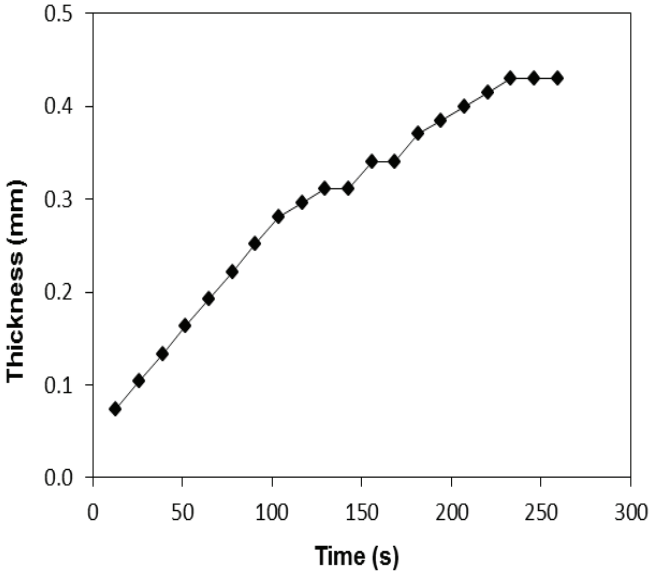

Figure 48: Thickness of boundary layer of ice melting in 10wt% $MgSO_4$

Growth rate and thickness of boundary layer

Between 525 to 1572 seconds after nucleation, the average growth rates of ice in de-ionised water and 10 wt% $MgSO_4$ solutions were 3.199 and 2.053 μm/s**.** During this period, the thickness of the boundary layer varied slightly. As the thickness of ice increased, the thicknesses of the boundary layers increased slightly as shown in Figure 49 and Figure 50. Figure 51 shows the thickness of the boundary layer as the ice grows in the 10 wt% $MgSO_4$ solution.

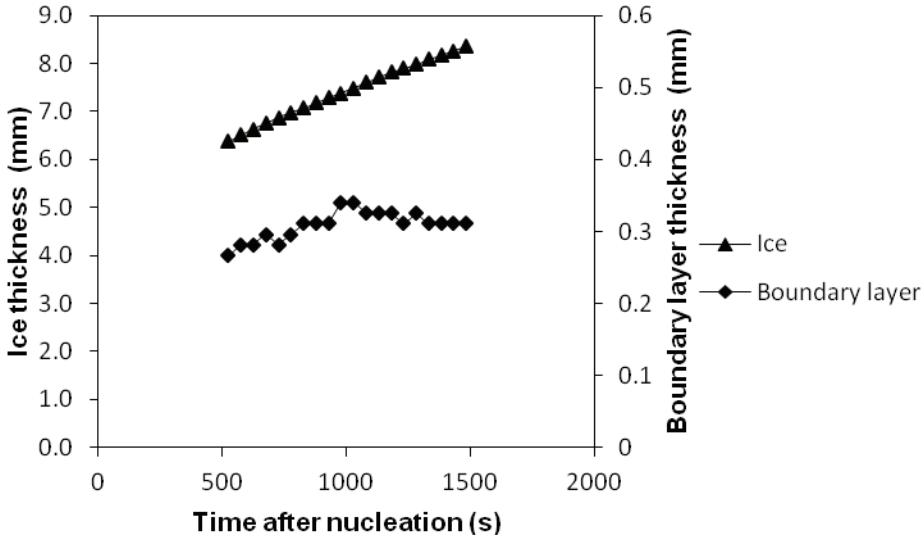

Figure 49: Thickness of ice and boundary layer of ice growing in 10wt% $MgSO_4$

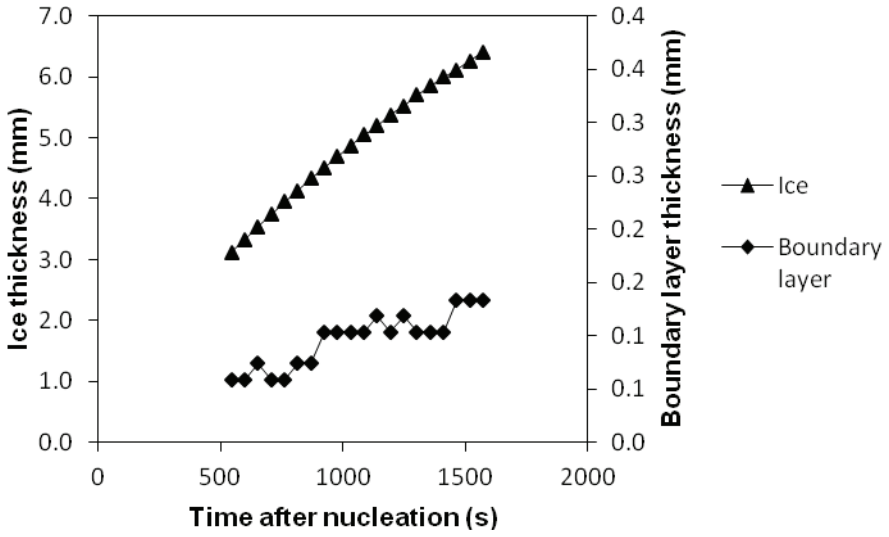

Figure 50: Thickness boundary layer of ice growing in pure water

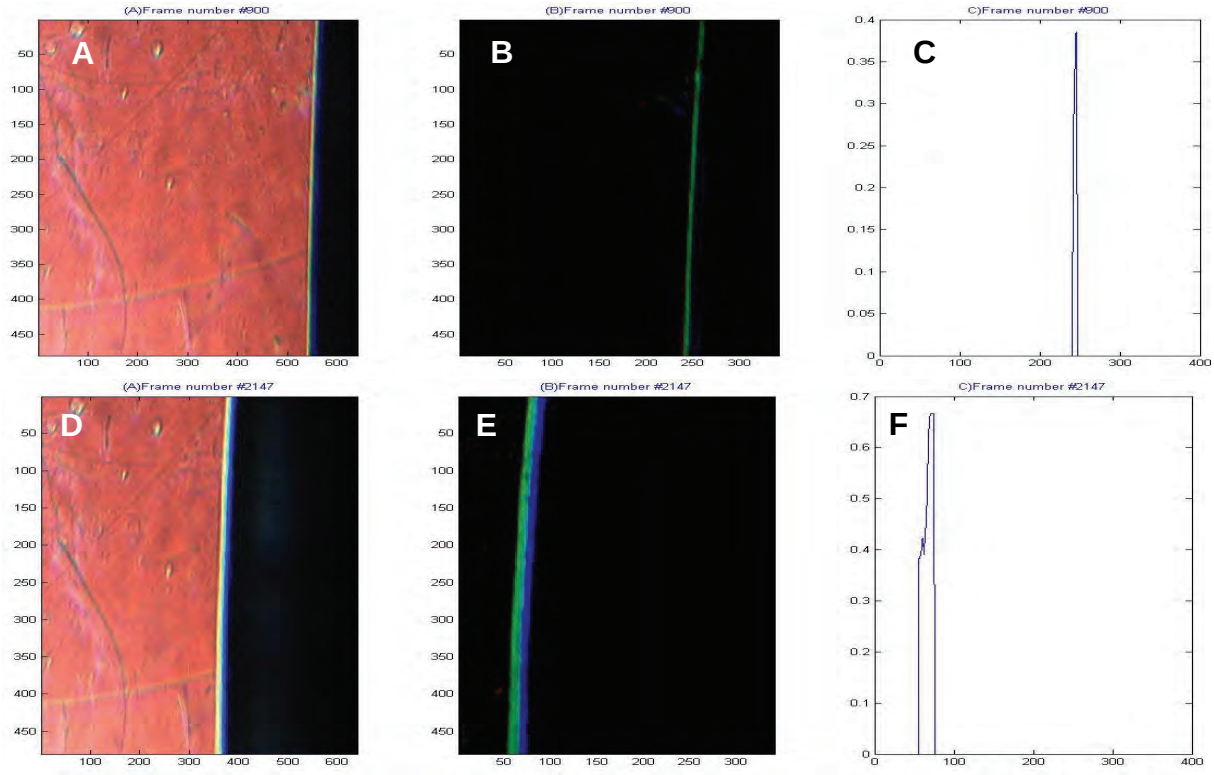

Figure 51: Thickness of boundary layer of ice growing in salt solution: thickness of ice after 14 minutes of nucleation and growth (A), boundary layer (B), changes in hue value along 250 pixel vertical axis (C), 24 minutes of nucleation and growth (D-F, same as A-C)

Diffusion

Figure 52 shows the ice crystal growing in a 10wt% $MgSO_4$ solution. Image (C) shows part of the solid-liquid boundary. It can be seen that the surface of the ice crystal is not smooth. The non-uniformity of the surface is due to diffusions of heat and solutes from the ice into the bulk solution.

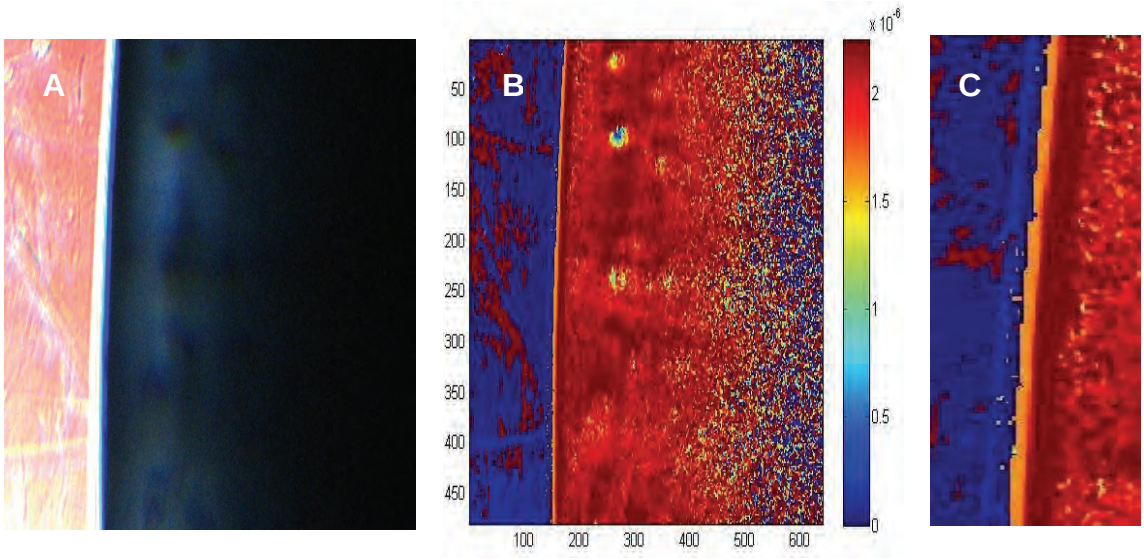

Figure 52: Ice crystal showing non-smooth interface

In the current set-up, the diffusion rates obtained during crystal growth were not detected due to the sensitivity of the equipment. However, during ice melting, diffusion rates were detected as can be seen in Figure 53 and Figure 54 . In order to clearly observe thermal diffusion, the background colour was removed as shown in images (B) and (E) of Figure 53. Images (C) and (F) of the same figure show the change in hue along the horizontal axis at 250 pixels which was used to calculate the rate of diffusion. When the temperature of the cooling unit was raised from -20°C to 10°C, the rate at which the heat diffused from the thermal boundary layer into the bulk solution was 0.0538 mm/s.

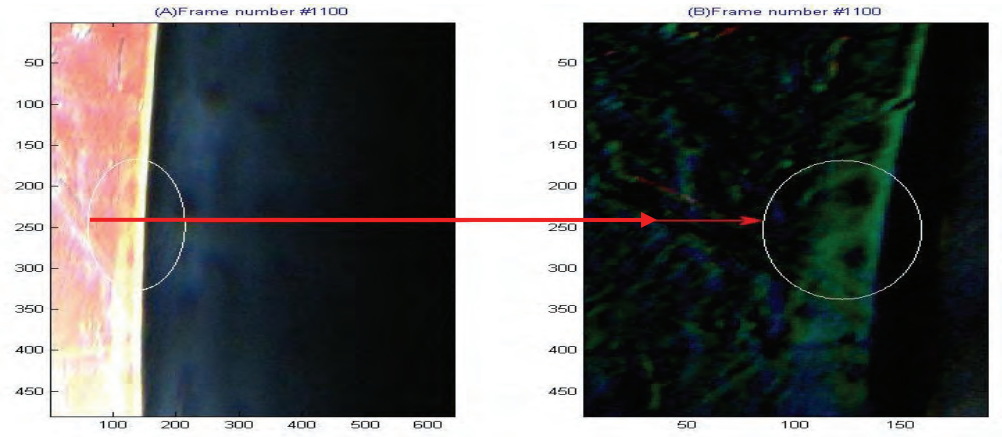

Figure 53: Heat diffusion during melting of ice in 10wt% $MgSO_4$

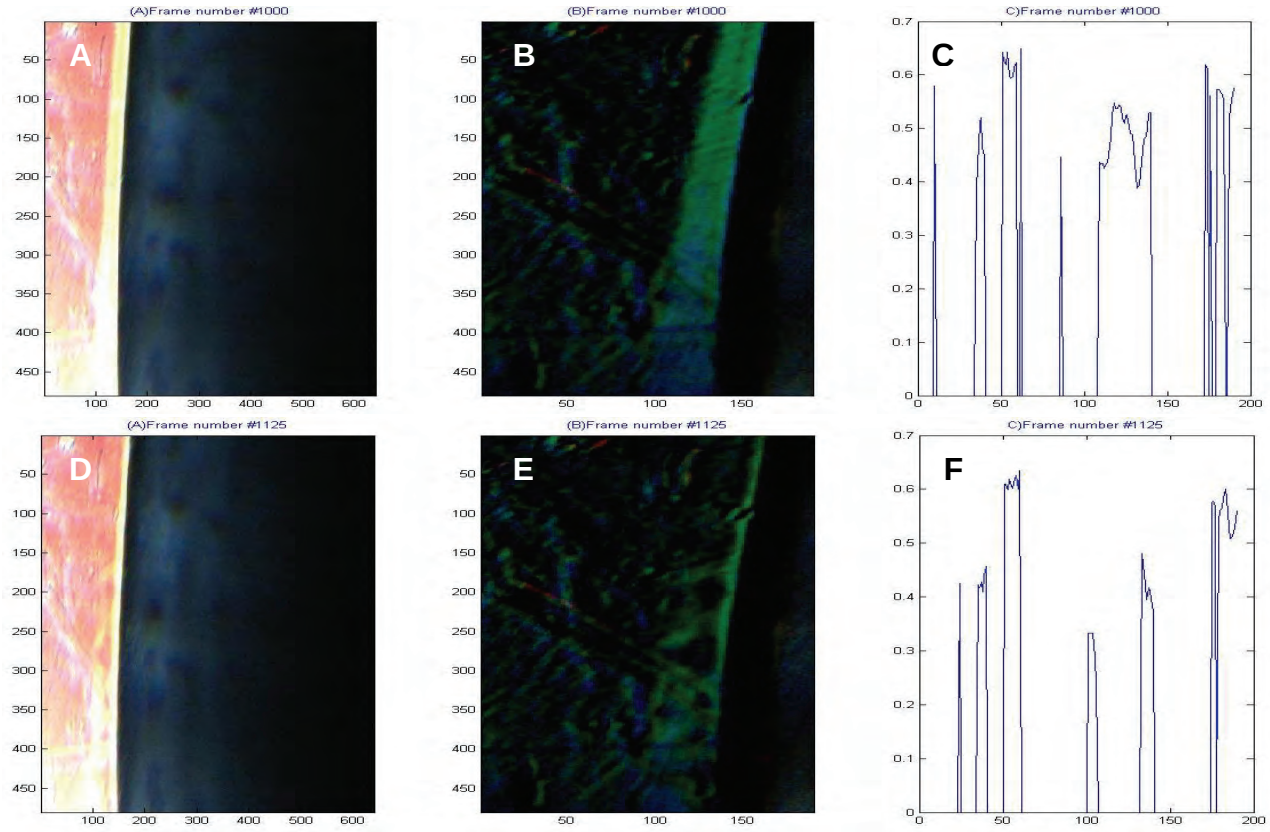

Figure 54: Heat diffusion at the interface before melting of ice (A-C) and after melting of ice (D-F); image of ice(A&D), thermal boundary layer (B&E), changes in hue value along 250 pixel (C&F).

In summary, this work has shown that ice crystallization is an extremely complex process that is not yet well understood. However, these preliminary results have generated some important knowledge about mechanisms of ice crystallization under EFC conditions. Future works will involve measurement of coupled heat and mass diffusion rates during crystal growth and a comparison of the boundary layer thickness and morphology of ice growth in different salt concentrations and at different growth rates. This will aid in the understanding of the effects of growth rates and diffusion processes on the boundary layer thickness and ice morphology which in turn affects the quality of ice crystals.

4.9.3 Ice washing

The concentration changes of the major components present in melted ice after washing with de-ionised are shown Figure 55. The product ice was formed during a freeze crystallization process of an inorganic brine and only ice was formed because the brine was too dilute for salt formation to also occur. The concentration limits in the melted ice are within acceptable South African water drinking standards after one wash (DWAF, 1996). These results indicate that washing can significantly reduce the entrainment of the brine with the ice crystals and also indicated that the impurities were not part of the crystal.

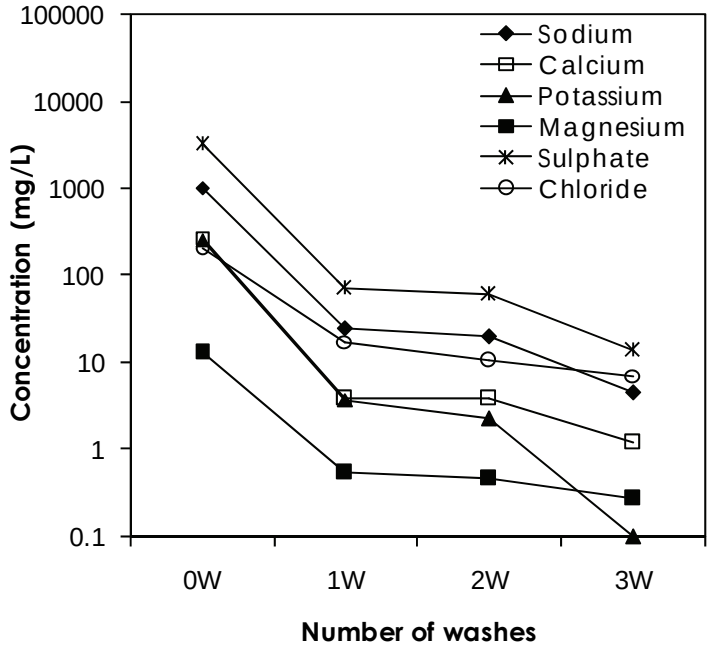

Figure 55: Change in ion concentrations for ice as a function of washes

Thus, the best strategy to improving the purity of ice formed under EFC conditions involves the incorporation of agitation in a settling vessel with a large settling surface area and washing of the ice crystals, as indicated Figure 56.

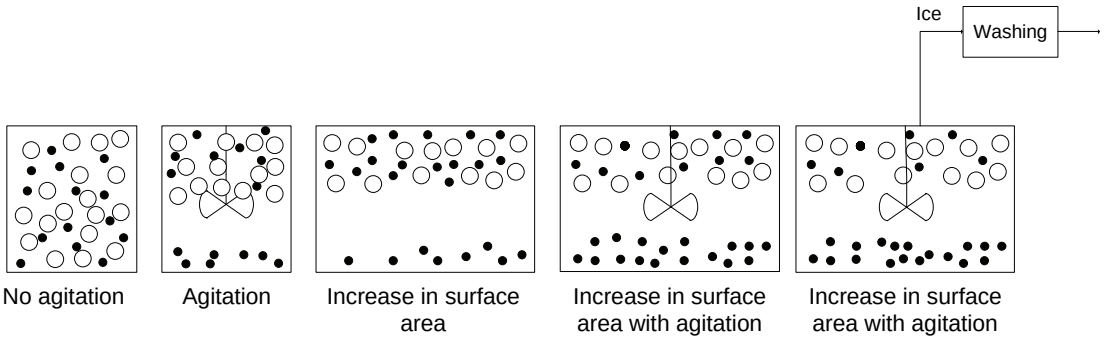

Figure 56: Strategy to improve ice purity in an EFC process

4.10 OBJECTIVE 5

4.10.1 Effect of operating temperature on yield

The effect of temperature on yield and purity in eutectic freeze crystallization processes appears at first glance to be a simple and straightforward relationship. In some cases, this is true. However, there are many factors that the operating temperature influences, both directly and indirectly, and hence it is worthy of investigation.

Previous work with sodium carbonate systems indicates a eutectic temperature of -2.1°C (van Spronsen, 2010). However, preliminary experimental runs showed a large depression of this eutectic, with the first signs of ice appearing in the system at -9.7°C. By modelling the cooling of the brine using OLI Stream Analyzer (2012), it was shown that this behaviour is the result of impurities present in the

brine, namely sodium chloride which results in a freezing point depression (Figure 57). These calculations are necessary for any eutectic freeze crystallization process, as it determines the theoretical operating temperature minima for salt and ice production. Thus, using thermodynamic modelling calculations with existing databanks of physical properties, it is possible to predict how temperature will affect yield.

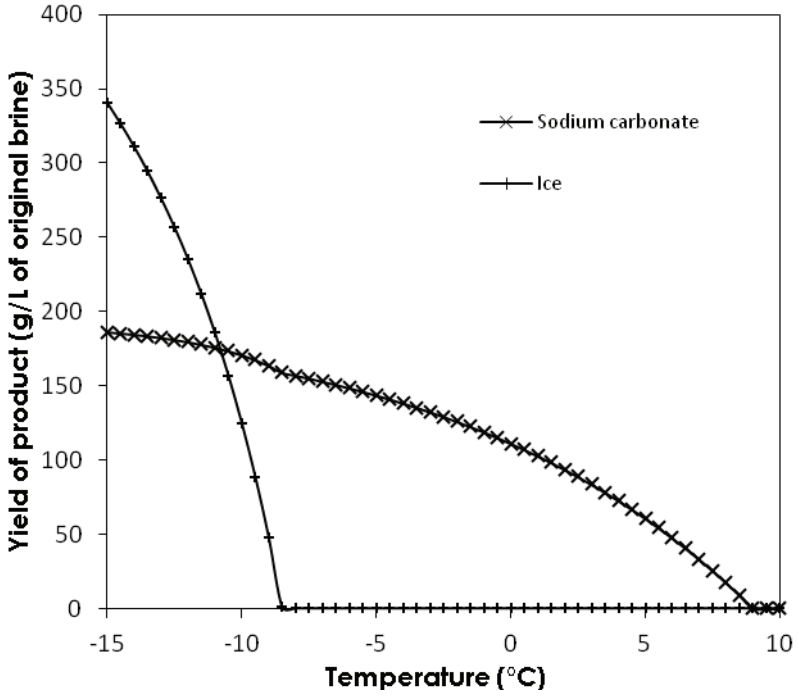

Figure 57: Theoretical modelling of alkaline wastewater brine

In practice, the measured eutectic temperature is -9.7°C, compared to the predicted value of -8.5°C. Additionally, yields are slightly less than predicted thermodynamically. However, this is to be expected if the predicted yield curve shifts to align with the actual eutectic point. Furthermore, the kinetic aspects of the system must be considered, especially as equilibrium is approached when growth rates will be at their slowest. The end result of this analysis is that, although theoretical modelling software is useful for providing first estimates of saturation and eutectic temperatures, and yields thereafter, actual operating temperatures and yields may be quite different due to kinetic factors.

For the first test run at 1°C, the full mass balance is represented schematically in Figure 58. In the figure, the width of the arrows is proportional to the mass flow rate of each stream.

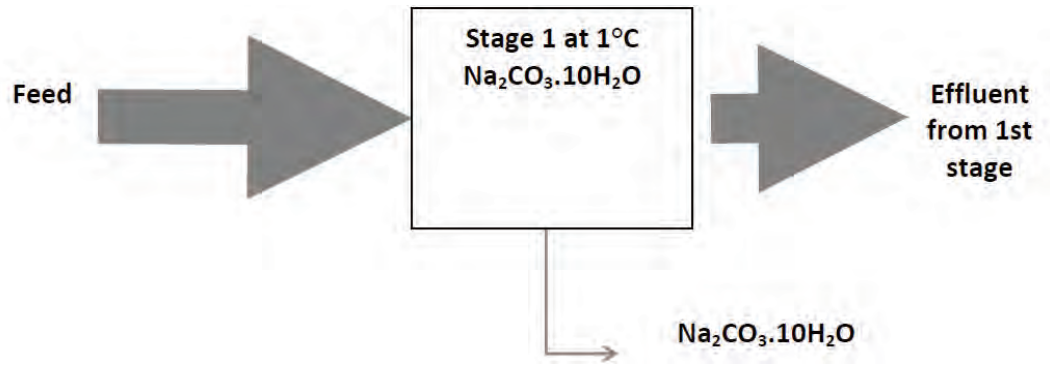

Figure 58: Mass balance for the test run at 1°C

The full mass balance is given in Table 12. From both Figure 58 and Table 12, it can be seen that the brine volume reduction is minimal. After 2 hours, the yield of salt is only 56 g, compared to the 218 g predicted at theoretical equilibrium, in other words, 26% of the equilibrium yield. This clearly indicates, not only that equilibrium has not been attained after 2 hours, but also that the time to reach equilibrium at this very small supersaturation (driving force) is likely to be much longer than a few hours.

Table 12: Mass balance for the test run at 1°C

	Mass in g
Brine feed	**1132**
Water in feed	**962**
Stage 1 operated at 1 °C	
Ice recovery	**0**
$Na_2CO_3 \cdot 10H_2O$	**56**
Effluent out of Stage 1	**1028**

For the second test run at -4°C, the full mass balance is represented schematically in Figure 59.

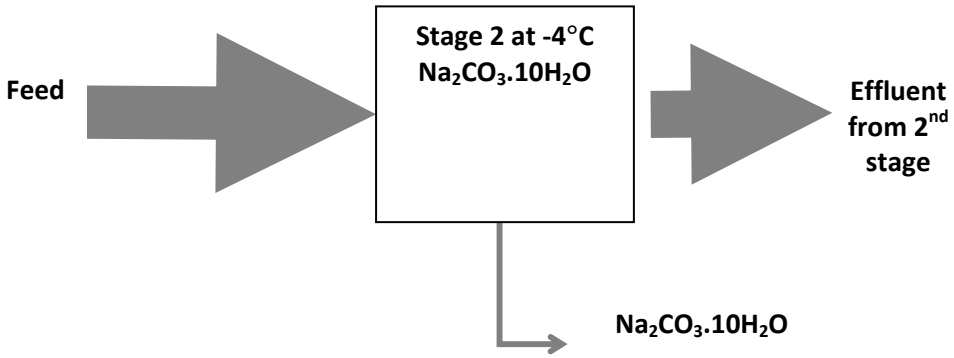

Figure 59: Mass balance for the test run at -4°C

The full mass balance is given in Table 13. From both Figure 59 and Table 13, it can be seen that the volume reduction of the incoming effluent feed has slightly improved by operating at -4°C. After 2 hours, the yield of salt is 128 g, compared to the 248 g predicted at theoretical equilibrium. This is 52% of the equilibrium yield, compared to only 26% when operating at 1°C. This indicates that, although equilibrium has still not been attained after 2 hours, the system approaches equilibrium more rapidly due to the slightly higher driving force imposed by operating at the lower temperature.

Table 13: Mass balance for the test run at -4°C

	Mass in g
Brine feed	**1134**
Water in feed	**963**
Stage 2nd operated at -4 °C	
Ice recovery	**0**
$Na_2CO_3.10H_2O$	**123**
Effluent out of Stage 2	**1001**

For the third test run at -9.7°C, the full mass balance is represented schematically in Figure 60 and given in Table 14. From both Figure 60 and Table 14, it can be seen that operation at -9.7°C results in the recovery of both ice and salt. The ice recovery at this temperature was found to be 26 g, 59% of the equilibrium yield, which is 44 g. The salt recovery was only 110 g, 40% of the equilibrium yield, which is 273 g. This is less than the salt recovered at -4°C, both in terms of absolute mass as well as in terms of percentage yield. This indicates that either the analysis of the brine is incorrect or that the thermodynamic modelling has underestimated the yield.

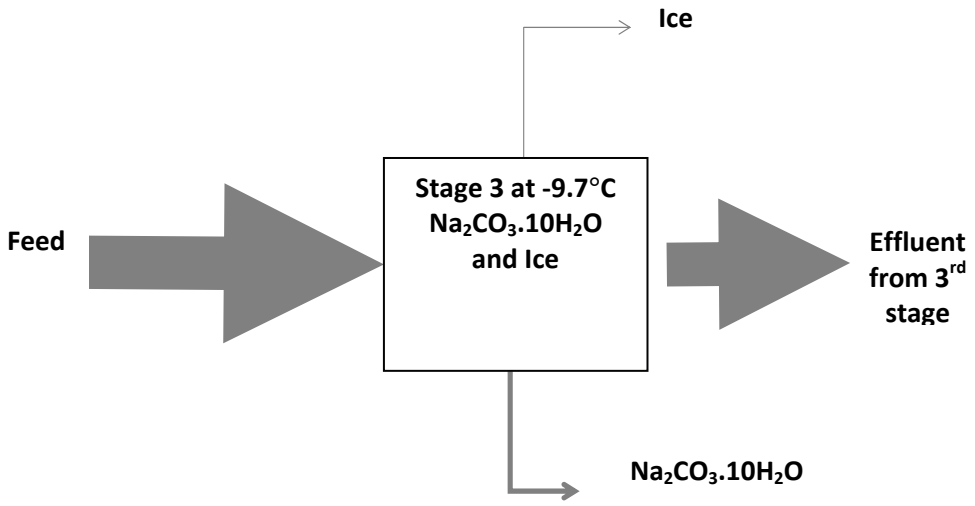

Figure 60: Mass balance for the test run at -9.7°C

Table 14: Mass balance for the test run at -9.7°C

	Mass in g
Brine feed	1134
Water in feed	964
Stage 3 operated at -9.7°C	
Ice recovery	26
$Na_2CO_3.10H_2O$	110
Effluent out of Stage 3	931

For the fourth test run at -11.3°C, the full mass balance is represented schematically in Figure 61 and given in Table 15. From both Figure 61 and Table 15, it can be seen that operation at -11.3°C results in the recovery of both ice and salt, but less salt than at -9.7°C. The ice recovery at this temperature was found to be 357 g, almost double the equilibrium yield of ice predicted. The salt recovery was only 41 g, much less than that at pre-eutectic temperatures, and far less than the predicted mass produced. A total brine reduction of 56%, on a mass basis, and 58% on a volume basis was achieved.

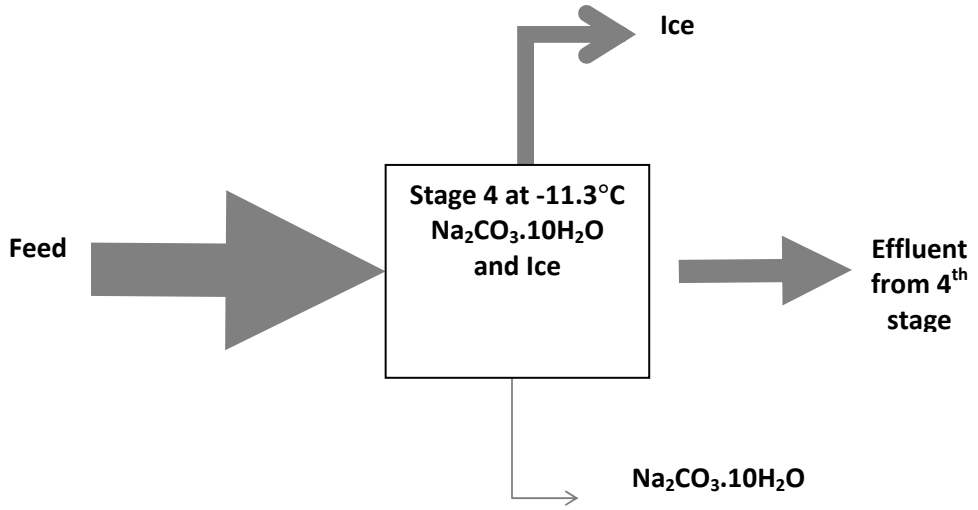

Figure 61: Mass balance for the test run at -11.3°C

Table 15: Mass balance for the test run at -11.3°C

	Mass in g
Brine feed	1133
Water in feed	962
Stage 1 operated at -9.7°C	
Ice recovery	357
$Na_2CO_3.10H_2O$	41
Effluent out of Stage 1	494

Unexpected behaviour is seen in the experimental results of mass-based salt yields from batch cooling crystallization experiments carried out on the alkaline brine. This behaviour is illustrated in Figure 62, which shows that, contrary to expectations, the mass of salt formed does not increase as the operating temperature decreases.

From Figure 62, it is apparent that, at the eutectic point and below, the yield of sodium carbonate decahydrate decreases substantially, relative to the yield at temperatures above than the eutectic temperature. Typically, it is expected that below the eutectic temperature, salt yield should further increase, as can be demonstrated by thermodynamic modelling of various systems. For example, in a mixed brine system (modelled in Figure 24 and Figure 57) recovery of salts in solution approach 100% as they crystallize out at their respective eutectic points.

However, as can be seen in Figure 62, the opposite effect is observed. The question as to why this contradictory behaviour is observed is currently the subject of on-going investigation. Analysis of the existing data can reveal some of the nature of the problem. For example, it is not likely not to be a kinetic problem of crystallization of a new hydrate or salt. It is known that, when operating at temperatures before the eutectic, there is a high salt content in the crystallizer, but at the eutectic temperature and below decreases, suggesting a dissolving of salt, and not a failure of the salt to nucleate and form.

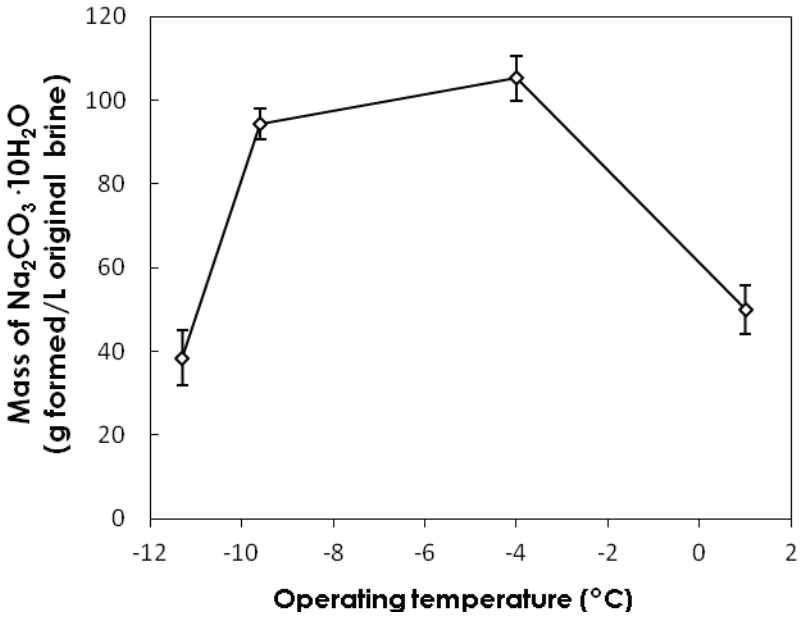

Figure 62: Mass yield of sodium carbonate decahydrate at varying operating temperatures

At operating temperatures far below the eutectic (for example, -11.3°C), the ice content of the crystallizer is substantial (greater than 40% solids content by mass), and it is possible that salt is trapped within the ice, resulting in lower salt yields. This has been observed to some degree in other studies; however, the resulting yields of salt at those low temperatures cannot be accounted for by capture within the ice. Further analyses of the purity of the ice is still pending, and should provide evidence to test this theory.

Another explanation for this behaviour may be found by comparing it to the behaviour of another system. In this case, the simplified solution chemistry for the crystallization of sodium sulphate decahydrate from aqueous solutions is given by

$$2Na^+ + SO_4^{2-} \rightleftharpoons Na_2SO_{4(s)} \quad \textbf{(13)}$$

By comparison, the sodium carbonate system is somewhat more complex:

$$CO_3^{2-} + H^+ \rightleftharpoons HCO_3^- \quad \textbf{(14)}$$

$$HCO_3^- + H^+ \rightleftharpoons H_2CO_3 \quad \textbf{(15)}$$

$$H_2CO_3 \rightleftharpoons H_2O + CO_2 \quad \textbf{(16)}$$

$$2Na^+ + CO_3^{2-} \rightleftharpoons Na_2CO_{3(s)} \quad \textbf{(17)}$$

Thus, the system behaviour is a strong function of pH, and not just of temperature. It is possible that, upon removal of ice from solution, particularly at sub-eutectic temperatures, the equilibria shift in accordance with Le Chatelier's Principle.

Operating temperatures also affect the yield of ice. Below the eutectic point, modelling indicates an increased yield of ice as temperature decreases. Experimental results validate this prediction, with increasing yields at lower temperatures.

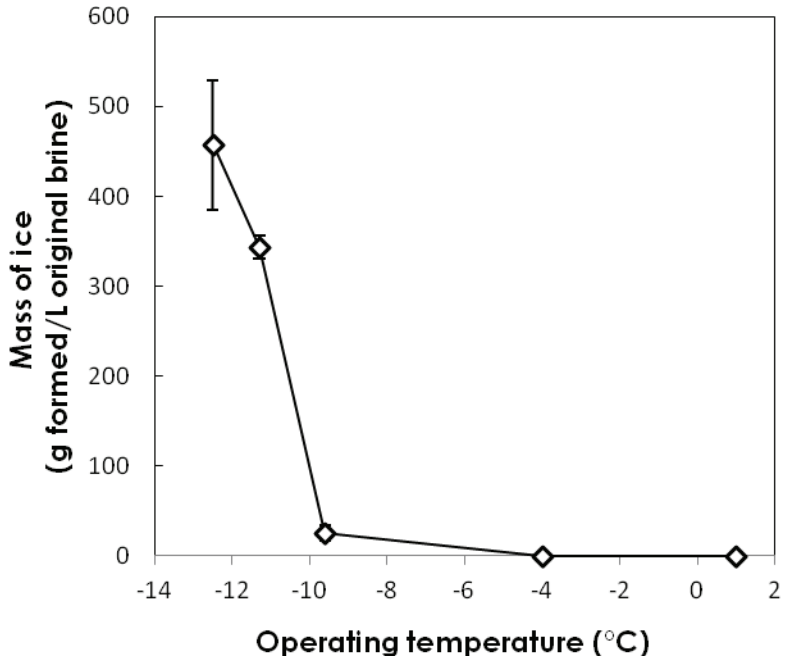

Figure 63: Yield of ice at various operating temperatures in a batch EFC crystallization

The operation of the EFC process at lower temperatures hinges on the thermodynamic driving force of the super-cooling. At colder temperatures, this driving force is greater, and hence, more ice crystallizes out of the brine. Furthermore, a greater thermodynamic driving force also accelerates the kinetics of the system, meaning that, in the same period of time, solutions at a colder temperature produce more ice. This kinetic effect is strongly observed in the EFC systems under study, as well as the batch experiments carried out allow for sufficient time for significant growth. It is recommended that to see how the kinetics change in continuous systems with lower residence times, but that is outside of the scope of the current objective.

This is not to a problem for the EFC process because by understanding where yield begins to decrease and why, it is possible to design a multi-stage process to optimise both salt and ice yields. Based on the experimental data, a two stage process should be sufficient, with the first stage operating at a temperature of -9°C to optimise salt yield and a second stage operating at a sub-eutectic point to produce large quantities of ice with a small quantity of additional salt (see Figure 64).

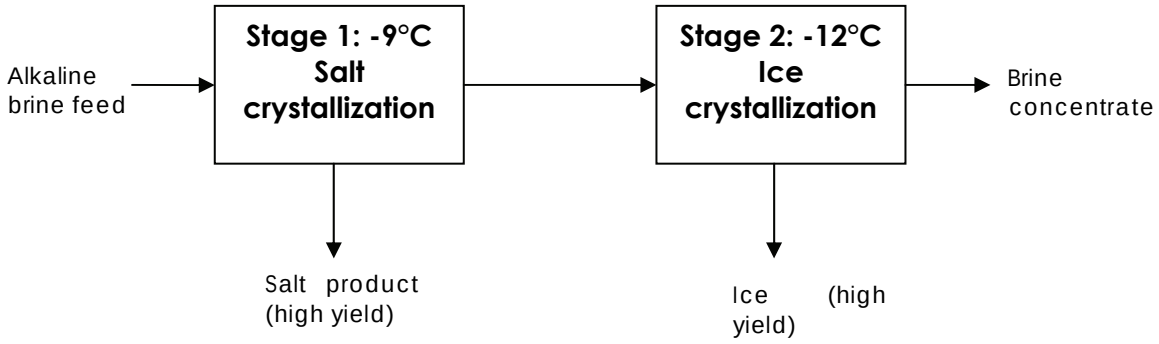

Figure 64: Proposed two-stage process to optimize yields with an alkaline brine by manipulating operating temperatures

4.10.2 Effect of operating temperature on purity

The second part of Objective 5 investigated how temperature affects purity. Ice purity will not be discussed here as, at the time of writing, analytical results were not yet available. However, analysis was completed on the salt produced from the eutectic freeze crystallization of the alkaline brine discussed above.

Figure 65 shows the purity of sodium decahydrate as a function of temperature. It is clear that, within all data sets, it is possible to produce a salt of purity greater than 90 % at temperatures above the eutectic point. This is indicative that the error in the results lies in the washing steps of the process.

This in itself reveals much about the EFC process with respect to product purity, as washing evidently plays a far more significant role in product purity than temperature. However, the highly repeatable purity data at -9.7°C suggests that washing was more effective at this temperature, with much less variability. This could be explained by the fact that at a lower temperature, more growth has been promoted with the greater supersaturation. With larger particles, one can expect less exposed surface area, and hence the total entrained brine is less (Myerson, 2002). This would lead to a product that is easier to wash, resulting in a greater purity.

Analysis of well-washed salts at varying temperatures revealed that the major impurities found within the feed brine do not appear within the salt (Table 16). This suggests that the major source of impurities in the sodium carbonate decahydrate system occur as a result of entrained brine on the surface of the product crystal.

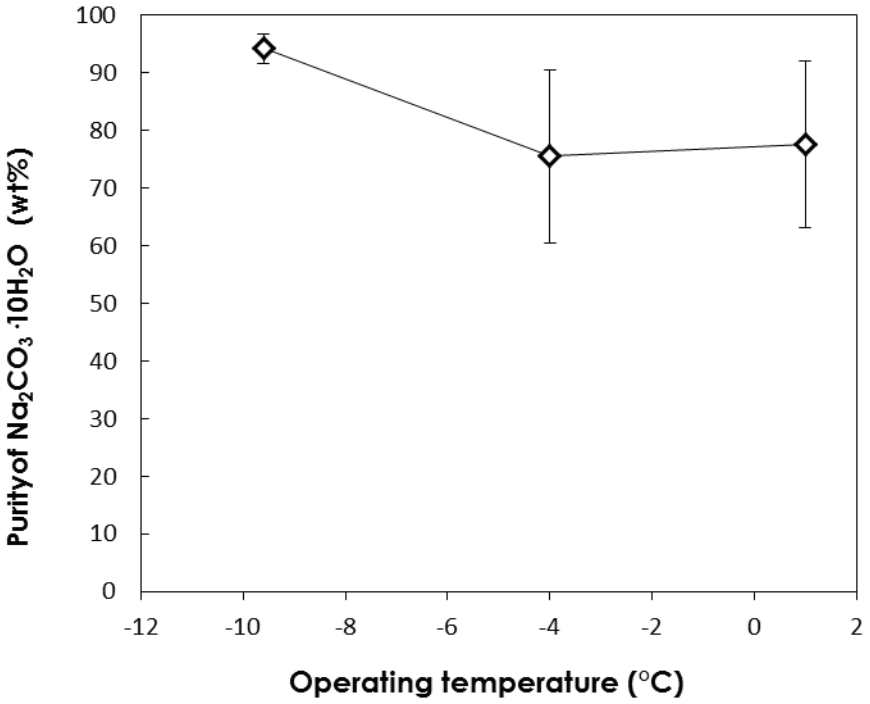

Figure 65: Purity of sodium carbonate decahydrate as a function of temperature

Table 16: Concentrations of dominant impurities in feed and product salts

Species	Feed mg/L	1°C mg/g	-4°C mg/g	-9.6°C mg/g
Ca	2.13	$5.15 * 10^{-3}$	$3.74 * 10^{-3}$	$3.67 * 10^{-3}$
Fe	1.56	$6.15 * 10^{-4}$	$8.3 * 10^{-5}$	$4.57 * 10^{-3}$
K	104.4	$2.09 * 10^{-2}$	$5.92 * 10^{-2}$	$1.16 * 10^{-1}$
Si	33.4	$6.54 * 10^{-2}$	$3.42 * 10^{-2}$	$5.21 * 10^{-2}$

5 CONCLUSIONS AND RECOMMENDATIONS

Eutectic Freeze Crystallization has the potential to treat brines being operated near the eutectic temperature of the desired salt product. When EFC conditions are reached, not only is water produced in the form of ice, but relatively pure salts are also produced. The problem of salt contamination is avoided by the fact that each salt has its own unique eutectic temperature, therefore providing the possibility of crystallizing many pure salts from the brine. Eutectic Freeze Crystallization is an attractive water treatment technology, but to date it has not been utilized for complex systems such as brines.

Although EFC has been shown to be effective in separating a single salt and water, it had yet to be applied to the complex hypersaline brines that are typical of reverse osmosis retentates in South Africa. This project investigated the applicability of EFC to the hypersaline brines and inorganic effluents produced by major South African industries. The objectives of this research project were:

1. Establish the thermodynamic and kinetic factors governing the operation of a Sequential EFC processes;
2. Establish how the treatment of real brines differs from that of synthetic brines;
3. Investigate the effect of impurities and contaminants on the salt product formed during an EFC process.
4. Investigate the effect of impurities and contaminants on the ice product formed by an EFC process.
5. Investigate how operating temperatures affect the yield and purity of the final products formed during an EFC process

5.1 Brine Analysis

The complexity and importance of the brine analysis step is often overlooked. The ion imbalance for a brine analysis is an important measure of the accuracy of the analysis. It was established that the ion imbalance had to be less than 10% to ensure sufficient accuracy for the thermodynamic modelling. It was found that the ion imbalances from the analysis of two of the four brine samples, **Brine 1** and **Brine 2**, were 5.8% and 6.3% respectively. The brines were also very dilute with a total dissolved solids concentration of 29.77 g/L for **Brine 1** and 31.26 g/L for **Brine 2**.

5.2 Thermodynamic modelling

The brine analysis was used in a thermodynamic modelling exercise using OLI Stream Analyser (2010). The model predicted that the system was already saturated with respect to $CaSO_4 \cdot 2H_2O$. It also predicted that water (in the form of ice) would crystallize at -0.8°C followed by $Na_2SO_4 \cdot 10H_2O$ at -1.5°C. A double salt, $K_2SO_4 \cdot CaSO_4 \cdot 1H_2O$, would crystallize at -2.2°C followed by KCl at a lower temperature of -19.6°C for the first brine sample and -16.6°C for the second.

It was determined that there was a correlation between the cation and anion concentration of the salt and the crystallization temperature of the corresponding salt. For example, the brine with the lowest Na^+ concentration resulted in the lowest crystallization temperature of $Na_2SO_4 \cdot 10H_2O$ while the brine with the lowest Cl^- concentration resulted in the lowest crystallization temperature of KCl. The thermodynamic results also showed that a high overall ion recovery (85% for **Brine 1** and 71% for **Brine 2**) would be obtained at an operating temperature of -5°C. The thermodynamic modelling provided the first indication of what could be expected during an EFC process. It showed, for example, that the brines were initially saturated with respect to calcium sulphate. This was identified as a possible problem to EFC because the calcium sulphate would potentially affect the purity of the dominant sodium sulphate salt.

5.3 Kinetic aspects

The kinetic investigations incorporated the results and techniques of the previous aspects of the project in order to investigate the feasibility of using Sequential EFC as a brine treatment method. The results from these investigations showed that a 97% waste conversion to viable products (pure water and salts) could be achieved. Pure calcium sulphate (98.0% purity) and pure sodium sulphate (96.4% purity) were produced along with potable water. In addition, these investigations showed that the initial concern with the saturation of calcium sulphate could be avoided by understanding the kinetics of the system. The experimental work indicated that, although the thermodynamics predicted the solution was saturated with calcium sulphate, calcium sulphate precipitated after 1 week. The results also showed that calcium sulphate could be removed along with ice, under EFC conditions, in a period of 3 to 4 hours. Thus, the removal of calcium sulphate under EFC conditions resulted in a similar aqueous calcium ion concentration to that obtained after 1 week under ambient conditions (0.68 g/L compared to 0.67 g/L) but in a shorter period of time.

5.4 Real vs. synthetic brines

The validity of using synthetic versus real brines was established. The conductivity, pH, density measurements and ion imbalance were identified as important parameters when considering the makeup of a synthetic brine. The current research successfully showed that a real brine could be approximated by a synthetic brine provided these key parameters were similar. The same nucleation temperatures for ice and salt were obtained for both the synthetic brine and the real brine.

5.5 Salt purity

Impurity incorporation was investigated using a platinum brine and it was shown that, only in this instance, the purity of sodium sulphate crystals formed had selenium, in the form of selenate, incorporated in the crystal product due to isomorphic substitution. Previous work focusing on salt purity showed the product purity was >96% with no washing.

5.6 Ice purity

The results showed that the separation of ice and salt plays a significant role in the purity and yield of both crystalline phases. Salt crystals were trapped between ice crystals which made the separation

process inefficient. The addition of gentle agitation at the top of the separation vessel released the trapped salt resulting in an increased yield of salt and a purer ice product.

The increase in the surface area of the settling vessel caused no significant improvement in ice purity compared to that of the addition of agitation in a single sized vessel. However, it is hypothesized that a combination of agitation together with a vessel having a larger surface area will result in purer ice. Also, washing of the ice crystals should be considered to improve the purity of ice even further.

The purity of ice is influence by the growth rate of the ice crystals. The phenomena that characterise crystal growth include heat and mass diffusion and depending on how they interact with each other, they affect crystal growth and morphology. It was observed that the coupled temperature and concentration gradient varied across the boundary layer at the ice interface. Both water and solution systems exhibited morphological instabilities. The boundary layer of ice growing in salt solution was thicker than that of ice growing in pure water and the growth rate of ice in pure water was faster than ice in salt solution. These results ultimately show how complex the ice crystallization process is in a freeze crystallization process and how a fundamental understanding of the phenomena involved in the process can lead to better quality ice and ultimately purer water.

5.7 Effect of temperature on yield and purity

The temperature dependence of yield and purity in the EFC processes should be analysed on a case-by-case basis. The conclusions drawn from thermodynamic modelling must be verified by kinetic experimentation.

In the sodium carbonate system, high yields of salt were observed above the eutectic temperature and ice yields increased substantially below eutectic temperatures.

The concentration of impurities in the sodium carbonate decahydrate salt is very low, indicating a highly pure crystal product affected largely by entrained impurities, and not liquid inclusions or isomorphous incorporations.

5.8 Overall Conclusions

This project, as well as the previous one (Randall 2012), has consisted of 6 years of an extensive experimental programme focussing on the use of Eutectic Freeze Crystallization. This programme has been carried out in collaboration with TU Delft and has been funded by a range of organisations and industrial partners, including the Water Research Commission, as well as CoalTech, Eskom TESP, Impala, Anglo Coal, Sasol, Proxa and DTI's THRIP.

These investigations have shown positive proof of concept for EFC as a feasible treatment for multi-component hypersaline brines.

Firstly, it was shown that thermodynamic modelling (using a model that takes non-idealities into account) can accurately predict the identities of the recovered salts, as well as their recovery temperatures (Lewis et al., 2010, Lewis et al., 2009); secondly, it was shown that EFC can be used for the treatment of hypersaline brines and inorganic effluents produced by major South African industries(Reddy et al., 2010); thirdly, it was shown that EFC can be used to recover multiple salts from multicomponent brines (Randall et al., 2011); lastly it was shown that EFC can produce relatively pure salts as well as pure ice (Jivanji et al., 2011, Lewis and Randall, 2011, Randall et al., 2009, Randall et al., 2011, Reddy et al., 2009).

5.9 Recommendations

Although this work has shown that EFC is an extremely promising technology for the recovery of both salts and ice from hypersaline brines, so far all of the work has been done in batch mode, an essential mode for testing proof of concept, as well as for initial feasibility testing. The next challenge is to be able to develop the technology to the point that it can be used in continuous mode. This is the focus of our current work.

6 REFERENCES

AMBROSINI D, PAOLETTI D, RASHIDNIA N, Overview of diffusion measurements by optical techniques, Optics and lasers in engineering 46 (2008) 852-864.

AYEL V, LOTTIN O, FAUCHEUX M, SALLIER D, PEERHOSSAINI H, Crystallisation of undercooled aqueous solutions: Experimental Study of Free Dendritic Growth in Cylindrical Geometry, International Journal of Heat and Mass Transfer 49 (2006) 1876-1884.

BAKER R.A, Trace organic contaminant concentration by freezing – I. Low inorganic aqueous solutions, Water Res. 1 (1967) 61-77.

BARDUHN A, MANUDHANE A, Temperature required for eutectic freezing of natural waters, Desalination 28 (1979) 233-241.

BREDIKHIN V.I, GALUSHKINA G.L, KUZNETSOV S.P., Schlieren technique to in situ monitor rapidly-growing KDP crystal surface. Journal of Crystal Growth 219 (2000) 83-90.

CARVALHO L, Costly mistakes in water treatment plant design for power plant projects, Conference of Electric Power Supply Company, Macau, China, 2008.

CHEN P, CHEN X.D, FREE K.W, An experimental study on the spatial uniformity of solute inclusion in ice formed from falling film flows on a sub-cooled surface, Journal of Food Engineering 39 (1999) 101-105.

CHEN S, WANG P, LEE T, An experimental investigation of nucleation probability of supercooled water inside cylindrical capsules, Experimental Thermal and Fluid Sciences 188 (1998) 299-306.

CORCORAN E, NELLEMANN C, BAKER E, BOS R, OSBORN D, SAVELLI H, Sick Water? The central role of wastewater management in sustainable development. A Rapid Response Assessment, United Nations Environment Programme, UN-HABITAT, 2010 http://www.grida.no/publications/rr/sickwater/ebook.aspx. [accessed on 21 May 2011]

CORK R.H, PRITCHARD D.C, TAM W.Y, Local concentration measurements in electrochemical deposition using a schlieren method, Physics Review 44, 10 (1991) 6940-6943.

DEPARTMENT OF WATER AFFAIRS AND FORESTRY, South African water quality guidelines, 2nd ed, vol. 1, Department of Water Affairs and Forestry, Pretoria, South Africa, 1996 http://www.dwaf.gov.za/IWQS/wq_guide/domestic.pdf. [accessed on 21 May 2011]

DRUMMOND L.S, VAESSEN R, HIMAWAN C, SECKLER M.M, WITKAMP G.J, A method for rapid development of eutectic freeze crystallization processes: application to potassium sulphate solution contaminated with organics, Chemical Engineering Transactions AIDIC 1 (2002) 921-926.

ERIBIL H.Y, Surface chemistry of solid and liquid interface, Blackwell Publishing, 2006.

GENCELI F.E, Eutectic Freeze Crystallization, Phd Thesis. Netherlands: Technical University of Delft, 2008.

GENCELI F.E, PASCUAL M.R, KJELSTRUP S, WITKAMP G, Coupled heat and mass transfer during crystallization of MgSO4.7H2O on a cooled surface, Crystal growth and design 9, no. 3 (2009) 1318-1326.

ZHANG G.G.Z, GRANT D.J.W, Incorporation mechanism of guest molecules in crystals: solid solution or inclusion? International journal of pharmaceutics (1999). Vol 181. 61-70.

GREENBERG P.S, KLIMEK R.B, BUCHELE D.R, Quantitative rainbow schlieren deflectometry." Applied Physics 34 (1995) 3810-3822.

GUPTA A.S, PANIGRAHI P.K, MURALIDHAR K, GUPTA R, Color Schlieren deflectometry for characterization of crystal growth, Journal of Crystal growth 312 (2010) 817-830.

HALDE R, Concentration of impurities by progressive freezing, Water Research 14 (1980) 575 580.

HARGATHER M.J, SETTLES G.S, A comparison of three quantitative schlieren techniques,Optics and Lasers in Engineering, 50 (2012) 8-17.

HERRERA C.A, HERNANDEZ D.M, GARCIA B.B, VIRAMONTES J.A, Temperature measurement of air convection using a schlieren system, Optics and Laser Technology 41 (2009) 233-240.

HIMAWAN C, WITKAMP G.J, Crystallization kinetics of MgSO4.12H2O from different scales of batch cooling scraped crystallizers, Crystal Research Technology 41 (2006) 865-873.

http://www.tulane.edu/~sanelson/geol212/ternaryphdiag.htm [accessed on 21 May 2011]

JIVANJI, R., NATHOO, J., MERWE, W. V. D., HUMAN, A. LEWIS, A. 2011. Application of Eutectic Freeze Crystallization to the Treatment of Mining Wastewaters. 22nd World Mining Congress. Istanbul.

JOHNSON W.E, State of the art freezing processes, their potential and future, Desalination 19 (1976) 349-358.

KIM K, ULRICH J, Theoretical and experimental studies on the behaviour of liquid impurity in solid layer melt crystallization." Journal of Physics 34 (2001): 378-396.

KIRKOVA E, DJAROVA M, DONKOVA B, Inclusion of Isomorphous Impurities during Crystallization from Solutions, Prog. Crystal Growth and Charact., 32 (1996) 111-134.

KLEINEA H, GRONIGB H, TAKAYAMA K, Simultaneous shadow, schlieren and interferometric visualization of compressible flows, Optical and Laser in Engineering 44 (2006) 348-361.

KUBOTA N, A new interpretation of metastable zone widths measured for unseeded solutions, Journal of Crystal Growth, 310 (2008) 629-634.

LEWIS A.E, NATHOO J, REDDY S.T, RANDALL D.G, Novel technology for recovery of water and solid salts from hypersaline brines: Eutectic Freeze Crystallization, Water Research Commission, South Africa, Progress Report 2, 2008.

LEWIS, A. & RANDALL, D. 2011. Using Eutectic Freeze Crystallization to treat a Range of Brines. Desalination and Environment: A Water Summit. Rotana Beach, Abu Dhabi.

LEWIS, A. E., NATHOO, J., THOMSEN, K., KRAMER, H. J., WITKAMP, G. J., REDDY, S. T. RANDALL, D. G. 2010. Design of a Eutectic Freeze Crystallization process for multicomponent waste water stream. Chemical Engineering Research & Design, 88, 1290-1296.

LEWIS, A. E., RANDALL, D. G., REDDY, S. T., JIVANJI, R. NATHOO, J. 2009. Worth its Salt – How Eutectic Freeze Crystallisation Can be Used to Recover Water and Salt from Hypersaline Mine Waters. In: FONG, O. T. (ed.) Water in Mining 2009. Perth: Austalasian Institute of Mining & Metallurgy

LEWIS, A.E., NATHOO, J., RANDALL, D., ZIBI, L AND JIVANJI, R. 2010. Novel Technology for Recovery of Water and Solid Salts from Hypersaline Brines: Eutectic Freeze Crystallization, Research Report 1727/1/10, Water Research Commission, Private Bag, X03, Gezina, 0031, South Africa

LOFFELMANN M, MERSMANN A, How to measure supersaturation, Chemical Engineering Science 57 (2002) 4301-4310.

LORAIN O, THIEBAUD P, BADORC E, AURELLE Y, Potential of freezing in wastewater treatment: soluble pollutant applications, Water Research 35 (2001) 541-547.

LUO C, CHEN W, HAN W, Experimental study on factors affecting the quality of ice crystal during the freezing concentration for the brackish water, Desalination 260 (2010) 231-238.

MAEDA K, FUKUI K, Effects of crystal growth rate and heat and mass transfer on solute distribution, Chemical Engineering Science 57 (2002) 3133-3140.

MERSMANN A, Crystallization Technology Handbook. 2nd. New York: Marcel Dekker Inc, 2011.

MULLIN J.W, Crystallization and Precipitation, Ullmann's Encyclopaedia of Industrial Chemistry, (2002) 6750-6796.

MULLIN J.W, Crystallization. 4th. London: Butterworth Heinemann, 2001.

MYERSON A, Handbook of Industrial Crystallization. 2nd edn, Butterworth Heinemann, USA, 2002.

MYERSON A, Impurity capture during crystal growth [Report] : Ph.D Dissertation

NYVLT J, Industrial Crystallization from solutions, 1st edn, Butterworth, London, 1971.

NYVLT J, RYCHLY R, GOTTFRIED J, WURZERLOVA J, Metastable zone-width of some aqueous solutions, Journal of Crystal Growth 6 (1970) 151-162.

OLI Systems Inc., OLI Stream Analyser, Version 3.0, Morris Plains, New Jersey, USA, 2010.

PETZOLD G, AQUILERA J.M, Ice morphology: Fundamental and technological application in foods, Food biophysics 4 (2009) 378-396.

PULLES W, Mine water reference manual, Pulles Howard & de Lange Incorporated, 1993.

RAHMAN M.S, AHMED M, CHEN X.D, Freezing-melting process and desalination: review of present status and future prospects, International Journal of Nuclear Desalination 2 (2007) 253-264.

RAMSDELL L.S, E.P. Partridge E.P, The crystal forms of calcium sulphate. Mineralogical Society of America, 14 (1929) 59-74.

RANDALL, D. G., NATHOO, J. & LEWIS, A. E. 2009. Seeding for selective salt recovery during Eutectic Freeze Crystallization. In: TAYLOR, C. (ed.) International Mine Water Conference. Pretoria.

RANDALL, D. G., NATHOO, J. LEWIS, A. E. 2011. A case study for treating a reverse osmosis brine using Eutectic Freeze Crystallization--Approaching a zero waste process. Desalination, 266, 256-262

REDDY, S. T., KRAMER, H. J. M., LEWIS, A. E. & NATHOO, J. Investigating factors that affect separation in a eutectic freeze crystallisation process. International Mine Water Conference, 19-22 October 2009 Pretoria, South Africa. 649-655

REDDY, S. T., LEWIS, A. E., WITKAMP, G. J., KRAMER, H. J. M. & VAN SPRONSEN, J. 2010. Recovery of Na2SO4•10H2O from a reverse osmosis retentate by eutectic freeze crystallisation technology. Chemical Engineering Research and Design, 88, 1153-1157.

SANGWAL K, Novel approach to analyze Metastable Zone Width determined by the polythermal method: physical interpretation of various parameters, Crystal Growth and Design 9 (2009) 942-950.

SATO K, Y. FURUKAWA Y, K.W. FREE K.W, Advances in crystal growth research, Elsievier, 2001.

SHIRAI Y, WAKISAKA M, MIYAWAKI O, SAKASHITA S, Effect of seed ice on formation of tube ice with high purity for a freeze wastewater treatment system with a bubble-flow, Elsevier 33 (1999) 1325-1329.

SHLICHTA S, VERMA P.J, Imaging techniques for mapping solution parameters, growth rate, and surface features during the growth of crystal from Solution, Progress in crystal growth and characterization of materials 54 (2008) 1-120.

SONG C, WANG P, MAKSE H.A, A phase diagram for jammed matter, Nature Letters 453 (2008) 629-632.

SRIVASTAVA A, MURALLIDHA K, PANIGRAHI P.K, Comparison of Interferometry, schlieren and shadowgraphy for visualizing convection around KDP, Crystal Growth 261 (2004) 348-361.

STEPAKOFF G.L, D. SIEGELMAN D, JOHNSON R, W. GIBSON W, Development of eutectic freezing process for brine disposal, Desalination 14 (1974) 25-38.

TAI C.Y, TAI C, CHANG M, Effect of interfacial supersaturation on secondary nucleation, Journal of the Taiwan Institute of Chemical Engineers 40 (2009) 439-442.

TAO Y, JUN M, LI-QIU Z, Study of factors affecting ice crystal purity during freeze concentration process for urine treatment, Harbin Institute of Technology 14 (2007) 1005-9113. Ternary phase diagrams, 2008.

THOMSEN K, Aqueous electrolytes: model parameters and process simulation, PhD Thesis, Technical University of Denmark, Denmark, 1997.

ULRICH J, TORSEN S, Kirk-Othmer Encyclopedia. John Willey and Sons, 2011.

ULRICH J, JONES M.J, Heat and Mass Transfer Operations-Crystallization. Oxford: Eolss, 2006.

University of Virginia – Virginia (1977)

VAESSEN R, Development of scraped eutectic crystallizers. PhD Thesis. Technical University of Delft, The Netherlands, 2003.

VAN DER HAM F, Eutectic Freeze Crystallization. PhD Thesis. Technical University of Delft, The Netherlands, 1999.

VAN DER HAM F, WITKAMP F, DE GRAAUW G.J, VAN ROSMALEN J, Eutectic Freeze Crystallization: Simultaneous formation and separation of two solid phases, Journal of Crystal Growth 199 (1999b) 744-748.

VAN DER HAM F, WITKAMP F, DE GRAAUW G.J, VAN ROSMALEN J, Eutectic Freeze Crystallization: Application to process streams and waste water purification, Chemical engineering process 37 (1998) 207-213.

VAN SPRONSEN J, RODRIGUEZ PASCUAL M, GENCELI F.E, TRAMBITAS D.O, EVERS H, WITKAMP G.J, Eutectic Freeze Crystallization from the ternary Na2CO3.10H2O – NaHCO3 – H2O system: A novel scraped wall crystallizer for the recovery of soda from an industrial aqueous stream, Chemical Engineering Research and Design 88 (2010) 1259-1263.

WIEGANDT H.F, VON BERG R.L, Myths about freeze desalting, Desalination 33 (1980) 287-297.

ZHANG G, GRANT D, Incorporation mechanism of guest molecules in crystals: solid solution

ZIBI L.M, Industrial brine characterisation and modelling, MSc. Thesis. University of Cape Town, South Africa, 2010.